

Diss. ETH No. 13210



# Modeling and Control for the Isothermal Extrusion of Aluminum

A dissertation submitted to the  
SWISS FEDERAL INSTITUTE OF TECHNOLOGY  
ZURICH  
for the degree of  
Doctor of Technical Sciences

presented by  
CARLOS FERNANDO CUÉLLAR MATAMOROS

Dipl. Chem.-Ing. ETH  
born October 28, 1967  
citizen of El Salvador

accepted on the recommendation of

Prof. M. Steiner, examiner  
Prof. Dr. P. Hora, co-examiner  
Dr. A. Schmid, co-examiner

1999

# Abstract

As competitiveness in the metal and metal forming industry grows more and more, great efforts must be paid to achieve targets on product quality. Within the aluminum industries, extrusion plays an important role. In this process, it is of superior importance to achieve uniform product quality while minimizing the discard. The exit temperature of the extrudate profile is a measure of product quality. It is desired to run the process in such a manner, that this temperature remains constant throughout the whole extrusion cycle. This is known as isothermal extrusion. Developing model-based control strategies to achieve isothermal extrusion was the aim of this thesis.

Starting from industrial data, empirical in-house process knowledge shared by the industrial partner of this thesis, as well as from literature on metal-forming processes, a first-principles model of the aluminum extrusion process investigated was developed. The motivation for developing such a model was driven by the fact that other solution approaches, such as system identification methods, would have required disturbing the production through extensive experimenting on the plant. This was clearly undesirable and a strong constraint on the development of any type of model. In addition, a model based just on experimental data would have only been valid for the plant from which the data originated. This would have meant developing numerous models, one for each machine, so as to capture the dynamics of each particular system.

This detailed model was the starting point for developing control strategies for the isothermal extrusion of aluminum. As a consequence of the complexity and thoroughness of this first-principles model, an open-loop control strategy was chosen as a first solution to the problem. This choice had two motivations: on the one hand open-loop strategies were simpler to implement in the existing

distributed control system (DCS) at the plant. Additionally, this type of approach was more likely to be understood and accepted by the plant personnel. On the other hand, more sophisticated closed-loop strategies could be developed subsequently, exploiting the existing detailed model and the open-loop trajectories derived therefrom.

This led to the second part of this work where, starting from the understanding and knowledge gained through the more sophisticated first-principles model, a simplified model of the aluminum extrusion process was derived. This step was a natural consequence of the mathematical as well as computational requirements imposed by a closed-loop control strategy, which could hardly have been met based on the model derived in the first part of this thesis. The development of closed-loop control strategies is of advantage to exploit the valuable information provided by the measurement of the temperature of the extrudate. This allows to take into account process/model mismatches and disturbances (e.g. noise) entering the system, two factors neglected by any open-loop strategy. At the same time, constraints on the system had to be taken into account. This led to the choice of model predictive control (MPC). This methodology allows various types of constraints on the system to be considered directly during the design of the control strategy.

Relying on the measurements of the temperature of the extrudate for closed-loop control obviously means ensuring that this information is accurate. As the temperature sensors found in industrial practice are prone to partial failure, a monitoring algorithm was designed to detect faults on this sole source of information for the closed-loop controller. Here, statistical methods based on cumulative sum (CUSUM) algorithms were chosen. Once again the choice of this strategy was driven by the simplicity with which this algorithm may be implemented in industrial practice. In addition, the introduction of such a monitoring scheme could increase the acceptance of closed-loop controllers by the operators.

# Zusammenfassung

Wettbewerbsfähigkeit in der Metallindustrie verlangt, dass die Prozesse möglichst effizient und produktiv laufen. Innerhalb der Aluminiumverarbeitungsindustrie spielt das Strangpressen eine zentrale Rolle. Hier ist es vor allem wichtig, dass man eine homogene Produktqualität gewährleistet, bei minimalem Ausschuss. Ein Mass für die Qualität des Produktes ist die Austrittstemperatur des gepressten Profils. Es ist erwünscht, den Prozess so zu betreiben, dass die Temperatur des gepressten Profils während des ganzen Presszyklus möglichst konstant bleibt. Dies nennt man isothermes Strangpressen von Aluminium. Die Entwicklung einer modellbasierten Regelstrategie für diesen Zweck ist das Ziel dieser Arbeit.

Im ersten Teil dieser Arbeit wird ein Modell des Prozesses entwickelt. Dafür sind experimentelle Methoden wenig geeignet, da diese umfangreiche Versuchskampagnen an der Anlage voraussetzen. Dies hätte zu unerwünschten Störungen oder gar Unterbrüchen des Produktionsbetriebs geführt. Zudem ist ein empirisches Modell lediglich für genau die Anlage gültig, auf welcher die Experimente durchgeführt werden. Dies bedeutet, dass die Herleitung eines Modells für jede Maschine wiederholt werden muss, um die Dynamik des jeweiligen Systems zu beschreiben. Somit kommt nur die Herleitung eines auf der Physik des Prozesses basierten Modells in Frage.

Dieses detaillierte physikalische Modell ist der Ausgangspunkt für die Entwicklung von Regelstrategien für das isotherme Strangpressen von Aluminium. Bedingt durch die Komplexität des physikalischen Modells werden zunächst Open-loop-Regelstrategien entworfen. Dieser Entscheid beruht auf drei Überlegungen: Erstens sind Open-loop-Regelstrategien einfacher in das vorhandene Leitsystem zu integrieren. Zweitens werden Open-loop-Regelstrategien vom Personal der Anlage rascher verstanden und akzeptiert. Drittens kann ein späterer Entwurf anspruchsvollerer Closed-loop-Regelstrategien auf



die Erfahrungen mit dem vorhandenen physikalischen Modell und die Open-loop-Strategien gestützt werden.

Im zweiten Teil der Arbeit werden der Entwurf und die Untersuchung von Closed-loop-Regelstrategien in Angriff genommen. Dafür wird ein vereinfachtes Modell des Prozesses hergeleitet. Dies wird durch die bei der Entwicklung des detaillierten physikalischen Modells gewonnenen Erfahrungen und Prozesskenntnisse ermöglicht. Die Herleitung eines vereinfachten Modells ist auch die logische Konsequenz der mathematischen bzw. rechen-technischen Ansprüche, die eine Closed-loop-Regelstrategie erfordert. In diesem Zusammenhang sind hauptsächlich die Anforderungen an die Rechenzeiten bei der Simulation des Prozesses mit dem komplexeren Modell nicht erfüllt. Eine Closed-loop-Regelstrategie ist dazu noch vorteilhaft, um die Messung der Temperatur des Profils ausnutzen zu können. Somit können eventuelle Modellfehler und Störungen (z.B. Rauschen), die das System beeinflussen, beim Entwurf der Regelstrategien in Betracht gezogen werden. Gleichzeitig müssen auch physikalische Begrenzungen des Systems betrachtet werden, was zur Wahl der Methode der Modell-prädiktiven Regelung führt. Verschiedene Begrenzungen des Systems können somit direkt beim Entwurf des Reglers berücksichtigt werden.

Um die Temperaturmessung des Profils ausnutzen zu können, muss man ihre Genauigkeit gewährleisten. Da die Temperatursensoren, die in der Regel beim Strangpressen eingesetzt werden, dazu neigen, Fehler zu entwickeln (z.B. Drifts, Bias), ist es nötig, diese Sensoren zu überwachen. Dafür wird im dritten Teil der Arbeit ein statistischer Algorithmus eingesetzt, um Fehler bei der Messung der Temperatur zu detektieren. Dieser Algorithmus wird aufgrund seiner Einfachheit hinsichtlich Implementierung in einer industriellen Umgebung gewählt.

# Resumen

A medida que la competitividad en la industria metalúrgica aumenta, mayor énfasis y esfuerzo se deben poner para poder garantizar y cumplir con las normas de calidad establecidas. En la industria del aluminio el proceso de extrusión juega un papel central. En este proceso es imprescindible garantizar una calidad homogénea de los productos, manteniendo siempre al mínimo los desperdicios de material. La temperatura del perfil de extrusión es una medida importante de la calidad del producto. Es necesario que el proceso corra de tal manera que esta temperatura permanezca constante durante todo el ciclo de extrusión. Esto se conoce como *extrusión isotérmica*. El fin de esta tesis es el desarrollo de estrategias de control basadas en un modelo del proceso que garanticen una extrusión isotérmica de aluminio.

En la primera parte de la tesis se desarrolla un modelo fundamentado en la física del proceso de extrusión de aluminio. Este modelo está basado en conocimientos empíricos sobre el proceso proporcionados por la empresa conjunto a la cual se llevo a cabo el proyecto, así como también en la literatura referente a procesos metalúrgicos. El desarrollo de un modelo experimental, basado quizás en métodos como la identificación de sistemas, no fue posible ya que ésto hubiera significado perturbar la producción con extensas campañas experimentales en la planta. Esto último era claramente inaceptable y representa una gran limitante al desarrollar cualquier tipo de modelo del proceso, sea éste un modelo experimental o un modelo basado en la física del proceso. Por otra parte, un modelo empírico del proceso basado solamente en datos experimentales hubiera sido válido sólo para la máquina de la cual se originaban los datos. Esto hubiera implicado desarrollar un modelo para cada una de las máquinas presentes en la planta que reflejase la dinámica particular de cada sistema.

El modelo detallado, fundamentado en la física del proceso, forma

la base para el diseño de estrategias de control para la extrusión isotérmica de aluminio. Debido a la complejidad del modelo detallado, una estrategia de control de lazo abierto fue seleccionada como primera solución a este problema. Otros aspectos de tipo práctico tales como la facilidad de implementación de las estrategias de control de lazo abierto en el sistema de control distribuido presente en la planta, así como también la aceptación de este tipo de estrategias por el personal técnico, fueron determinantes para inclinarse por esta decisión.

En la segunda parte de la tesis se deriva un modelo simplificado del proceso para poder desarrollar estrategias de control de lazo cerrado. Esto fue posible gracias a los conocimientos del proceso obtenidos al desarrollar el modelo detallado en la primera parte. El desarrollo de un modelo simplificado es también una consecuencia lógica de los requerimientos computacionales que una estrategia de control de lazo cerrado suponen, los cuales no hubieran podido ser cumplidos con el modelo desarrollado en la primera parte. El control de lazo cerrado es ventajoso para poder explotar la información proporcionada por el sensor de temperatura del perfil de extrusión. Esto último permite tomar en cuenta factores como incongruencias entre el modelo y la planta, así como también perturbaciones que entran en el sistema (e.g. ruido). Por otra parte, en el proceso de diseño de un controlador es imperativo tomar en cuenta los límites físicos del sistema. Para este fin se utilizó el método de modelo de control predictivo.

Para hacer uso de la medición de la temperatura del perfil es necesario garantizar su exactitud. Puesto que los sensores de temperatura que se utilizan en este tipo de procesos tienden a desarrollar bias y otros tipos de errores, se utilizó un algoritmo para la detección de fallas en los sensores. Este algoritmo está basado en métodos estadísticos y adicionalmente ofrece la ventaja de una fácil implementación en condiciones industriales.

# Acknowledgments

First and foremost I would like to acknowledge all the persons to whom I am beholden and by whom I have been influenced throughout the course of this thesis and my entire sojourn here in Europe.

I would like to thank Prof. M. Steiner for granting me full independence and confidence to pursue my research interests in the manner I considered most proper. My deepest gratitude goes to Prof. Dr. Pavel Hora, from the Institute of Forming Technology of the ETH, for his helpful comments and suggestions, as well as for accepting to serve as co-examiner. I am indebted to Dr. Andreas Schmid, who not only helped in getting the project started and guided me during the complete course of this thesis, but also agreed to act as co-examiner.

The late Prof. Dr. D.W.T. Rippin I thank for providing me with the opportunity to start my PhD studies in his Systems Engineering Group and for encouraging me to pursue my interests in the field of automatic control. I will always remember him as an exemplary and dedicated scholar. A real gentleman!

I wish to express my sincere gratitude to Alusuisse Technology Management AG for its support during the first part of this dissertation. In particular I would like to thank Ronald Stiem, and Edgard Steigmann, for their support, patience, and their willingness to share their engineering experience. I owe much to Dr. W. Maletinsky who agreed to start the cooperation between Alusuisse and the Measurement and Control Laboratory.

I am indebted to Dr. Ayman Hamdy. His wonderful engineering knowledge and great personality were a great support during the initial phase of my life as a "control engineer". I also wish to thank Iwona Bärtsch, Hans Musch, and Adriana Horníková with whom I had the pleasure of sharing the office. I owe much to Mr. Georges

Bammatter and Esther Baumann for their patience, competence, and constant support regarding the computer network. My greatest respect and gratitude go to Ms Brigitte Rohrbach who supported me throughout the whole project. Her constant advice regarding the English language and personal matters, was of great value to me.

My days at the Measurement and Control Laboratory have been full of excitement from the technical, and what is more important to myself, from the personal point of view. Days usually started with a morning coffee where "the gang" met and where we discussed and joked about many topics. I have to thank everybody usually present in these coffee rounds. It must certainly not have been easy having to constantly react to my provocations regarding "Swiss mentality". I always had fun there, and many times while riding the tram to the ETH during the gray and depressive mornings of winter in Zurich, I looked forward to these meetings which I found the best way to kick-off the day.

I am beholden to Roberto Cirillo, Michael Simons, Mengbin Zhang, Oliver Tanner, and Christoph Eck my immediate office neighbours and after-work "buddys". Indeed, without their moral and many times technical support I would have never made it through the rough waters of this dissertation. Again, and again they attacked my frustrations and my stress during these PhD years with the best remedy: a fantastic sense of humor! I will miss them and hope that our friendship will continue after I have left the Institute and Switzerland.

My deepest gratitude goes to the "Latino Community & Co." of the ETH. In particular I would like to thank Javier de Oñate, Philip Moscoso, and Christian Roduner. Throughout the years I have enjoyed their sincere friendship and advice. Their support when I did not see "any light at the other side of the tunnel" was invaluable. I am deeply beholden to them and can only hope I will be able to make

up for all their patience and tolerance.

My earlier years in Germany cannot go unnoticed. In particular I wish to thank Danilo Marengo, with whom I certainly have spent some of the most interesting and exciting times here in Europe. His strong personality and very refined sense of humor, have marked my character and indeed he has become my "greater family" overseas.

To my family: thanks to my brothers and sister. In the last years I have enjoyed the company and time with my oldest brother Alfredo. His advice and presence in my life have been invaluable to withstand my long years of education. My respect to my brother José Ernesto and sister Lygia for their constant moral support.

To my parents! What can I say to these two wonderful human beings to whom I had the luck to have been born to. They have always encouraged me, and have taught me to be persistent and confident in myself. My desire to pursue my PhD studies undoubtedly came from the special atmosphere that reigned in our house. Looking back throughout the years I am always amazed of what the love and determination of these two people was capable of achieving. Hopefully, I will be able to pay with love all the love and support that I have received from them.

From all the experiences here in Europe, having met my girlfriend Maureen has been by far the most wonderful and rewarding of them all. Maureen's sharp mind, open-mindedness, and great sense of humor were always a reassurance and a motivation to keep going. I thank her for all her patience, encouragement, and understanding. In short: I love you very much Maureen, and thank you for all the great things you have given to me.



# Nomenclature

## Notation for Extrusion Processes

Notation	Meaning	Units
$T$	Temperature.	$[^{\circ}C]$
$W$	Work.	$[J]$
$F$	Force.	$[N]$
$F_{die}$	Die Force.	$[N]$
$F_{friction}$	Friction Force.	$[N]$
$P$	Work per unit of time.	$[W]$
$Q$	Heat generation rate.	$[W]$
$Q_{friction}$	Heat generation rate due to friction.	$[W]$
$Q_{deformation}$	Heat generation rate due to deformation.	$[W]$
$A_0$	Cross-sectional area of billet.	$[m^2]$
$A_1$	Cross-sectional area of extrudate profile.	$[m^2]$
$A_{i/j}$	Contact area between sections $i$ and $j$ .	$[m^2]$
$V$	Volume.	$[m^3]$
$V_i$	Volume of section $i$ .	$[m^3]$
$c_p$	Specific heat.	$\left[ \frac{J}{kg^{\circ}C} \right]$
$cp_{Al}$	Specific heat of aluminum.	$\left[ \frac{J}{kg^{\circ}C} \right]$
$cp_{Fe}$	Specific heat of steel.	$\left[ \frac{J}{kg^{\circ}C} \right]$
$R$	Radius of billet or inner radius of container.	$[m]$
$R_1$	Outer radius of container.	$[m]$
$L_0$	Initial length of billet.	$[m]$
$Re$	Reynolds Number.	$[-]$
$k$	Thermal conductivity.	$\left[ \frac{W}{m^{\circ}C} \right]$



$k_{Al}$	Thermal conductivity of aluminum.	$\left[ \frac{W}{m^{\circ}C} \right]$
$k_{Fe}$	Thermal conductivity of steel.	$\left[ \frac{W}{m^{\circ}C} \right]$
$r$	Radial coordinate.	$[m]$
$x$	Axial coordinate.	$[m]$
$q$	Heat flux per unit area.	$\left[ \frac{W}{m^2} \right]$
$v_x$	Axial velocity component.	$\left[ \frac{m}{s} \right]$
$v_r$	Radial velocity component.	$\left[ \frac{m}{s} \right]$
$h_c$	Contact conductance.	$\left[ \frac{W}{m^{2\circ}C} \right]$
$h$	Heat transfer coefficient.	$\left[ \frac{W}{m^{2\circ}C} \right]$
$h_R$	Heat transfer coefficient billet/container.	$\left[ \frac{W}{m^{2\circ}C} \right]$
$g$	Gravitational acceleration.	$\left[ \frac{m}{s^2} \right]$
$g_i$	Component of $g$ in direction $i$ .	$\left[ \frac{m}{s^2} \right]$
$p$	Pressure.	$\left[ \frac{N}{m^2} \right]$
$v_{ram}$	Ram velocity.	$\left[ \frac{m}{s} \right]$
$r_{die}$	Radius of die.	$[m]$
$d$	Diameter of die.	$[m]$
$t$	Time.	$[s]$
$k_f$	Flow stress.	$\left[ \frac{N}{m^2} \right]$

## Greek Symbols

Notation	Meaning	Units
$\alpha$	Thermal diffusivity.	$\left[\frac{m^2}{s}\right]$
$\rho$	Density.	$\left[\frac{kg}{m^3}\right]$
$\rho_{Al}$	Density of aluminum.	$\left[\frac{kg}{m^3}\right]$
$\rho_{Fe}$	Density of steel.	$\left[\frac{kg}{m^3}\right]$
$\phi$	Angular coordinate.	$[^\circ]$
$\tau_{ij}$	Shear stress in direction $j$ on a fluid surface of constant $i$ .	$\left[\frac{N}{m^2}\right]$
$\mu$	Viscosity.	$\left[\frac{kg}{m \cdot s}\right]$
$\sigma_i$	Normal stress in direction $i$ .	$\left[\frac{N}{m^2}\right]$
$\sigma_m$	Mean principal stress.	$\left[\frac{N}{m^2}\right]$
$\nu_{fr}$	Coefficient of friction.	$[-]$
$\Psi$	Stream function.	$[-]$
$\epsilon$	Strain.	$[-]$
$\dot{\epsilon}$	Strain rate.	$\left[\frac{1}{s}\right]$
$\varphi$	Logarithm of extrusion ratio.	$[-]$

## Notation for State-Space Models and Systems

### Notation    Meaning

$A$	System matrix.
$B, D$	Input-to-state (input-to-ouput) gain matrix.
$C$	State-to-ouput gain matrix.
$x, X$	State vector.
$y, Y$	Output vector of the system.
$u, U$	Control/manipulated input.
$\hat{x}, \hat{X}$	State estimate.
$Y_0^N = \begin{pmatrix} y_0 \\ y_1 \\ \vdots \\ y_N \end{pmatrix}$ or $Y_0^N = \begin{pmatrix} Y_0 \\ Y_1 \\ \vdots \\ Y_N \end{pmatrix}$	Output sequence.
$K$	Kalman gain.
$W$	Noise sequence on state equation.
$V$	Noise sequence on observation equation.
$P$	Covariance matrix of state estimation error.
$Q$	Covariance matrix for $\omega$ or $W$ .
$R$	Covariance matrix for $\nu$ or $V$ .
$J$	Performance index.
$T_s$	Sampling time.
$r$	Reference trajectory vector.
$p$	Prediction horizon.
$m$	Control horizon.

### Greek Symbols

#### Notation    Meaning

$\epsilon$	Innovation.
$\Sigma$	Covariance matrix of innovation $\epsilon$ .
$\Upsilon_x$	Direction of additive change in the state vector.
$\Upsilon_y$	Direction of additive change in the output vector.
$\Gamma$	Gain matrix for $\Upsilon_x$ .

$\Xi$	Gain matrix for $\Upsilon_y$ .
$\alpha$	Signature of additive change on the state.
$\beta$	Signature of additive change on the state's estimate.
$\rho$	Signature of additive change on the innovation.
$\omega$	Noise sequence on state equation.
$\nu$	Noise sequence on observation equation.

## Notation for Statistics and Change Detection

Notation	Meaning
$\mathcal{H}$	Hypothesis.
$T$	Stopping time.
$P(B)$	Probability of the event $B \in \mathcal{B}$ .
$S_i^j = S_j$	Log-likelihood ratio for observations $y_i$ until $y_j$ .
$\tilde{S}_i^j$	Weighted log-likelihood ratio for observations $y_i$ until $y_j$ .
$\bar{T}$	Mean time between false alarms.
$\mathbf{E}$	Expectation.
$\mathcal{L}$	Probability law; $\mathcal{L}(Y) = \mathbf{P}_\theta$ .
$\mathcal{N}$	Normal (or Gaussian) law.
$t_0$	Change time.
$t_a$	Alarm time.
$g_k$	Decision function.
$p(y)$	Probability density, pdf.
$p_\theta(y)$	Parametrized probability density, pdf.
$h, -a$	Thresholds.
$b$	Minimum magnitude of change.

## Greek Symbols

Notation	Meaning
$\Lambda_i^j$	Likelihood ratio for observations $y_i$ until $y_j$ .
$\tilde{\Lambda}_i^j$	Weighted likelihood ratio for observations $y_i$ until $y_j$ .
$\Upsilon$	Direction of change in a vector parameter.

$\Sigma$	Covariance matrix of the vector random variable $Y$ .
$\theta$	Parameter.
$\theta_0$	Parameter before change.
$\theta_1$	Parameter after change.
$\lambda$	Threshold.
$\sigma^2$	Variance of the scalar random variable $Y$ .
$\bar{\tau}$	Mean detection delay.
$\delta$	Magnitude of change.
$\alpha$	Error probability.
$\beta$	Power of a statistical test.

# Contents

Abstract	i
Zusammenfassung	iii
Resumen	v
Acknowledgments	vii
Nomenclature	xi
<b>1 Introduction</b>	<b>1</b>
1.1 Motivation . . . . .	1
1.2 Scope of the Thesis . . . . .	2
1.3 Control of Aluminum Extrusion: A Review . . . . .	4
1.4 Structure of the Thesis . . . . .	8
<b>2 Dynamic Modeling and Optimal Control Strategies for Aluminum Extrusion</b>	<b>13</b>
2.1 Introduction . . . . .	13
2.2 Extrusion Processes . . . . .	15
2.2.1 Direct Extrusion . . . . .	16
2.2.2 Indirect Extrusion . . . . .	18
2.2.3 Material Flow in Extrusion Processes . . . . .	19
2.2.4 Thermal Dynamics in Extrusion Processes . . . . .	20
2.2.5 Isothermal Extrusion . . . . .	21
2.3 Dynamic Model of the Extrusion Process . . . . .	22
2.3.1 Modeling the Billet . . . . .	23

2.3.2	Modeling the Container, Die, and Ram . . . . .	41
2.4	Simulating the Extrusion Process . . . . .	42
2.5	Qualitative Comparison of the Model with the Program PressForm . . . . .	51
2.6	Model Validation . . . . .	63
2.7	Process Control and Control Objectives . . . . .	64
2.8	Conclusions and Outlook . . . . .	69
<b>3</b>	<b>Nonlinear Model Predictive Control for the Isothermal Extrusion of Aluminum</b>	<b>77</b>
3.1	Introduction . . . . .	77
3.2	Deriving a Simplified Model . . . . .	78
3.2.1	Simplified Model of the Extrusion Process . . . . .	79
3.2.2	Validation of the Simplified Model . . . . .	84
3.2.3	Validation of the Model with Data from an In- dustrial Aluminum Extruder . . . . .	91
3.3	Nonlinear Model Predictive Control of Exit Temperature . . . . .	93
3.3.1	MPC: Background . . . . .	94
3.3.2	Isothermal Extrusion via Nonlinear Model Pre- dictive Control . . . . .	99
3.4	Conclusions . . . . .	111
<b>4</b>	<b>Monitoring and Fault Detection of Sensors in Alu- minum Extrusion via Statistical Methods</b>	<b>117</b>
4.1	Introduction . . . . .	117
4.2	Preliminaries . . . . .	120
4.2.1	Additive Changes in Dynamic Systems . . . . .	120
4.3	Detection of Faults in Sensors for Aluminum Extrusion . . . . .	128
4.3.1	Tuning of the Algorithm . . . . .	129
4.3.2	Simulation Results . . . . .	131
4.4	Conclusions . . . . .	134

<b>Contributions of the Thesis</b>	<b>139</b>
<b>Appendices</b>	<b>141</b>
<b>A Assumed Geometry of Profile</b>	<b>141</b>
<b>B Method of Separation of Variables for the Solution of a Fourth Order Linear Partial Differential Equation</b>	<b>143</b>
<b>C Solving the Equation for the Distribution of Pressure</b>	<b>151</b>
<b>D Smoothing Algorithm</b>	<b>155</b>
<b>E Simulation of the Extrusion Process</b>	<b>161</b>
E.1 Simulation of the Container . . . . .	161
E.2 Simulation of the Die . . . . .	165
E.3 Simulation of the Mandrel . . . . .	169
<b>F Equations of the Simplified Model for the Various Bodies Involved</b>	<b>173</b>
F.1 Equations of the Model Before the First Disc is Extruded	173
F.2 Equations of the Model Before the Second Disc is Extruded . . . . .	176
<b>G State Estimation via Extended Kalman Filtering</b>	<b>179</b>
<b>Curriculum Vitae</b>	<b>183</b>





# Chapter 1

## Introduction

### 1.1 Motivation

As competitiveness in the metal and metal forming industry grows more and more, great efforts must be paid to achieve targets on product quality. At the same time other aspects, such as productivity, safety, and maintenance issues, must be taken into consideration as well. In order to hit all these targets, processes must be run in operating regions that may be difficult to achieve or even unknown to personnel. Model-based automatic control of industrial processes offers new possibilities within this context. If a model of the process exists, the process may be investigated carefully and limitations – inherent to every system – may be identified. More effective control strategies for the process may be first designed and tested on the model, prior to implementation on the real plant. This has already been partially recognized by the metal industry and the trend during the last fifteen years has been to move in this direction.

Albeit all of the arguments previously mentioned and despite the fact that aluminum extrusion has a long tradition within the metal forming industry [1], little automatic control is used there. Processes are mostly run manually by the operators who, based on extensive practical experience, adjust the extrusion velocity so as to achieve the desired product quality. The main reason for the lack of model-based control strategies for aluminum extrusion lies in the complexity of the process. Highly nonlinear flow and heat phenomena take place in

extrusion. If these phenomena are to be described accurately, coupled partial differential equations must be used [2]. Solving these differential equations is a cumbersome task. Nevertheless, models of the extrusion process exist and are mainly used for the design of the tooling. However, these models are not suited for model-based control purposes since the solution of the equations describing them requires massive computation times. Nevertheless, there are strong incentives for the development of a model of the extrusion process upon which a control strategy may be based. One of the main problems arising in the extrusion of aluminum is that of controlling the exit temperature of the extrudate. A model-based approach to tackle this problem is desirable for the following reasons:

- Extrusion of complex profiles by hand is difficult and unreliable.
- Extrusion of new profiles requires extensive "experimenting" until the operator has acquired the know-how to extrude in such a manner as to achieve the desired product quality.
- Manual operation leads to rather conservative extrusion velocity trajectories. Model-based control strategies would help to extrude at the maximum velocity that the alloy can withstand without melting. This would lead to an increase in productivity.
- A model of the process is helpful to give the operators more insight into the process.
- Maintenance issues can be addressed more properly by means of a model by simulating the behavior of the process under abnormal situations.

## 1.2 Scope of the Thesis

This thesis started as a joint project with Alusuisse Technology and Management AG, Neuhausen, Switzerland. The development and implementation of model-based control strategies to run the process in an optimal manner, therefore achieving isothermal extrusion were

the main goals of the project. For this purpose a dynamic model of the process was required. The development of such a model of the extrusion process as well as the design of open-loop optimal control strategies to achieve isothermal extrusion for the whole product range (profile geometries) present at Alusuisse was the focus of the first phase of the project.

A model was to be derived based on first principles and on physical understanding of the process. This was due to the fact that the model had to be applicable for different types of extrusion presses and a wide range of extrudate profiles. Therefore, models suited only for a certain type of profiles or machines and that could have been based on system identification methods were not acceptable. The model had to be validated with real industrial data, prior to implementing any control strategy derived therefrom. Although the physics of the extrusion process is well known, the main challenge at deriving a first-principles dynamic model of the process that is suited for control purposes lies in achieving reasonable computation times. Computation times had to be kept low so as to facilitate the design and implementation of the model-based control strategies. By treating the metal as a highly viscous fluid and making appropriate assumptions regarding its flow, the velocities, pressure, and strain rates distributions needed for the modeling of the process are solved analytically leaving therefore only the temperature distributions to be solved numerically. This *semi-analytical* approach allows for a considerable reduction in computation times as compared to the usual Finite Elements Method for the modeling of extrusion processes.

In a second phase of the project closed-loop control strategies based on modern control techniques were to be designed and tested, the implementation of these closed-loop control strategies being dependent on practical issues such as availability of the plant. Closed-loop control was envisioned so as to exploit the valuable information provided by the measurement of the temperature of the extrudate.

In addition, uncertainties such as the uncertainty in the knowledge of the initial temperature gradient of the billet prior to loading it into the container as well as disturbances (e.g. noise) entering the system were to be at least partially counterbalanced by the use of closed-loop control.

Closed-loop control strategies rely on the measurement of the temperature of the extrudate. However, since the temperature sensors used in aluminum extrusion are prone to partial failure, the detection of faults in these devices is an important task. The problem of monitoring these sensors was to be addressed. For this purpose statistical methods were chosen. The onset of bias in these sensors is treated as a jump in the mean of a stochastic process, and the detection of these jump is tackled using an on-line cumulative sum (CUSUM) algorithm. Drifts in the temperature measurement may also be diagnosed by means of this CUSUM algorithm. This algorithm was to be tested on simulation examples. However, its eventual implementation in an industrial environment should be investigated. Within this context the algorithm had to satisfy certain conditions. Primarily it was not to pose any major difficulties with regards to computational burden.

### **1.3 Control of Aluminum Extrusion: A Review**

Earlier contributions to the problem of controlling the temperature of the extrudate for the aluminum extrusion process may be found in the literature. This section presents a review of previous work in this direction. It is by no means an exhaustive review of earlier contributions, but only a highlight of what are personally considered to be the most important contributions.

Akeret [3] presents one of the first approaches to the derivation of a model of the thermal processes that take place in the aluminum extrusion process. The potential of model-based control to achieve

isothermal extrusion is mentioned, however no steps towards deriving these strategies are presented. In subsequent investigations ([4], [5]), empirical methods are presented for the extrusion of aluminum with isothermal extrusion as the main goal. In particular, it is remarked that the problem of isothermal extrusion of aluminum should be investigated from the systems and control engineering point of view. That is, the problem should be tackled by means of a model to describe all the physical phenomena taking place in extrusion and not just by trial-and-error methods.

An important contribution to the modeling of the extrusion process is due to Lange. An analytical model is presented in [6] to determine the temperature distribution within the deformation zone of the billet. It is postulated that the heat flux generated through friction and the heat flux due to conduction between the billet and container must compensate each other at every moment in time in order to achieve isothermal extrusion. It is assumed that no heat flows from the deformation zone to the back of the billet. Particular attention is paid to the friction between the extrudate section and the die, as well as to the effect on the temperature of the extrudate section derived therefrom. Under these assumptions, ways of predetermining velocity trajectories to achieve various goals are described. However, only theoretical results are presented in this investigation.

Stüwe [7] approaches the problem of isothermal extrusion in an ad-hoc manner. Combining rules of thumb from practitioners with basic physical understanding of the process, he roughly estimates changes in the temperature of the extrudate due to the various heat phenomena that take place during the process. Proper extrusion velocity profiles to reach isothermal extrusion for certain configurations are recommended, however only simulations results are presented in this work, and it is questionable whether these results are transferable to more complex extrudate profiles as the ones presented.

The effects of extrusion ratio, extrusion speed, and speed changes on the emergent temperature of lead and high-purity aluminum have been investigated by Singer et al. [8]. Here as well, an attempt was made to correlate the observations with theoretical calculations based on considerations of heat flow during the process. The experimental data presented reasonably agrees with the theoretical calculations proposed. One drawback of this approach is the fact that all the experiments presented were conducted on a laboratory scale press and under conditions rarely found in an industrial environment. Furthermore, the extrusion ratio range studied in this investigation is limited, and nothing is mentioned as to whether the observations may be extrapolated to a wider range of extrusion ratios or more industrial-like extrusion conditions.

Grandhi and co-workers have derived a method for controlling temperatures in deformation processes, such as forging and extrusion ([9], [10]). These approaches are based on modern control theory and involve deriving state space models directly from available models of material behavior and hot deformation processes. The nonlinear finite element method (FEM) is used to model and simulate the metal-forming process. Nonlinear open-loop control strategies for producing required microstructural characteristics, uniformity of deformation, and temperature distribution within the metal are derived based on these models. Recognizing the weakness of this approach as far as computation time is concerned, reduced-order state space models for the control of metal-forming processes are derived in [11]. The objective of the design process is to maintain specified effective strain rates in certain critical elements of the workpiece. Numerical case studies with discussions are presented in these investigations. However, even with the reduced-order state space models, computation times are not feasible for any practical use. Nevertheless, the work presented by Grandhi et al. is significant from the point of view of gaining insight into the physics of the process and the systematic development of a model that is suited to

theoretically designing control strategies.

Isothermal extrusion of aluminum via iterative learning control is presented by Pandit and Buchheit [12], [13]. This control scheme improves the control of the temperature of the extrudate, from extrusion cycle to extrusion cycle, by iteratively optimizing an appropriate performance index [14]. The method employs the gradient of a functional which is derived using a Frechet differential. The model used for this approach is derived via system identification methods and, strong assumptions are made regarding process linearity, actuators behavior, and constancy of disturbances. Although theoretically this approach could be applied for a wide variety of extrusion presses and extrusion profiles, this would involve carrying out identification experiments for the whole variety of production configurations in order to identify each model. In practice this may turn into a cumbersome task as in most cases production may not be disturbed and, for practical and acceptance reasons conducting the identification experiments is nearly impossible. In addition, in certain cases this control strategy has the disadvantage of requiring too many iterations (extrusion cycles) until isothermal extrusion is attained. In industrial practice various types of profiles are extruded batchwise in the same press. To achieve isothermal extrusion the iterative learning control may require more learning cycles than are available for a certain profile.

Recently, Tibbetts et al. [15] have presented very promising results for round-to-round extrusions. This work offers the advantage of resolving the spatial temperature variations in the deformation region, not just the time-dependence of an averaged value. It is unclear, however, whether the models presented in that investigation can actually be implemented in real-time. It is also unclear whether these models can be extended to more complicated geometries.

From the above mentioned research contributions, only the work by Pandit and Buchheit ([12], [13]), has been validated with industrial



data and actually implemented in an industrial press. The remaining contributions limit themselves to either simulation examples or to laboratory results under carefully controlled experimental conditions. In addition, no model-based closed-loop control strategies for the control of exit temperature in the extrusion process have been investigated yet. This thesis is an attempt at tackling the problem of isothermal extrusion from the industrial point of view, and at adding to the state-of-the-art knowledge of systems engineering of metal-forming processes by presenting a closed-loop control strategy for the isothermal extrusion of aluminum.

## 1.4 Structure of the Thesis

This thesis is divided in three parts. Each part is written in form of a chapter dealing with one of the three main subproblems and can be read independently of the others.

For each subproblem a methodology – and not an ad-hoc procedure based on trial and error – was developed. Consequently, the solution procedure for each of these subproblems could be systematically applied in various industrial environments without major adjustments.

The first part deals with the derivation of a detailed dynamic model of the extrusion process and the design of open-loop control strategies. Of superior importance while deriving this detailed dynamic model were computation times. To achieve low computation times the partial differential equations describing the flow of the metal are solved analytically, while the equations describing the temperature distributions are solved numerically. As mentioned earlier this was possible by treating the metal as a highly viscous fluid and making appropriate assumptions regarding its flow. The accuracy of this model was suited for the purposes of designing control strategies. However, the model is by no means a substitute of other available models based on Finite Element Methods, when construction and design purposes have first priority. The model is compared to

industrial data, and open-loop optimal control strategies are then designed to achieve isothermal extrusion. The effectiveness of these control strategies is shown through simulations. These strategies have been successfully implemented on an industrial plant, covering a wide range of extrudate profiles and leading not only to guaranteed product quality but to an increase in productivity.

The second part of the thesis deals with the design of a closed-loop control strategy for the isothermal extrusion of aluminum. As the model derived in part one is still too complex to form the basis for a closed-loop control strategy, a simplified model is derived and validated with data from an industrial scale aluminum extrusion press. Further, it is shown that with the aid of this simplified dynamic model, the problem of isothermal extrusion of aluminum can be posed and solved as a model predictive control (MPC) problem, wherein constraints inherent to the system are directly taken into consideration.

In part three of the dissertation the problem of monitoring and fault detection of the aluminum extrusion process is addressed. In particular the application of a strategy to detect faults in the temperature sensors used in the process is investigated. This strategy is based on statistical methods to detect abrupt changes in systems. The onset of bias in sensors is thus modelled as an abrupt change taking place at an unknown time and the goal is to detect the change and possibly estimate the change time. The dissertation closes with an overview of its contributions.

# Bibliography

- [1] K. Laue and H. Stenger. *Extrusion: Processes, Machinery, Tooling*. American Society for Metals, Ohio, 1981.
- [2] H. S. Carslaw and J. C. Jaeger. *Conduction of Heat in Solids*. Oxford University Press, Oxford, second edition, 1959.
- [3] R. Akeret. A Numerical Analysis of Temperature Distribution in Extrusion. *J. Inst. of Metals*, vol. 95, pp.204–211, 1967.
- [4] R. Akeret. Untersuchungen über das Strangpressen unter besonderer Berücksichtigung der thermischen Vorgänge. *Aluminium*, vol. 7, pp.412–415, 1968.
- [5] R. Akeret. Das Verhalten der Strangpresse als Regelstrecke. *Metall*, vol. 8, pp.737–741, 1980.
- [6] G. Lange. Der Wärmehaushalt beim Strangpressen. *Z. für Metallkunde*, 62, pp.571–584, 1971.
- [7] H. P. Stiiwe. Einige Abschätzungen zum Strangpressen. *Metall*, vol. 12, pp.1197–1200, 1968.
- [8] A. R. E. Singer and S. H. K. Al-Samarrai. Temperature Changes Associated with Speed Variations during Extrusion. *J. Inst. of Metals*, vol. 89, pp.225–231, 1960/61.
- [9] J.C. Malas, R.D. Irwin, and R.V. Grandhi. An Innovative Strategy for Open Loop Control of Hot Deformation Processes. *J. Mat. Eng. Perf.*, vol.2, pp.703–714, 1993.
- [10] R.V. Grandhi, A. Kumar, A. Chaudhary, and J.C. Malas. State-Space Representation and Optimal Control of Non-Linear Mate-

- rial Deformation Using the Finite Element Method. *Int. J. Num. Methods in Eng.*, vol.36, pp.1967–1986, 1993.
- [11] R.V. Grandhi, R. Thiagarajan, J.C. Malas, and D. Irwin. Reduced-order State Space Models for Control of Metal-forming Processes. *J. Optimal Control Appl. Methods*, vol.16, pp.19–39, 1995.
- [12] M. Pandit and K. Buchheit. Isothermes Strangpressen von Aluminium, Teil I. *Aluminium*, vol. 4, pp.483–487, 1995.
- [13] M. Pandit and K. Buchheit. Control Schemes for a Cyclically Operating Aluminum Extruder Plant. In *Proc. 3th IEEE Conf. on Contr. Applicat.*, Glasgow, Scotland, vol.1, pp.525–531, 1994.
- [14] M. Pandit and K. Buchheit. Iterativ lernende Regelung zyklischer Produktionsprozesse. *Automatisierungstechnik*, vol. 1, pp.21–31, 1996.
- [15] B. R. Tibbetts and J. Weng. Extrusion Process: Control, Identification, and Optimization. *IEEE Trans. on Control Systems Technology*, 6, (2), pp.134–145, 1998.



## Chapter 2

# Dynamic Modeling and Optimal Control Strategies for Aluminum Extrusion

This chapter presents a new approach to the modeling of extrusion processes. Although the physics of the extrusion process is well known, the main challenge and first priority at deriving a first-principles dynamic model of the process that is suited for control purposes lies in achieving reasonable computation times. The model developed in this chapter is based on the heat conduction equation for a moving body with heat generation terms. By treating the metal as a highly viscous fluid and making appropriate assumptions regarding its flow, the velocities, pressure, strain, and strain rates distributions needed for the modeling of the process are solved analytically leaving therefore only the temperature distributions to be solved numerically. This *semi-analytical* approach allows for a considerable reduction in computation times as compared to the usual Finite Elements Method for the modeling of extrusion processes. The model is validated with data from an industrial aluminum extrusion press. The validated model is then used to design various open-loop optimal control strategies according to different performance criteria.

### 2.1 Introduction

Extrusion is one of the various methods of deformation processing of materials. Revenues from this industry in the U.S. are reported to

amount to U.S. \$ 4.5 billion, processing 1.2 billion kilograms of aluminum in 1991 [1]. Although the need for modern control techniques to guarantee product quality and increase productivity has been recognized, still virtually no automatic control is used on this process. The operator controls the process manually by adjustment of the ram speed. This adjustment of the ram speed to respond to variations in the temperature of the extrudate is mostly based on the experience of the operator. Model-based control of the process could improve performance, therefore leading to an increase in productivity and not least product quality. A precise and tractable model of the extrusion process could not only build the framework of a model-based control strategy but would give the operators more insight into the process, this perhaps leading to improvement of safety and maintenance issues as well. The development of such a model, as well as the design of optimal control strategies to guarantee product quality, are the primary goals of this chapter.

To fully describe the extrusion process, the relationships between the heat phenomena in the process and the flow of the metal have to be accounted for. These phenomena are described by partial differential equations, which in order to model the extrusion process are usually solved by means of the Finite Element Method (*FEM*). This technique has been applied to the prediction of flow patterns, strains, and temperature distributions, in order to facilitate the design and optimization of the dies and of the tooling.

In a control framework, the interest lies in the relation of temperature changes, specifically changes in the temperature of the extrudate, associated to the variations of the speed of the ram (extrusion velocity). Early approaches to this problem may be found in [2], [3], [4]. Within this context state space models as well as reduced state space models have been derived using the *FEM* method [5], [6], the goal being the design of open-loop control strategies for metal-forming processes [7]. However, solving the equations that describe the metal-forming process by means of the *FEM* requires lengthy numerical computations. Because of this fact, a *semi-analytical* approach for solving

the equations which describe the extrusion process is proposed in this chapter. This approach consists of treating the metal as a highly viscous Newtonian fluid. Appropriate assumptions regarding its flow are made, so that the velocities, pressure, strain, and strain rates distributions needed for the modeling of the process are solved analytically. Only the temperature distributions are thus solved numerically, this allowing for a considerable reduction in computation times.

This chapter is divided as follows: in section 2.2 extrusion processes are presented briefly. Although the focus of this investigation is the direct extrusion process, the different types of extrusion processes are reviewed for the sake of clarity and completeness. For a more thorough and detailed description of extrusion processes the interested reader is referred to the work of Laue et al. [8]. In section 2.3 a model of the direct extrusion process is developed based on the heat conduction equation for a moving body with heat generation terms. This equation is solved numerically using finite differences. The velocity distributions, which are required for the solution of this equation, are provided by solving analytically a modified momentum equation. The process is simulated in section 2.4. In sections 2.5 and 2.6 the model is compared to *PressForm*, an established program for the simulation of metal forming processes, and validated with data from an industrial aluminum extrusion press. In section 2.7 performance criteria are formulated, taking into account practical performance measures of product quality as well as physical constraints of the system. Extrusion velocity trajectories are then designed to minimize these target functions. The chapter closes with some concluding remarks in section 2.8.

## 2.2 Extrusion Processes

Extrusion is a deformation process used to produce long, straight, semi-finished metal products such as bars, solid and hollow sections, tubes, wires, and strips. The principle behind this process is simple: under a high load, a billet is squeezed from a closed container through



a die to give a reduction in size. Cross-sections of varying complexity can be extruded, depending on the material and the dies used. The conditions at which this process takes place vary depending on the alloy and the extrusion method used. Thus, extrusion can be carried out at high temperatures as well as at room temperatures. Four main characteristic differences exist among the various methods of extrusion and the processes used:

- The movement of the extrusion relative to the ram – direct or indirect processes.
- The position of the press axis – horizontal or vertical presses.
- Type of drive – hydraulic (water or oil) or mechanical presses.
- Method of load application – conventional or hydrostatic extrusion.

Different alloys present different characteristics while being extruded. Thus, it is impossible to use the same method of extrusion for all materials. The flow characteristics of the alloy under consideration play a decisive role in choosing the method to be employed, so as to obtain optimum quality and productivity. The most common methods are:

- Direct or forward extrusion.
- Indirect or backward extrusion (using a hollow ram).

### **2.2.1 Direct Extrusion**

The direct process is the most widely used method for extrusion. Figure 2.1 illustrates the main bodies involved in the process, whose main characteristics are described next. The load is transmitted to the billet via a hydraulically or mechanically driven ram through an intermediate dummy block.

After the billet is upset to fill the container, extrusion begins to produce the extrudate. Heat is generated by the friction of the surface

of the billet against the container, by the deformation of the billet, as well as by the shearing at the dead metal zone. Part of this heat is transported towards the die as the material flows through it (convective heat transfer). Another portion dissipates due to conduction through the tooling (container, and ram) as well as through the billet and the extrudate. Direct extrusion can be performed with or without a lubricant, and in the latter case with or without a shell. Some materials have a strong tendency to stick to the container wall so that nonuniform flow occurs. The central region of the billet first flows towards the die and the peripheral region is extruded only towards the end of the process. The separation of the pure material, forming the inside of the billet, from the outside layer, which usually has a rough cast surface and is coated with oxide and impurities, can be improved still further by leaving this layer in the container. This is known as extrusion with a shell and is used mainly with heavy metal alloys to suppress the formation of pipe in the rear of the extrusion. Aluminum alloys are preferably extruded using a dummy block with a very close fit in the container. Consequently, hardly any shell is sheared off. The surface is not drawn into the billet because, in contrast to heavy metals, aluminum sticks to the container wall and impurities on the surface are held back. There is also a small temperature difference between the billet and the container, and the difference in velocity between the center of the billet and the periphery is much less than in the case of heavy metals. As the dummy block advances, impurities on the billet surface and the peripheral segregation are sheared off

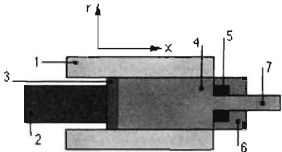


Figure 2.1: *Direct Extrusion: 1 Container, 2 Ram, 3 Dummy Block, 4 Billet, 5 Die, 6 Die Holder, 7 Extrudate.*

and collected in the discard, which must be large enough to meet the quality desired. In summary, the complete direct extrusion process may be viewed as consisting mainly of the following steps:

- Loading the billet and dummy block into the press.
- Extruding the billet.
- Decompression of the press and opening the container to expose the discard and the dummy block (stripping).
- Shearing the discard.
- Returning the shear, container and ram to the loading position.

## 2.2.2 Indirect Extrusion

In indirect extrusion the die at the front end of the hollow ram moves relative to the container but there is no relative displacement between the billet and the container. The main feature of this process is the absence of friction between the billet and the surface of the container. The load required for extrusion is therefore less than that of the direct extrusion process. Figure 2.2 shows this process.

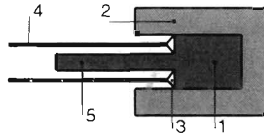


Figure 2.2: *Indirect Extrusion: 1 Billet, 2 Container, 3 Die, 4 Ram, 5 Extrudate.*

The advantages of indirect extrusion are partly related to the lower load needed and partly to the more uniform flow pattern developed because of the absence of relative motion between the billet and the container. Some other advantages of this process are:

- No heat is produced by friction between the billet and the walls of the container, and thus no temperature increase occurs at the

billet surface towards the end of extrusion. The surfaces and edges tend to crack less in this type of process and significantly higher extrusion speeds can be used.

- The life of the tooling is longer, because of the almost total absence of friction.

The disadvantage of indirect extrusion is that impurities or defects on the billet surface affect the surface of the extrudate profile and are not automatically retained as a shell or discard in the container as in the direct extrusion process. In addition, the cross-sectional area of the extrusion is limited by the size of the hollow ram. The individual steps characteristic of the working cycle in the indirect extrusion process can be summarized as:

- Loading of the die holder and die.
- Loading of the billet.
- Extrusion.
- Separation of the die holder with the die and the discard from the extrudate.

### 2.2.3 Material Flow in Extrusion Processes

Extrusion is a discontinuous process. A billet is not loaded until the one preceding it has been completely extruded. Temperature variations in the billet, due to friction between the container and the billet as well as heat transfer between the ram and the billet arise while it is being extruded. These temperature variations cause a nonsteady state flow of material. Changes in the extrusion load throughout the cycle, as well as temperature differences that lead to variations in the material properties over the cross-section and length of the extrudate are the results of a nonuniform flow from the front of the billet to its end. The flow characteristics of many metals during extrusion processes have been studied before. Dürschnabel [9] presents a detailed literature survey of studies carried out on the material flow in non-ferrous metal extrusion. The method of *Visioplasticity* [10], has been

suggested for analyzing the flow patterns of any metal or nonmetal material. This method consists of first defining a surface of symmetry along the direction in which the material is going to flow. A grid of orthogonal lines on that surface is then drawn. These lines deform to streamlines while the material flows and lines perpendicular to them are called potential lines. From the deformation of the grid one can draw conclusions about the deformation state in the flow zone. Despite the differences in material and extrusion conditions at which the different investigations have been carried out, all the flow patterns are alike. They present a dead zone at the corner between the container and the die and there is almost no relative velocity at the point where the ram touches the billet.

#### **2.2.4 Thermal Dynamics in Extrusion Processes**

The product quality of the extrudate is in the main determined by the thermal processes taking place in the extrusion process. Temperature is one of the most important parameters in extrusion. As the temperature within the metal increases, the flow stress is reduced and deformation is easier. However, at the same time, the maximum speed at which the metal may be extruded is reduced, since localized temperature peaks can lead to the melting of the metal. This leads to a torn surface. Complex thermal processes commence once the hot billet is loaded into the container and extrusion begins. They mainly consist of the following:

- Production of heat by deformation.
- Production of heat by friction between the billet and container.
- Convection of heat as the billet moves towards the die.
- Conduction of heat within the billet and the tooling.
- Heat transfer from the deformation zone to the billet, to the container, and to the die.
- Heat transfer between the billet and container and ram, respectively.

Decisive in extrusion is the temperature of the extrudate section, which depends on all of the above mentioned phenomena. The temperature of the extrudate section increases if the heat produced by deformation and friction exceeds the heat losses, and decreases if the reverse is true. Heat conduction requires a certain time, depending on the alloy and the extrusion conditions. Thus, heat production predominates above a certain ram speed. This explains the dependence of the temperature profile along the length of the extrudate on the ram speed. If this temperature is to be controlled a thorough understanding of the thermal processes occurring in extrusion is needed.

### **2.2.5 Isothermal Extrusion**

The interest of extruding at a constant exit temperature arises from the fact that, by doing so, a uniform product quality can be guaranteed. The goal is to achieve the maximum extrusion speed that the alloy can withstand without melting over the complete cycle, while maintaining the temperature of the extrudate section at a particular setpoint. In practice isothermal extrusion may be performed in one of the following ways:

- Adjusting the extrusion speed while extruding, based on measurements of the exit temperature.
- Reduction of the extrusion speed according to a preset speed program.
- Taper heating the billet. This method involves forcing an axial temperature gradient along the length of the billet, the cooler end being at the back of the billet. In this manner, the additional heat produced by friction/shear at the container/billet interface is compensated for [11].

From the theoretical point of view, taper heating is the best solution from all the methods mentioned hitherto. Extrusion could then be performed at the maximum possible speed throughout the extrusion

length, enabling to exploit the full power of the press. Some difficulties, however, are intrinsic to this method. Achieving a controlled temperature gradient in extruders with gas furnaces is a cumbersome task. As for extruders with induction furnaces, producing the necessary complicated temperature profiles quickly and accurately is not feasible. Taper heating is usually used in combination with one of the other methods.

## 2.3 Dynamic Model of the Extrusion Process

The complex phenomena that take place in extrusion include nonsteady-state flow, nonuniform distribution of strains, strain rates, and temperatures in the deforming metal. The Finite Element Method (*FEM*) is the method most widely used to model and simulate metal forming processes. The theory underlying this method has been described by several authors [12], [13]. The *FEM* is used to predict flow patterns, strain, and temperature distributions, in order to facilitate the design and optimization of the dies and the tooling. However, the solution of the equations that describe the metal-forming process by means of the *FEM* requires lengthy numerical computations. A *semi-analytical* approach for solving the equations which describe the extrusion process is proposed in this section. A dynamic model for the direct extrusion process is developed based on the heat conduction equation for a moving body with heat generation terms. This equation is solved numerically using finite differences. The metal is considered to be a highly viscous Newtonian fluid. Thus, the velocity, pressure, strain, and strain rate distributions required for the solution of the equations of motion and continuity are provided by solving these equations analytically. This *semi-analytical* approach allows for reasonable computation time as compared to the *FEM*.

### 2.3.1 Modeling the Billet

#### Heat Balance

To model the billet it is assumed that the metal flows. If a fixed coordinate system is chosen, the equation to be solved is the heat conduction equation for a moving body. Heat source terms are added to the equation to account for the heat which evolves due to friction and to deformation of the metal. Axial symmetry is assumed and cylindrical coordinates are chosen. The complete derivation of this equation can be found in [14]. The equation is the following:

$$\frac{\partial T}{\partial t} = \alpha \left( \frac{\partial^2 T}{\partial x^2} + \frac{\partial^2 T}{\partial r^2} + \frac{1}{r} \frac{\partial T}{\partial r} \right) - v_x \frac{\partial T}{\partial x} - v_r \frac{\partial T}{\partial r} + \frac{q(x, r, t)}{\rho c_p}, \quad (2.1)$$

where:

- $T$  = temperature,
- $\alpha = \frac{k}{\rho c_p}$  thermal diffusivity,
- $k$  = thermal conductivity,
- $\rho$  = density,
- $c_p$  = specific heat,
- $r$  = radial coordinate,
- $x$  = axial coordinate,
- $q$  = heat source term,
- $v_x$  = axial velocity component,
- $v_r$  = radial velocity component.

This equation is written more compactly as:

$$\frac{DT}{Dt} = \alpha \nabla^2 T + \frac{1}{\rho c_p} q(\mathbf{p}, t) \quad (2.2)$$



which is strictly applicable for constant  $\rho c_p$ . Here,  $\mathbf{p}$  is a position vector,  $\frac{D}{Dt}$  stands for the substantial (or total) derivative defined by

$$\frac{D}{Dt} \equiv \frac{\partial}{\partial t} + v_x \frac{\partial}{\partial x} + v_r \frac{\partial}{\partial r}$$

and the operator  $\nabla^2$  is defined for cylindrical coordinates as follows:

$$\nabla^2 \equiv \frac{\partial^2}{\partial x^2} + \frac{\partial^2}{\partial r^2} + \frac{1}{r} \frac{\partial}{\partial r}. \quad (2.3)$$

All the material properties like density, heat capacity, thermal conductivity, and therefore thermal diffusivity are considered to be independent of the temperature and of the space. Since the thermal conductivity is taken as being independent of the space coordinates, the body is said to be *isotropic*. For the solution of equation (2.1), a velocity distribution  $\mathbf{v}(t, \mathbf{p})$  with an initial condition  $T(t_0, \mathbf{p}) = T_0(\mathbf{p})$  and a set of boundary conditions must be defined.

### Temperature Boundary Conditions

Two materials having different thermal conductivities,  $k_1$  and  $k_2$ , and being in imperfect contact are considered here. These materials share a common boundary as shown in Figure 2.3. The temperature profile through the solids experiences a sudden drop across the interface between the two materials. This temperature drop can be explained as follows: the actual metal-to-metal contact takes place at a limited number of spots and the void between them is filled with air, which is the surrounding fluid. Since the thermal conductivity of air is much smaller than that of the metal, a steep temperature drop occurs across the gap. The boundary condition for such an interface can be developed by formulating a heat balance:

$$\begin{aligned} (\text{Conduction through solid 1}) &= \\ (\text{Heat transfer across gap}) &= (\text{Conduction through solid 2}) \end{aligned}$$

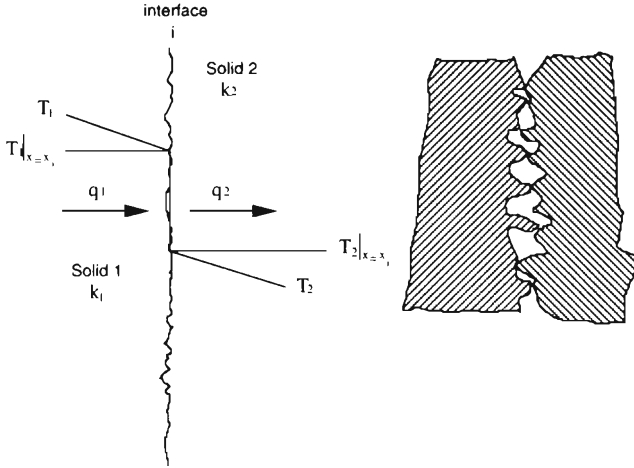


Figure 2.3: *Interface Boundary Condition.*

$$-k_1 \left. \frac{\partial T_1}{\partial x} \right|_i = h_c (T_1 - T_2)_i = -k_2 \left. \frac{\partial T_2}{\partial x} \right|_i. \quad (2.4)$$

The subscript  $i$  denotes the interface and  $h_c$  in  $\left(\frac{W}{m^2 \cdot ^\circ C}\right)$  is the *contact conductance*. The surface of the billet is in contact with the surface of the container so that for this surface the boundary conditions can be postulated as described above. Such a boundary condition is generally called an *interface boundary condition* [14]. The frontal surfaces of the cylinder may be treated similarly. One of these surfaces is in contact with the ram, the other with the die. This is taken into account by using the appropriate contact conductances corresponding to the different materials. Since rotational symmetry to the central axis of the billet is assumed, another boundary condition must be introduced for the points lying on the axis of symmetry. For these points the following boundary condition is formulated:

$$\left. \frac{\partial T}{\partial r} \right|_{r=0} = 0. \quad (2.5)$$

The following is an overview of all temperature boundary conditions:

$$\left. \frac{\partial T}{\partial x} \right|_{x=L} = -\frac{h_c}{k} (T_{billet} - T_{dir}) \quad (2.6)$$

$$\left. \frac{\partial T}{\partial r} \right|_{r=R} = -\frac{h_c}{k} (T_{billet} - T_{container}) \quad (2.7)$$

$$\left. \frac{\partial T}{\partial x} \right|_{x=0} = -\frac{h_c}{k} (T_{billet} - T_{ram}) \quad (2.8)$$

$$\left. \frac{\partial T}{\partial r} \right|_{r=0} = 0 \quad (\text{symmetry}), \quad (2.9)$$

where:

$R$  = radius of the billet,

$L$  = length of the billet,

$h_c$  = contact conductance,

$k$  = thermal conductivity.

## Momentum and Mass Balance

For the solution of equation (2.1) the velocity distribution is still required. This is done by taking into account the equations of continuity and motion. The general equation of continuity for cylindrical coordinates is the following [15]:

$$\frac{\partial \rho}{\partial t} + \frac{1}{r} \frac{\partial (\rho r v_r)}{\partial r} + \frac{1}{r} \frac{\partial (\rho v_\phi)}{\partial \phi} + \frac{\partial (\rho v_x)}{\partial x} = 0.$$

It may be written more conveniently in vector notation:

$$\frac{\partial \rho}{\partial t} = -(\nabla \cdot \rho \mathbf{v}). \quad (2.10)$$

This equation may be derived by writing a mass balance over a stationary differential volume element  $d\mathbf{V}$ . The equation expresses how the density of a fluid varies with time at a fixed point when the mass

velocity vector  $\rho \mathbf{v}$  changes. In the last equation,  $(\nabla \cdot \rho \mathbf{v})$  is the *divergence* of  $\rho \mathbf{v}$ . Its significance is the net rate of mass efflux per unit volume. The equation of motion can be similarly derived by writing a momentum balance over a stationary differential volume element  $d\mathbf{V}$ . Expressed in cylindrical coordinates it takes the general form [15]:

$$\begin{aligned} \text{r-component} \quad \rho \left( \frac{\partial v_r}{\partial t} + v_r \frac{\partial v_r}{\partial r} + \frac{v_\phi}{r} \frac{\partial v_r}{\partial \phi} - \frac{v_\phi^2}{r} + v_x \frac{\partial v_r}{\partial x} \right) = \\ - \frac{\partial p}{\partial r} - \left( \frac{1}{r} \frac{\partial (r \tau_{rr})}{\partial r} + \frac{1}{r} \frac{\partial \tau_{r\phi}}{\partial \phi} - \frac{\tau_{\phi\phi}}{r} + \frac{\partial \tau_{rx}}{\partial x} \right) + \rho g_r, \end{aligned} \quad (2.11)$$

$$\begin{aligned} \text{x-component} \quad \rho \left( \frac{\partial v_x}{\partial t} + v_r \frac{\partial v_x}{\partial r} + \frac{v_\phi}{r} \frac{\partial v_x}{\partial \phi} + v_x \frac{\partial v_x}{\partial x} \right) = \\ - \frac{\partial p}{\partial x} - \left( \frac{1}{r} \frac{\partial (r \tau_{rx})}{\partial r} + \frac{1}{r} \frac{\partial \tau_{r\phi}}{\partial \phi} + \frac{\partial \tau_{xx}}{\partial x} \right) + \rho g_x, \end{aligned} \quad (2.12)$$

$$\begin{aligned} \phi\text{-component} \quad \rho \left( \frac{\partial v_\phi}{\partial t} + v_r \frac{\partial v_\phi}{\partial r} + \frac{v_\phi}{r} \frac{\partial v_\phi}{\partial \phi} + \frac{v_r v_\phi}{r} + v_x \frac{\partial v_\phi}{\partial x} \right) = \\ - \frac{1}{r} \frac{\partial p}{\partial \phi} - \left( \frac{1}{r^2} \frac{\partial (r^2 \tau_{r\phi})}{\partial r} + \frac{1}{r} \frac{\partial \tau_{\phi\phi}}{\partial \phi} + \frac{\partial \tau_{\phi x}}{\partial x} \right) + \rho g_\phi. \end{aligned} \quad (2.13)$$

Written in vector notation, this is:

$$\frac{\partial}{\partial t} \rho \mathbf{v} = -[\nabla \cdot \rho \mathbf{v} \mathbf{v}] - \nabla p - [\nabla \cdot \tau] + \rho \mathbf{g}. \quad (2.14)$$

The terms  $[\nabla \cdot \rho \mathbf{v} \mathbf{v}]$  and  $[\nabla \cdot \tau]$  are not simple divergences due to the tensorial nature of  $\rho \mathbf{v} \mathbf{v}$  and  $\tau$ . The quantity  $[\nabla \cdot \rho \mathbf{v} \mathbf{v}]$  represents the rate of momentum loss (a vector) by fluid flow,  $-\nabla p$  the net pressure force,  $[\nabla \cdot \tau]$  the rate of momentum gain by viscous force, and  $\rho \mathbf{g}$  the gravitational force per unit volume. For the solution of the equations of continuity (2.10) and motion (2.14), a number of

assumptions are made which are stated next. The metal is treated as a highly viscous, noncompressible Newtonian fluid with density  $\rho$ , and viscosity  $\mu$  assumed to be independent of time, position, and temperature. With these assumptions the equation of motion can be expressed in terms of velocity gradients as follows:

$$\begin{aligned} \text{r-component} \quad \rho \left( \frac{\partial v_r}{\partial t} + v_r \frac{\partial v_r}{\partial r} + \frac{v_\phi}{r} \frac{\partial v_r}{\partial \phi} - \frac{v_\phi^2}{r} + v_x \frac{\partial v_r}{\partial x} \right) = \\ - \frac{\partial p}{\partial r} + \mu \left[ \frac{\partial}{\partial r} \left( \frac{1}{r} \frac{\partial}{\partial r} (r v_r) \right) + \frac{1}{r^2} \frac{\partial^2 v_r}{\partial \phi^2} - \frac{2}{r^2} \frac{\partial v_\phi}{\partial \phi} + \frac{\partial^2 v_r}{\partial x^2} \right] + \rho g_r, \end{aligned} \quad (2.15)$$

$$\begin{aligned} \text{x-component} \quad \rho \left( \frac{\partial v_x}{\partial t} + v_r \frac{\partial v_x}{\partial r} + \frac{v_\phi}{r} \frac{\partial v_x}{\partial \phi} + v_x \frac{\partial v_x}{\partial x} \right) = \\ - \frac{\partial p}{\partial x} + \mu \left[ \frac{1}{r} \frac{\partial}{\partial r} \left( r \frac{\partial v_x}{\partial r} \right) + \frac{1}{r^2} \frac{\partial^2 v_x}{\partial \phi^2} + \frac{\partial^2 v_x}{\partial x^2} \right] + \rho g_x, \end{aligned} \quad (2.16)$$

$$\begin{aligned} \phi\text{-component} \quad \rho \left( \frac{\partial v_\phi}{\partial t} + v_r \frac{\partial v_\phi}{\partial r} + \frac{v_\phi}{r} \frac{\partial v_\phi}{\partial \phi} + \frac{v_r v_\phi}{r} + v_x \frac{\partial v_\phi}{\partial x} \right) = \\ - \frac{1}{r} \frac{\partial p}{\partial \phi} + \mu \left[ \frac{\partial}{\partial r} \left( \frac{1}{r} \frac{\partial}{\partial r} (r v_\phi) \right) + \frac{1}{r^2} \frac{\partial^2 v_\phi}{\partial \phi^2} + \frac{2}{r^2} \frac{\partial v_r}{\partial \phi} + \frac{\partial^2 v_\phi}{\partial x^2} \right] + \rho g_\phi \end{aligned} \quad (2.17)$$

Additionally, gravitational forces are neglected and rotational symmetry is assumed. The latter implies that  $\frac{\partial}{\partial \phi} = 0$  and  $v_\phi = 0$ . Thus, terms related to  $v_\phi$ , and to variations with respect to  $\phi$  in the equation of motion vanish. With this, the equation of motion is further reduced to:

$$\begin{aligned} \text{r-component} \quad \rho \left( \frac{\partial v_r}{\partial t} + v_r \frac{\partial v_r}{\partial r} + v_x \frac{\partial v_r}{\partial x} \right) = \\ - \frac{\partial p}{\partial r} + \mu \left[ \frac{\partial}{\partial r} \left( \frac{1}{r} \frac{\partial}{\partial r} (r v_r) \right) + \frac{\partial^2 v_r}{\partial x^2} \right] \end{aligned} \quad (2.18)$$

$$\begin{aligned}
\text{x-component} \quad & \rho \left( \frac{\partial v_x}{\partial t} + v_r \frac{\partial v_x}{\partial r} + v_x \frac{\partial v_x}{\partial x} \right) = \\
& -\frac{\partial p}{\partial x} + \mu \left[ \frac{1}{r} \frac{\partial}{\partial r} \left( r \frac{\partial v_x}{\partial r} \right) + \frac{\partial^2 v_x}{\partial x^2} \right]. \quad (2.19)
\end{aligned}$$

Considering the high loads, which translate into high pressures within the billet, as well as the high temperatures at which the extrusion is carried out, it may be assumed that the pressure forces are in equilibrium with the viscous forces and that the mass forces may be neglected. Therefore, the terms on the left hand side of the last two equations are assumed to be negligible when compared to the third term on the right hand side related to the viscosity. Taking into account all the assumptions previously mentioned, the continuity equation and the equation of motion take the following form:

$$\text{continuity} \quad 0 = \frac{1}{r} \frac{\partial (r v_r)}{\partial r} + \frac{\partial (v_x)}{\partial x} \quad (2.20)$$

$$\text{motion: r-component} \quad \frac{\partial p}{\partial r} = \mu \left[ \frac{\partial}{\partial r} \left( \frac{1}{r} \frac{\partial (r v_r)}{\partial r} \right) + \frac{\partial^2 v_r}{\partial x^2} \right] \quad (2.21)$$

$$\text{motion: x-component} \quad \frac{\partial p}{\partial x} = \mu \left[ \frac{1}{r} \frac{\partial}{\partial r} \left( r \frac{\partial v_x}{\partial r} \right) + \frac{\partial^2 v_x}{\partial x^2} \right] \quad (2.22)$$

Finally, elastic deformations within the billet and the deformation of the metal within the die are also neglected. Plug flow is assumed for the metal at the entrance of the die, and the flow of the metal within it is assumed to obey the *Hagen-Poiseuille* law. The geometry of the profile is assumed to be a ring with equivalent area and perimeter to the particular profile in question (see Appendix A for a detailed explanation and derivation). All of the aforementioned assumptions are restated and summarized in Table 2.1 to give a clear overview of

them<sup>1</sup> before continuing with the detailed discussion of the solution of the equations.

### Assumptions for solving equations of motion and continuity:

- Rotational symmetry is assumed (this means:  $\frac{\partial}{\partial \phi} = 0$ ;  $v_\phi = 0$ ,  $\phi$  is the polar angle in cylindrical coordinates).
- Metal is considered to be a Newtonian fluid.
- Mass forces are negligible:  

$$\rho \left( \frac{\partial v_r}{\partial t} + v_r \frac{\partial v_r}{\partial r} + v_x \frac{\partial v_x}{\partial x} \right) \ll \mu \left[ \frac{1}{r} \frac{\partial}{\partial r} \left( r \frac{\partial v_r}{\partial r} \right) + \frac{\partial^2 v_x}{\partial x^2} \right]$$

$$\rho \left( \frac{\partial v_x}{\partial t} + v_r \frac{\partial v_x}{\partial r} + v_x \frac{\partial v_x}{\partial x} \right) \ll \mu \left[ \frac{\partial}{\partial r} \left( \frac{1}{r} \frac{\partial}{\partial r} (r v_r) \right) + \frac{\partial^2 v_x}{\partial x^2} \right].$$
- Negligible gravitational forces.
- Elastic deformations within the billet are neglected.
- Plug flow at the entrance of the die is assumed.
- Deformation within the die is neglected.
- *Hagen-Poiseuille* law is valid for flow within the die.
- $\rho, \mu \approx \text{constant}$ .
- Reduction of profile geometry to a ring with equivalent area and perimeter.

Table 2.1: *Assumptions for solving equations of motion and continuity.*

### Velocity Boundary Conditions

The following boundary conditions are imposed on the system:

$$v_x|_{x=0} = v_{ram}; \forall r \quad (2.23)$$

$$v_x|_{r=R} = v_x(x, R); \forall x \quad (2.24)$$

$$v_x|_{x=L} = v(L, r) \quad (2.25)$$

$$v_r|_{r=0} = 0; \forall x \quad (\text{rotational symmetry}) \quad (2.26)$$

$$v_r|_{x=0} = 0; \forall r \quad (2.27)$$

$$v_r|_{r=R} = 0; \forall x \quad (2.28)$$

$$v_r|_{x=L} = 0; \forall r. \quad (2.29)$$

---

<sup>1</sup>These assumptions, with the exception of Newtonian fluid, are supported through experimental results [9], [16].

For steady flows with two nonvanishing velocity components and with constant  $\rho$  and  $\mu$ , the solution of the differential equations (2.20) – (2.22) may be simplified by introducing the *stream function*  $\Psi$ . Lines of  $\Psi = \text{constant}$  are called *streamlines*. In a steady-state flow, these are the curves actually traced out by the particles of the fluid. The velocity components are now expressed as derivatives of  $\Psi$  so that the equation of continuity is automatically satisfied. The two nonvanishing components of the equation of motion are then combined to eliminate the terms containing the components of  $p$ . The procedure is shown below:

$$v_r = -\frac{1}{r} \frac{\partial \Psi}{\partial x}, \quad v_x = \frac{1}{r} \frac{\partial \Psi}{\partial r}. \quad (2.30)$$

From equations (2.21) and (2.22) the following relationships may be derived:

$$\frac{\partial}{\partial x} \left( \frac{\partial p}{\partial r} \right) = \mu \frac{\partial}{\partial x} \left[ \frac{\partial}{\partial r} \left( \frac{1}{r} \frac{\partial (r v_r)}{\partial r} \right) + \frac{\partial^2 v_r}{\partial x^2} \right] \quad (2.31)$$

$$\frac{\partial}{\partial r} \left( \frac{\partial p}{\partial x} \right) = \mu \frac{\partial}{\partial r} \left[ \frac{1}{r} \frac{\partial}{\partial r} \left( r \frac{\partial v_x}{\partial r} \right) + \frac{\partial^2 v_x}{\partial x^2} \right] \quad (2.32)$$

$$\frac{\partial^2 p}{\partial x \partial r} = \frac{\partial^2 p}{\partial r \partial x}. \quad (2.33)$$

In the last equations, the terms for the derivatives of the velocities with respect to the radial and axial coordinates may be substituted for their corresponding terms as functions of  $\Psi$ , which are derived from (2.30), thus yielding the following fourth order partial differential equation:

$$\frac{\partial^4 \Psi}{\partial r^4} + 2 \frac{\partial^4 \Psi}{\partial r^2 \partial x^2} + \frac{\partial^4 \Psi}{\partial x^4} - \frac{2}{r} \frac{\partial^3 \Psi}{\partial r \partial x^2} - \frac{2}{r} \frac{\partial^3 \Psi}{\partial r^3} + \frac{3}{r^2} \frac{\partial^2 \Psi}{\partial r^2} - \frac{3}{r^3} \frac{\partial \Psi}{\partial r} = 0. \quad (2.34)$$



The velocity boundary conditions (2.23) – (2.29) are still valid. However, another boundary condition is introduced to account for the symmetry to the central axis. Expressed in terms of  $\Psi$  this yields:

$$\Psi(r = 0, x) = \text{constant}, \forall x. \quad (2.35)$$

Equation (2.34) may be solved by the method of separation of variables. The solution is presented here; the complete derivation may be found in Appendix B. First the stream function  $\Psi$  is expressed as a product of two functions. One of these functions is dependent on the radial coordinate only, the other only on the axial coordinate:

$$\Psi(r, x) = \Upsilon(r)\Xi(x). \quad (2.36)$$

Taking into account equations (2.30) and (2.36), the velocity boundary conditions may be expressed also in terms of the two functions  $\Upsilon(r)$  and  $\Xi(x)$ :

$$v_x|_{x=0} = \frac{1}{r} \Upsilon'(r) \Xi(x) \Big|_{x=0} = v_{ram} \implies \frac{1}{r} \Xi(x) \Big|_{x=0} = 0 \quad (2.37)$$

$$v_x|_{r=R} = \frac{1}{r} \Upsilon'(r) \Xi(x) \Big|_{r=R} = v_r(x, R) \quad (2.38)$$

$$v_x|_{x=L} = \frac{1}{r} \Upsilon'(r) \Xi(x) \Big|_{x=L} = v_r(L, r) \quad (2.39)$$

$$v_r|_{r=0} = \frac{1}{r} \Upsilon(r) \Xi'(x) = 0; \forall x \implies \frac{1}{r} \Upsilon(r) \Big|_{r=0} = 0 \quad (2.40)$$

$$v_r|_{x=0} = \frac{1}{r} \Upsilon(r) \Xi'(x) = 0; \forall r \implies \frac{1}{r} \Xi'(x) \Big|_{x=0} = 0 \quad (2.41)$$

$$v_r|_{r=R} = \frac{1}{r} \Upsilon(r) \Xi'(x) = 0; \forall x \implies \frac{1}{r} \Upsilon(r) \Big|_{r=R} = 0 \quad (2.42)$$

$$v_r|_{x=L} = \frac{1}{r} \Upsilon(r) \Xi'(x) = 0; \forall r \implies \frac{1}{r} \Xi'(x) \Big|_{x=L} = 0. \quad (2.43)$$

From equation (2.40) it can be concluded that the stream function  $\Psi(r, x)$  vanishes at the axis of symmetry. Equation (2.35) is therefore fulfilled. The introduction of some identities leads to the *Bessel* differential equation of zero order [17]:

$$f''(r) + \frac{1}{r} f'(r) + \omega^2 f(r) = 0. \quad (2.44)$$

Solutions of equation (2.44) are called the *Bessel* functions. In this case, since the *Bessel* differential equation is of zero order, its solutions are called *Bessel functions* of zero order. The solution of equation (2.34) by the method of separation of variables is bound to the eigenvalues of  $\Upsilon$  satisfying certain conditions (see Appendix B). All of the boundary conditions may eventually not be satisfied simultaneously. In the approach taken here, the following boundary condition was dropped:

$$v_x|_{r=R} = \frac{1}{r} \Upsilon'(r) \Xi(x) \Big|_{r=R} = v_x(x, R) - v_{ram}.$$

This implies that the axial velocity component at the outer surface of the cylinder will result from the solution and may not be predetermined. A detailed derivation of equation (2.44), including a more extensive explanation of the aforementioned characteristics of the solutions and its implications for the problem, can be found in Appendix B.

### Velocity Distribution at the Entrance of the Die

As mentioned before, plug flow is assumed for the metal flowing at the entrance of the die. Additionally, it is assumed that the metal flowing into the die obeys the *Hagen-Poiseuille* law. Such an assumption implies that the flow is laminar, incompressible, steady-state, and Newtonian. Furthermore it is assumed that the metal behaves as a

continuum, that there is no slip at the wall, and that end effects may be neglected. The latter conditions can be expressed mathematically in the following manner:

$$\begin{aligned}
 \frac{\partial v_x}{\partial x} &= 0, \\
 \frac{\partial p}{\partial r} &= 0, \\
 \rho &= \text{constant}, \\
 v_r &= 0, \\
 v_x|_{r=r_{die}} &= 0 \\
 Re &< 2100 \quad (\text{Re} = \text{Reynolds Number}).
 \end{aligned}$$

Under these last assumptions, the axial velocity is described as follows [18]:

$$v_x(r) = A \frac{r^2}{4} + B \ln(r) + C. \quad (2.45)$$

Let  $d$  be the diameter of the die's channel. The metal is treated as a Newtonian fluid. Thus the following is valid:

$$\begin{aligned}
 v_{exit} A_{die} &= v_{ram} A_0 \\
 \int_0^{\frac{d}{2}} v_x(r) r \, dr &= \frac{1}{2} v_{ram} R^2.
 \end{aligned} \quad (2.46)$$

Here,  $A_0$ ,  $A_{die}$ ,  $v_{ram}$ ,  $v_{exit}$ , and  $R$  stand for the cross-sectional area of the billet, cross-sectional area of the die's channel, velocity of the ram, velocity at the entrance of the die, and radius of the billet, respectively. From equations (2.45) and (2.46) the following expression for the axial velocity distribution within the die can be derived:

$$v_x(\varrho) = \frac{2}{\varrho_1^2} \left[ 1 - \frac{\varrho^2}{\varrho_1^2} \right] v_{ram}, \quad (2.47)$$

where  $\varrho$  and  $\varrho_1$  are normed variables defined as follows:

$$\varrho = \frac{r}{R}, \quad \varrho_1 = \frac{d}{2R}.$$

If the extruded profile in consideration is hollow (ring with inner diameter  $d_1$  and outer diameter  $d_2$ ), the following boundary conditions are valid:

$$v_x \left( \varrho_1 = \frac{d_1}{2R} \right) = 0, \quad v_x \left( \varrho_2 = \frac{d_2}{2R} \right) = 0. \quad (2.48)$$

In this case the condition of continuity is:

$$\int_{\varrho_1}^{\varrho_2} v_x(\varrho) \varrho d\varrho = \frac{1}{2} v_{ram} \quad (2.49)$$

and the following axial velocity distribution results:

$$v_x(\varrho) = C (A \varrho^2 + B \ln(\varrho) + 1) \quad (2.50)$$

where:

$$A = \frac{\ln(\varrho_2) - \ln(\varrho_1)}{\ln(\varrho_1)\varrho_2^2 - \ln(\varrho_2)\varrho_1^2},$$

$$B = \frac{\varrho_1^2 - \varrho_2^2}{\ln(\varrho_1)\varrho_2^2 - \ln(\varrho_2)\varrho_1^2},$$

$$C = \frac{2 [\ln(\varrho_1)\varrho_2^2 - \ln(\varrho_2)\varrho_1^2]}{[(\varrho_2^4 - \varrho_1^4) (\ln(\varrho_1) - \ln(\varrho_2)) + (\varrho_1^2 - \varrho_2^2)^2]} v_{ram}.$$

## Modeling the Heat Sources

Plastic deformations take place while the billet is being extruded. The heat generated within the billet in the course of the extrusion derives mainly from the transformation of the mechanical energy consumed during deformation. When the energy stored in the elastically deformed material prior to start flowing (yielding) reaches a critical value, plastic flow starts. This is called the *von Mises* yield criterion [19]. The mean principal stress for the cylindrical coordinates under consideration is:

$$\sigma_m = \frac{(\sigma_x + \sigma_r + \sigma_\phi)}{3} \quad (2.51)$$

where  $\sigma_x$ ,  $\sigma_r$  and  $\sigma_\phi$  denote the principal normal stresses for the principal axes. Expressed as a function of the principal stresses, the *von Mises* rule takes the following form:

$$k_f = \left\{ \frac{1}{2} [(\sigma_x - \sigma_r)^2 + (\sigma_r - \sigma_\phi)^2 + (\sigma_x - \sigma_\phi)^2] \right\}^{\frac{1}{2}}. \quad (2.52)$$

The term  $k_f$  is called the flow stress. Plastic flow starts when this critical value is reached. Combining equations (2.51) and (2.52) the following expression results:

$$k_f = \left\{ \frac{3}{2} [(\sigma_x - \sigma_m)^2 + (\sigma_r - \sigma_m)^2 + (\sigma_\phi - \sigma_m)^2] \right\}^{\frac{1}{2}}. \quad (2.53)$$

Consider a volume element  $dV$ . Assuming that elastic deformation can be neglected because of the high hydrostatic pressure, the deformation energy  $dW$  expended during a time element  $dt$  is [20]:

$$P = \frac{dW}{dt} = k_f \dot{\epsilon} dV \quad (2.54)$$

where  $\dot{\epsilon}$  denotes the strain rate. The strain rate is a function of the velocity distribution, which in turn is a function of the axial and radial coordinates. The strain rate may be calculated by the following equation [20]:

$$\dot{\epsilon} = \sqrt{\frac{2}{3} \left[ \left( \frac{\partial v_x}{\partial x} \right)^2 + \left( \frac{\partial v_r}{\partial r} \right)^2 + \left( \frac{v_r}{r} \right)^2 + \frac{1}{2} \left( \frac{\partial v_r}{\partial r} + \frac{\partial v_r}{\partial x} \right)^2 \right]}. \quad (2.55)$$

If the friction between the billet and the container is neglected, equations (2.54) and (2.55) may be used to calculate the heat sources within the billet during extrusion. In this case, the heat source term in equation (2.1) is given by:

$$q(x, r, t) = k_f \dot{\epsilon}. \quad (2.56)$$

The flow stress  $k_f$ , which is a function of the temperature and of the strain rate  $\dot{\epsilon}$ , may be determined experimentally. The following empirical relationship for  $k_f$  is found in the literature [21], [22]:

$$k_f = \Lambda (1 - \Theta \epsilon) \exp(-\Phi T) \dot{\epsilon}^\Omega. \quad (2.57)$$

The coefficients  $\Lambda$ ,  $\Theta$ ,  $\Phi$ , and  $\Omega$  depend on the alloy under consideration. Values for various alloys can be found in [21]. For uniaxial deformation, the strain  $\epsilon$  may be defined as [23]:

$$d\epsilon = \frac{dx}{x}. \quad (2.58)$$

To calculate the strain for the extrusion process, this equation must be integrated from the initial length of the billet  $L_0$  to the final length of the extrudate profile  $L_1$ . Thus:

$$\epsilon = \int_{L_0}^{L_1} \frac{dx}{x} = \ln \frac{L_1}{L_0}. \quad (2.59)$$

If the deformation is assumed to take place under constant volume the following is true:

$$A_0 L_0 = A_1 L_1 . \quad (2.60)$$

Here  $A_0$  and  $A_1$  stand for the cross-sectional areas of the billet and extrudate profile, respectively. From the last equation it follows that the strain may be approximated by:

$$\epsilon = \ln \frac{L_1}{L_0} = \ln \frac{A_0}{A_1} = \varphi . \quad (2.61)$$

The ratio  $\frac{A_0}{A_1}$  is known as the extrusion ratio.

If friction forces are considerable, another term must be added to equation (2.54) to account for this heat source. The heat generated per unit of time due to friction between the outer surface of the billet and the inner surface of the container is:

$$q_{fr} = \nu_{fr} p(R, x) v_x(R, x) . \quad (2.62)$$

Here,  $\nu_{fr}$  stands for the coefficient of friction.

### Modeling the Pressure Forces

The pressure distribution may be determined by means of equations (2.21) or (2.22). The introduction of the stream function into equation (2.21) leads to the following expression:

$$\frac{\partial p(r, x)}{\partial r} = \mu \left[ \frac{\partial}{\partial r} \left( -\frac{1}{r} \frac{\partial^2 \Psi}{\partial r \partial x} \right) - \frac{1}{r} \frac{\partial^3 \Psi}{\partial x^3} \right] . \quad (2.63)$$

This equation may be solved by using the method of separation of variables analogously to the way equation (2.34) was solved. In this

section the solution is just stated; a detailed solution may be found in Appendix C. Upon introduction of the separation functions  $\Upsilon$  and  $\Xi$  into equation (2.63), the following expression results:

$$\frac{\partial p(r, x)}{\partial r} = \mu \left[ -\frac{\partial}{\partial r} \left( \frac{1}{r} \Upsilon' \Xi' \right) - \frac{1}{r} \Upsilon \Xi''' \right]. \quad (2.64)$$

Further substitutions and transformations as indicated in Appendix C lead to the following equation:

$$p(r, x) = \mu \sum_i f_i(r) \left[ -\Xi'_i(x) + \frac{\Xi_i'''(x)}{\omega_i^2} \right] + c. \quad (2.65)$$

The integration constant may be determined by assuming zero pressure at the exit of the die. The assumptions mentioned before for the velocity and pressure distributions within the die (*Hagen-Poiseuille* flow) imply that:

$$\frac{\partial p(r, x)}{\partial x} = \mu \frac{1}{r} \frac{\partial}{\partial r} \left( r \frac{\partial v_x}{\partial r} \right) = \text{constant}. \quad (2.66)$$

This equation leads to the following expression for the pressure drop in the die:

$$\Delta p(x) = 4 \mu \Delta x \frac{C A}{R^2} \quad (2.67)$$

where  $\Delta x$  is the width of the die, while C and A are the constants defined in equation (2.50). The integration constant in equation (2.65) is readily derived from the following relationship:

$$\mu \sum_i f_i(0) \left[ -\Xi'_i(L) + \frac{\Xi_i'''(L)}{\omega_i^2} \right] - 4 \mu \Delta x \frac{C A}{R^2} + c = 0. \quad (2.68)$$



## Extrusion Force

The extrusion force may be considered to be equal to the sum of the die and friction forces. Each of these force components may be calculated from the pressure distribution described above.

## Die Force

The pressure distribution at the die is given by equation (2.65) evaluated at  $x = L$ :

$$p(r, L) = \mu \sum_i f_i(r) \left[ -\Xi'_i(L) + \frac{\Xi'''_i(L)}{\omega_i^2} \right] + c. \quad (2.69)$$

The force at the die may be calculated by integrating the following equation:

$$F_{die} = \int_0^R \int_0^{2\pi} p(r, L) r dr d\phi. \quad (2.70)$$

Inserting equation (2.69) into the last equation yields:

$$F_{die} = 2\pi\mu \int_0^R r f_i(r) \left[ -\Xi'_i(L) + \frac{\Xi'''_i(L)}{\omega_i^2} \right] dr + \pi c R^2. \quad (2.71)$$

With the help of equation (B.38) (see appendix B), this last equation transforms into:

$$F_{die} = 2\pi\mu \left[ \sum_i \Upsilon_i(r) \right] \left[ -\Xi'_i(L) + \frac{\Xi'''_i(L)}{\omega_i^2} \right]_0^R + \pi c R^2. \quad (2.72)$$

Recapturing equations (2.40) and (2.42):

$$v_r|_{r=0} = \frac{1}{r} \Upsilon(r) \Xi'(x) = 0; \forall x \implies \frac{1}{r} \Upsilon(r) \Big|_{r=0} = 0$$

$$v_r|_{r=R} = \frac{1}{r} \Upsilon(r) \Xi'(x) = 0; \forall x \implies \frac{1}{r} \Upsilon(r) \Big|_{r=R} = 0$$

finally yields:

$$F_{die} = \pi c R^2 \quad (2.73)$$

where:

$$c = 2 \mu \pi A C \Delta x v_{ram} . \quad (2.74)$$

### Friction Force

The friction force is given by:

$$F_{friction} = \int_0^{2\pi} \int_0^L \nu_{fr} R p(R, x) dx d\phi = 2\pi \nu_{fr} R \int_0^L p(R, x) dx . \quad (2.75)$$

In the last equation  $\nu_{fr}$  stands for the coefficient of friction. This integration gives:

$$F_{friction} = 2\pi \nu_{fr} R \left[ Lc + \mu \sum_i f_i(R) \left[ (\Xi_i(0) - \Xi_i(L)) + \left( \frac{\Xi''(L) - \Xi''(0)}{\omega_i^2} \right) \right] \right] . \quad (2.76)$$

### 2.3.2 Modeling the Container, Die, and Ram

The container can be modelled as a hollow cylinder, exchanging heat with diverse mediums. This implies different boundary conditions for the inner and outer surfaces. At the outer surface the container exchanges heat with the environment ( $T \approx 30^\circ C$ ), and at the inner surface it exchanges heat with the billet. Radiation of the outer surface of the container into the environment is neglected. The heat conduction

equation is set up for a hollow cylinder, assuming rotational symmetry to the central axis:

$$\frac{\partial T}{\partial t} = \alpha \left( \frac{\partial^2 T}{\partial x^2} + \frac{\partial^2 T}{\partial r^2} + \frac{1}{r} \frac{\partial T}{\partial r} \right) \quad (2.77)$$

taking into account the following boundary conditions:

$$\left. \frac{\partial T}{\partial r} \right|_{r=R_1} = -\frac{h}{k} (T - T_\infty) \quad (2.78)$$

$$\left. \frac{\partial T}{\partial r} \right|_{r=R} = -\frac{h_c}{k} (T - T_{billet}) \quad (2.79)$$

$$\left. \frac{\partial T}{\partial x} \right|_{x=0} = -\frac{h}{k} (T - T_\infty) \quad (2.80)$$

$$\left. \frac{\partial T}{\partial x} \right|_{x=L} = -\frac{h}{k} (T - T_\infty) \quad (2.81)$$

where  $T_\infty$ ,  $T_{billet}$ ,  $h_c$ ,  $h$ ,  $R$ , and  $R_1$  stand for temperature of the surroundings, temperature of the container/billet surface, contact conductance aluminum/steel, heat transfer coefficient steel/air, inner and outer radius of the container, respectively. Similarly, the die is modelled as a hollow cylinder, exchanging heat with the environment through the outer surface and with the extrudate section through the inner surface. The ram is modelled as a full cylinder similar to the billet. The equation to be solved is the same as for the container, with substitutions for the appropriate boundary conditions.

## 2.4 Simulating the Extrusion Process

Having set up the model for the billet and the different tooling pieces, the next step is to simulate the whole process. To simulate the billet, equations (2.1), (2.20), (2.21), and (2.22) have to be solved simultaneously to account for their respective boundary conditions. Solving

them numerically would require massive computation times and would be of no advantage over using the *FEM*. Therefore, the following approach was pursued: the velocity distributions and heat sources terms were calculated in an analytical way. At each time step, the main program invokes the velocities and heat sources needed to calculate the temperature distributions. The temperature distribution for that time interval is then calculated numerically using a finite differences method. The procedure is repeated for each time interval. Figure 2.5 shows a scheme of the calculation sequence for each time step. A Forward-Time-Central-Space (FTCS) finite difference approximation of the derivatives with respect to the time and spatial coordinates was used:

$$\frac{\partial T}{\partial t} = \frac{T_{i,j}^{n+1} - T_{i,j}^n}{\Delta t} \quad (2.82)$$

$$\frac{\partial T}{\partial r} = \frac{T_{i,j+1}^n - T_{i,j-1}^n}{2 \Delta r} \quad (2.83)$$

$$\frac{\partial T}{\partial x} = \frac{T_{i+1,j}^n - T_{i-1,j}^n}{2 \Delta x} \quad (2.84)$$

$$\frac{\partial^2 T}{\partial r^2} = \frac{T_{i,j+1}^n - 2T_{i,j}^n + T_{i,j-1}^n}{\Delta r^2} \quad (2.85)$$

$$\frac{\partial^2 T}{\partial x^2} = \frac{T_{i+1,j}^n - 2T_{i,j}^n + T_{i-1,j}^n}{\Delta x^2}. \quad (2.86)$$

The grid for the discretization of the billet is portrayed in Figure 2.4. At each time step the grid is readjusted, taking into account the changing geometry (decrease in length) of the billet. To simulate the remaining bodies (container, die) an identical finite-difference scheme was selected. In this case, however, neither heat sources nor velocity terms have to be taken into account as the equation to be solved is the homogeneous *heat conduction* equation (2.77). Table 2.2 presents some data relevant for the simulations. A simulation of an extrusion cycle was conducted and the evolution of the temperature distribution of the billet during the extrusion cycle is shown in Figures 2.6–2.11. Figures 2.12 and 2.13 show the temperature of the extrudate section

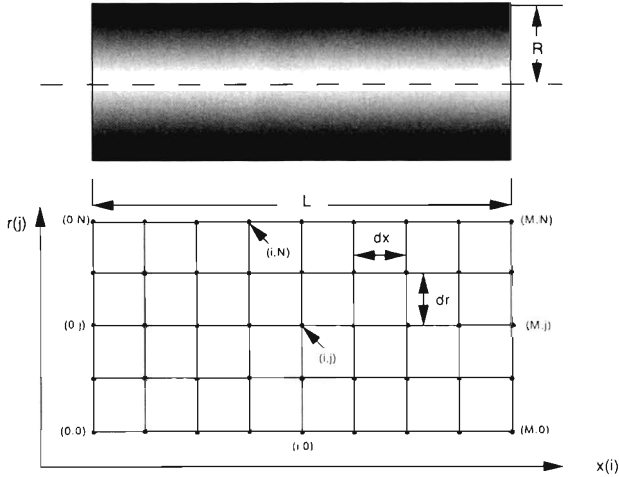


Figure 2.4: *Finite-difference network.*

and extrusion force, respectively. The plots corresponding to the temperature distributions for the remaining bodies (i.e. container, die holder, and die) may be found in Appendix E.

For this simulation a constant extrusion velocity of  $6 \text{ mm/s}$  was chosen. The initial temperature distribution of the billet was taken as a constant gradient with  $\Delta T = 70^\circ\text{C}$ .  $\Delta T$  stands for the difference between the initial temperatures at the front and rear ends of the billet which were chosen to be  $T_{front} = 515^\circ\text{C}$  and  $T_{rear} = 445^\circ\text{C}$ . The front part of the billet is where the higher temperatures may be found<sup>2</sup> (in Figures 2.6 – 2.11 zero length indicates the front of the billet). It is in this part of the body that deformation takes place. The energy used to deform the billet is transformed into heat, which is reflected in the higher temperatures found at the front of the body. As shown in the figures, temperature variations at the back of the billet are relatively small. The metal just flows into the deformation zone, however, no major thermal phenomena take place in that part of the body. As the extrusion proceeds, the temperature at the front of

<sup>2</sup>For the front part of the billet, a finer mesh was used for the discretization and a smoothing algorithm was developed to avoid numerical problems in this region (see Appendix D).

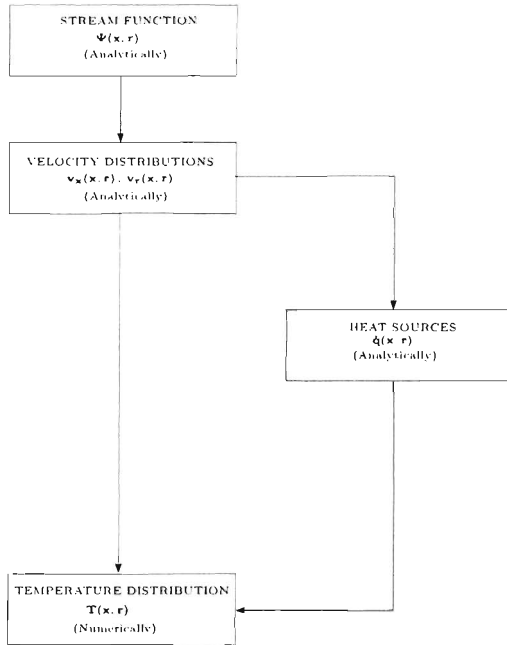


Figure 2.5: *Calculation sequence for each time step.*

the billet decreases. This is due to the fact that the remaining material cools down as it flows and eventually cools the front of the cylinder by convection. The friction force is linearly dependent on the length of the billet (see equation (2.76)). Thus, the extrusion force decreases as the billet length decreases. However, towards the end of the extrusion cycle an increase in the extrusion load is noticed (Figure 2.13). This occurs when the billet has been extruded to a small length and there is a high resistance to radial flow towards the center of the billet. An increase in the heat generation rate due to deformation is a consequence thereof. This increase in the heat of deformation cannot be dissipated quickly enough and the temperature at the front of the billet increases slightly again. This is more clearly noticed in the

## Physical and Material Constants

<b>Billet</b>		
Billet's initial length	(m)	1.2
Billet's diameter	(m)	0.3
Extrusion ratio	(-)	27.5
Density aluminum <sup>3</sup>	$(kgm^{-3})$	2700
Specific heat aluminum	$(Jkg^{-1}K^{-1})$	920
Thermal conductivity aluminum	$(Wm^{-1}K^{-1})$	165
Heat conductance Al/steel <sup>4</sup>	$(Wm^{-2}K^{-1})$	4000
<b>Container</b>		
Container's length	(m)	1.4
Container's outer diameter	(m)	1.120
Density of steel <sup>5</sup>	$(kgm^{-3})$	7900
Specific heat steel	$(Jkg^{-1}K^{-1})$	477
Thermal conductivity steel	$(Wm^{-1}K^{-1})$	14.5
Heat conductance Al/steel	$(Wm^{-2}K^{-1})$	4000
Heat transfer coefficient steel/air <sup>6</sup>	$(Wm^{-2}K^{-1})$	7
<b>Ram</b>		
Ram's diameter	(m)	0.224
Ram's length	(m)	1.0

Table 2.2: *Physical Constants, Tooling and Billet Data.*

temperature of the extrudate (Figure 2.12). The front part of the container which is in direct contact with the part of the billet that is being deformed (see Appendix E) also heats up. The temperature of the rest of the container remains more or less constant throughout the whole extrusion cycle. A slight decrease in temperature can be observed for the container near the outer surface. This surface is exchanging heat with the environment. The temperatures of the die and mandrel increase rapidly as the extrusion cycle proceeds. These bodies are in direct contact with the front part of the billet where most of the heat is being produced.

<sup>3</sup>Density, specific heat, and thermal conductivity of aluminum from reference [24].

<sup>4</sup>From reference [14].

<sup>5</sup>Density, specific heat, and thermal conductivity of steel from reference [24].

<sup>6</sup>As calculated by Dilger [25].

Temperature Distribution of the Billet at  $t = 25$  s

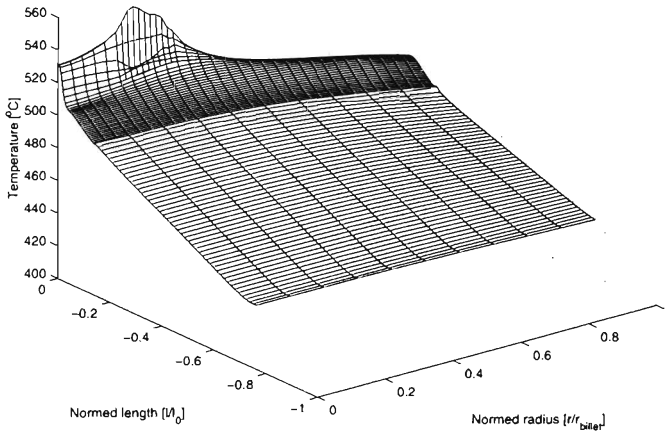


Figure 2.6: *Temperature distribution in the billet at  $t = 25$  s.*

Temperature Distribution of the Billet at  $t = 50$  s

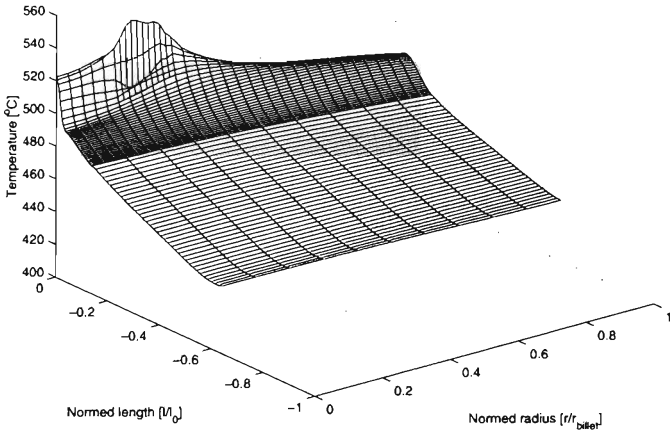


Figure 2.7: *Temperature distribution in the billet at  $t = 50$  s.*



Temperature Distribution of the Billet at  $t = 75$  s

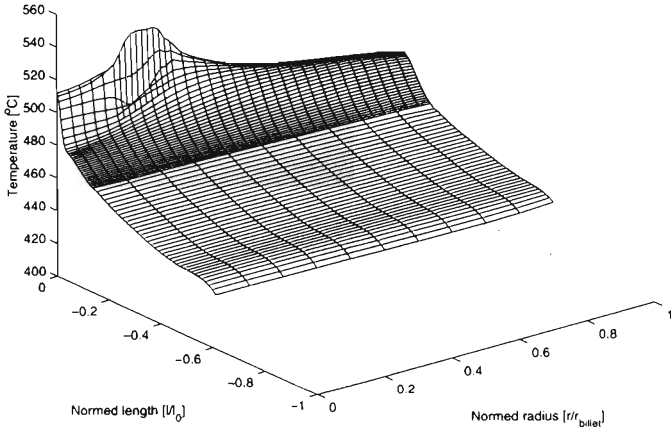


Figure 2.8: *Temperature distribution in the billet at  $t = 75$  s.*

Temperature Distribution of the Billet at  $t = 100$  s

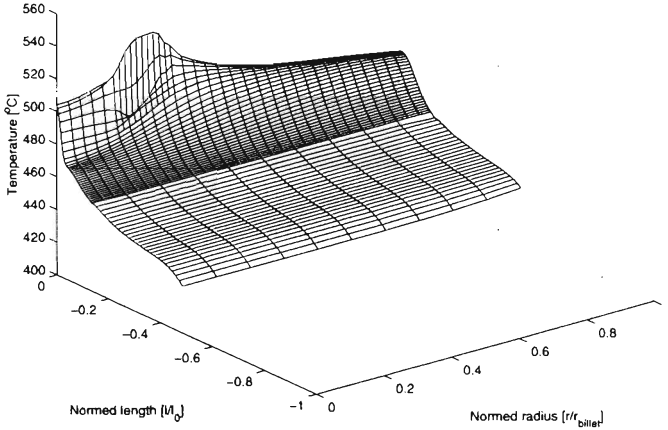


Figure 2.9: *Temperature distribution in the billet at  $t = 100$  s.*

Temperature Distribution of the Billet at  $t = 125$  s

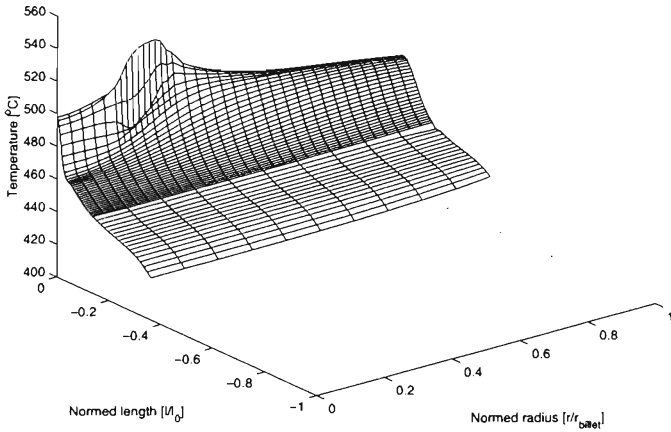


Figure 2.10: *Temperature distribution in the billet at  $t = 125$  s.*

Temperature Distribution of the Billet at  $t = 150$  s

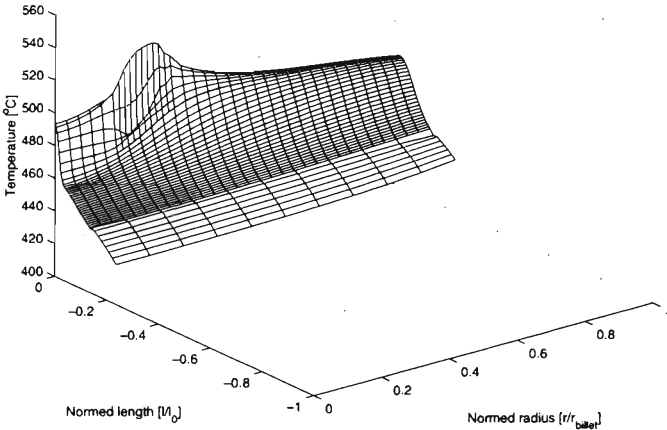


Figure 2.11: *Temperature distribution in the billet at  $t = 150$  s.*

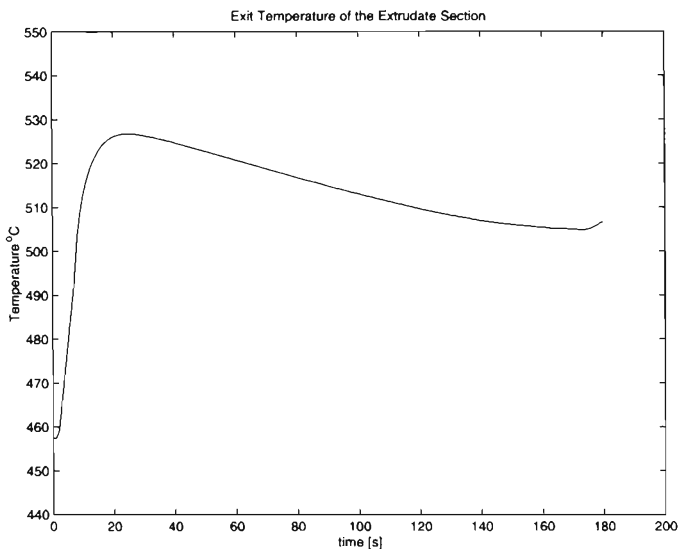


Figure 2.12: *Exit Temperature of the Extrudate.*

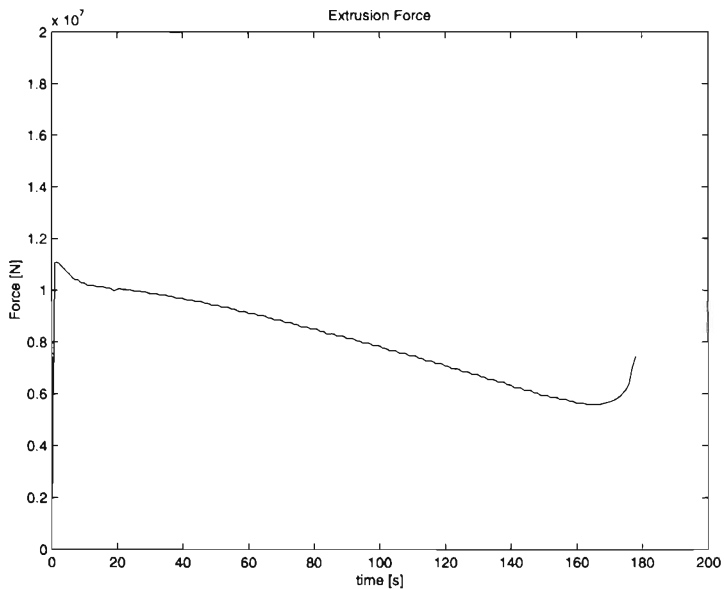


Figure 2.13: *Extrusion force.*

## 2.5 Qualitative Comparison of the Model with the Program *PressForm*

*PressForm* is a simulation package developed at the Institute of Forming Technology of the Swiss Federal Institute of Technology Zurich. The program is designed to simulate metal forming processes such as extrusion, rolling, and drawing. It is based on the Finite Element Method (*FEM*) and it is capable of simulating the forming processes in three or two dimensions for design purposes. Prior to validating the model presented in the previous sections with measurements from the plant a qualitative comparison with the program *PressForm* was performed. *PressForm* was to serve as a benchmark by means of which the capability of the detailed model presented in previous sections to reflect the physical phenomena taking place within the billet could be measured and judged. However, the results must only be compared qualitatively as there are some underlying differences between the two models. It must also be kept in mind that the model presented in this thesis is intended for control purposes, and as such it is expected to ultimately be quantitatively in agreement with the measurements of the plant. The differences between the two models are pointed out next. *PressForm* assumes a constant and homogeneous temperature of the tooling throughout the complete extrusion cycle. As mentioned in previous sections the model derived in this thesis is not restricted to this. The temperature of the tooling is taken as a function of time as well as of the radial and axial coordinates. An important difference lies also in the assumed behavior of the flow stress as a function of time, temperature, strain, and strain rate. *PressForm* assumes the following behavior:

$$k_f = C \left[ \dot{\epsilon} \exp \left( \frac{Q}{RT} \right) \right]^m. \quad (2.87)$$

Here  $C$  and  $m$  are experimentally determined constants.  $R$  stands for the universal gas constant,  $T$  for temperature,  $Q$  for internal energy,

and  $\dot{\epsilon}$  for strain rate. The model presented in this thesis assumes the following relationship:

$$k_f = \Lambda (1 - \Theta\epsilon) \exp(-\Phi T) \dot{\epsilon}^\Omega. \quad (2.88)$$

In the last equation  $\Lambda$ ,  $\Theta$ ,  $\Phi$ , and  $\Omega$  are experimentally determined constants dependent on the alloy being considered.  $\epsilon$  stands for the strain. The difference between these two approaches will be reflected in the temperature distributions within the billet, as the heat generation rate due to deformation is directly proportional to it (see equation (2.54)). For the comparison to be meaningful the flow stress  $k_f$  used in *PressForm* must be fitted to the flow stress given by equation (2.88) and the alloy in question. The strain in equation (2.88) is set equal to the logarithm of the extrusion ratio  $\varphi = \ln \frac{A_0}{A_1}$  where  $A_0$  and  $A_1$  stand for the cross-sectional area of the billet and cross-sectional area of the extrudate profile, respectively. For the comparison with *PressForm*, a particular geometry was chosen which is depicted in Figure 2.14.

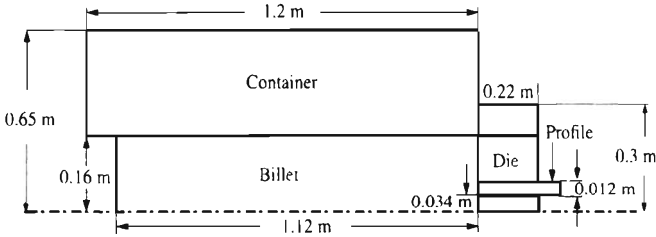


Figure 2.14: *Geometry for comparison with PressForm.*

The fit of the flow stress was conducted for the temperature range of  $400 - 700^\circ\text{C}$  and the strain rate range of  $0 - 20\text{ s}^{-1}$ . Figure 2.15 shows the flow stress  $k_f$  as a function of temperature and strain rate as given by the original parameters for the alloy in question and by equation (2.88), as well as the fitted flow stress as given by equation (2.87). For the comparison with *PressForm*, a homogeneous initial temperature of the billet of  $T_{billet} = 515^\circ\text{C}$  was chosen. The simulations were performed for a constant extrusion velocity of  $6\text{ mm/s}$  and an initial

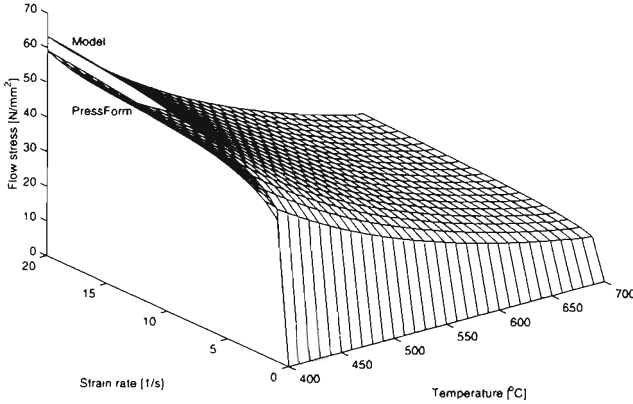


Figure 2.15: *Fit of flow stress as a function of strain rate and temperature.*

temperature of the tooling of  $T_{tooling} = 433\text{ }^{\circ}\text{C}$ . Table 2.3 summarizes the data for the comparison of the two models.

### Simulation Conditions for Comparison with PressForm

#### Initial Conditions

Initial temperature of billet	$(^{\circ}\text{C})$	515
Initial temperature of tooling	$(^{\circ}\text{C})$	433
Extrusion velocity	$(\text{mm}\cdot\text{s}^{-1})$	6
Extrusion ratio	(-)	3

Table 2.3: *Simulation Conditions for Comparison with PressForm.*

Since the most interesting and relevant physical phenomena of the extrusion process take place in the foremost part of the billet where deformation takes place and the metal flows into the die, this is the pertinent zone to be compared between the two models. Temperature and velocity distributions within the billet, as well as extrusion forces

for the two models are shown in Figures 2.16 – 2.27. The qualitative agreement between the two models is clear. As mentioned before, the disagreement between the two is more marked in the temperature distributions than in the flow patterns of the metal. This derives mostly from the different behaviors assumed for the flow stress as a function of temperature and strain rate and its relationship to the heat generated due to deformation. The lower temperatures at the rear end in Figure 2.17 are explained as follows: for computational purposes in the simulations with *PressForm* the length of the billet is assumed to be approximately equal to the deformation zone. Thus the rear part of the billet as shown in Figure 2.17 is exchanging heat with the ram, causing the temperature to drop at the rear end of the billet. The assumption of a shorter billet for the simulations with *PressForm* naturally influences the extrusion force calculated. In particular the friction forces are bound to be different. The marked difference in the extrusion forces could derive therefrom. Nonetheless, the overall qualitative behavior of the forces calculated by the two models coincides. Although the qualitative agreement for the velocity distributions is clearly reflected in Figures 2.18 – 2.21, comparison of the flow patterns in Figures 2.22 – 2.23 may at first lead to some misinterpretations. In particular the difference in axial velocities in the front part of the billet seem to be rather marked. Lets examine thus these figures in more detail to clarify the validity of the results. Both models make the assumption of the metal being an incompressible fluid. Thus a volumetric flow balance for the metal yields the following in both cases:

$$v_{ram}A_0 = v_{exit}A_{die} \quad (2.89)$$

where:

- $v_{ram}$  = Ram velocity,
- $v_{exit}$  = Velocity at entrance of die,
- $A_0$  = Cross-sectional area of billet,
- $A_{die}$  = Area of opening of die.

These calculations were performed by taking the velocity at the entrance of the die calculated by each of the models. The results are presented in Table 2.4.

### Calculation of Volumetric Flow

---



---

<b>PressForm</b>		
$A_0$	$(m^2)$	$8.3 \cdot 10^{-2}$
$A_{die}$	$(m^2)$	$3 \cdot 10^{-3}$
$v_{ram}$	$(ms^{-1})$	$6 \cdot 10^{-3}$
$v_{exit}$	$(ms^{-1})$	0.14
$v_{ram}A_0$	$(m^3s^{-1})$	$5 \cdot 10^{-4}$
$v_{exit}A_{die}$	$(m^3s^{-1})$	$4.3 \cdot 10^{-4}$
<b>Model</b>		
$A_0$	$(m^2)$	$8.3 \cdot 10^{-2}$
$A_{die}$	$(m^2)$	$3 \cdot 10^{-3}$
$v_{ram}$	$(ms^{-1})$	$6 \cdot 10^{-3}$
$v_{exit}$	$(ms^{-1})$	0.2
$v_{ram}A_0$	$(m^3s^{-1})$	$5 \cdot 10^{-4}$
$v_{exit}A_{die}$	$(m^3s^{-1})$	$6 \cdot 10^{-4}$

Table 2.4: *Volumetric flow balance.*

The condition of constant volumetric flow is satisfied for both models. The disagreement between the model presented in this thesis and the theoretically calculated value may originate from the rough size of the mesh used, and numerical inaccuracies derived therefrom. Overall, however, qualitative agreement of the model presented in this thesis with *PressForm* is satisfactory.

At this point the question may arise as to why not use *PressForm* directly to design model-based control strategies for the isothermal extrusion of aluminum. The answer to this question lies in the computation times demanded by *PressForm*. Simulating five seconds of an extrusion cycle with *PressForm* requires approximately three



and a half hours of CPU time on a SILICONGRAPHICS INDY, whereas the simulation of a complete extrusion cycle of 150 seconds requires approximately 4 minutes of CPU time on a COMPAQ Deskpro XL5133 (Pentium 133 MHZ).

A final remark with respect to this last question is appropriate at this point. Once again the point is stressed that the model developed in this thesis is for control purposes. Although the model should reflect the physical phenomena taking place within the billet, this should be done while maintaining low computation times. The whole development of the model by means of the *semi-analytical* approach was conducted with this goal in mind. If design purposes are of importance or if the accurate study of thermo-mechanical properties within the billet is intended, very fine discretization meshes are of interest and the model presented in this thesis is by no means a substitute of well established simulation packages such as *PressForm*.

Nevertheless, it was felt that a comparison of the model proposed in this thesis with *PressForm*, a well known and accepted program within the forming technology community, was indeed necessary to confirm the plausibility of the *semi-analytical* approach proposed in previous sections to accurately solve the equations that describe the extrusion process.

Temperature Distribution of the Billet at  $t = 5$  s

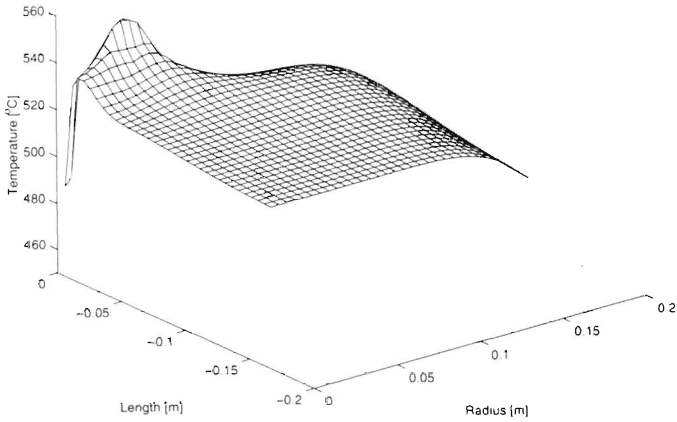


Figure 2.16: *Temperature distribution in the billet at  $t = 5$  s.*

Temperature of the Billet at  $t = 5$  s. Pressform.

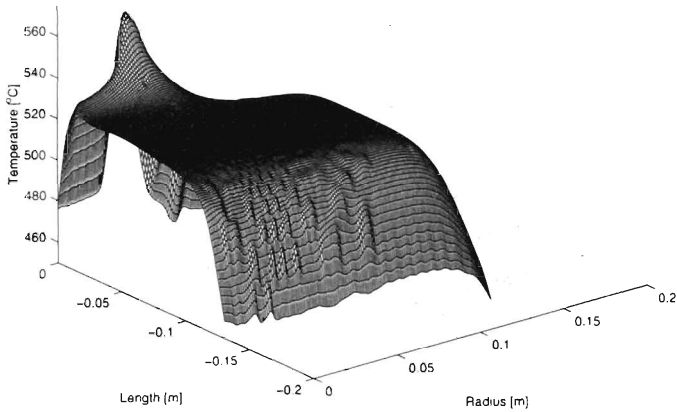


Figure 2.17: *Temperature distribution in the billet at  $t = 5$  s: Press-Form.*

Axial Velocity Distribution of the Billet at  $t = 5$  s

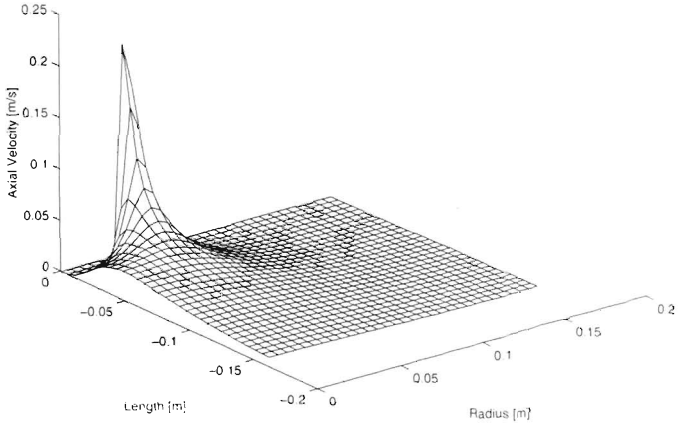


Figure 2.18: Axial velocity distribution within the billet at  $t = 5$  s.

Axial Velocity Distribution of the Billet at  $t = 5$  s: PressForm

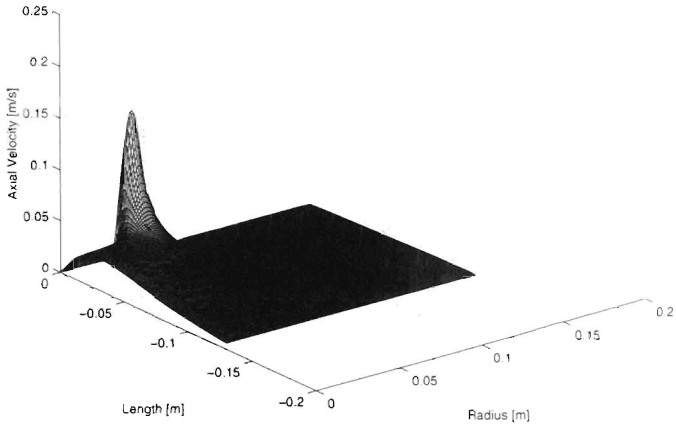


Figure 2.19: Axial velocity distribution within the billet at  $t = 5$  s: PressForm.

Radial Velocity Distribution of the Billet at  $t = 5$  s

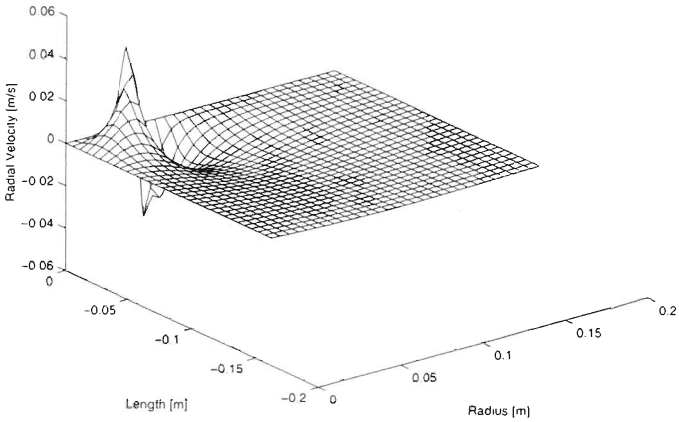


Figure 2.20: *Radial velocity distribution within the billet at  $t = 5$  s.*

Radial Velocity Distribution of the Billet at  $t = 5$  s. PressForm

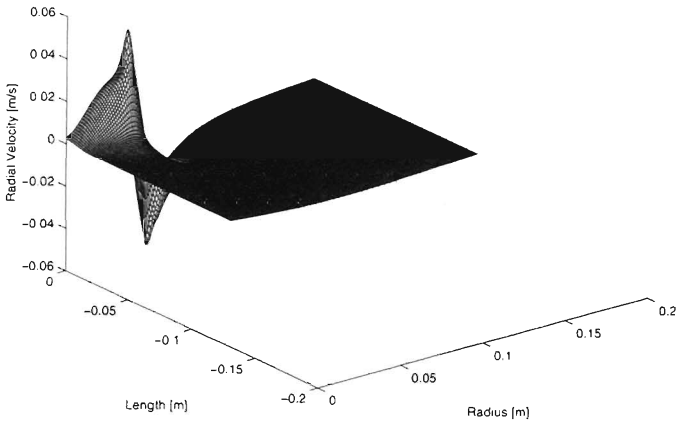


Figure 2.21: *Radial velocity distribution within the billet at  $t = 5$  s: PressForm.*

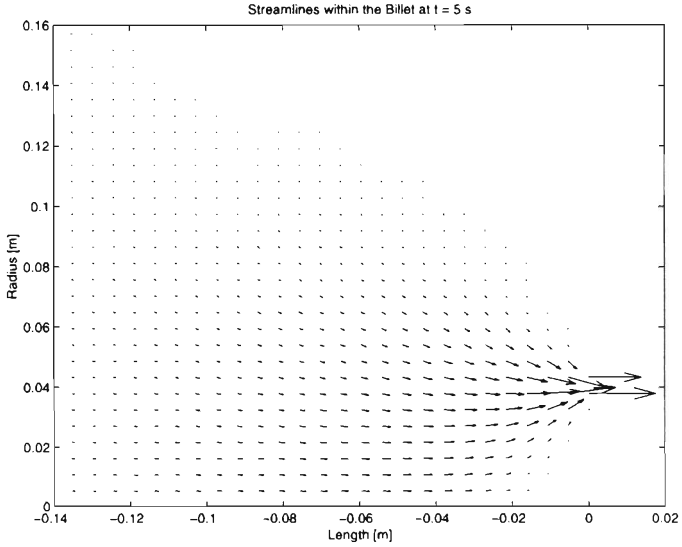


Figure 2.22: *Streamlines within the billet at  $t = 5$  s.*

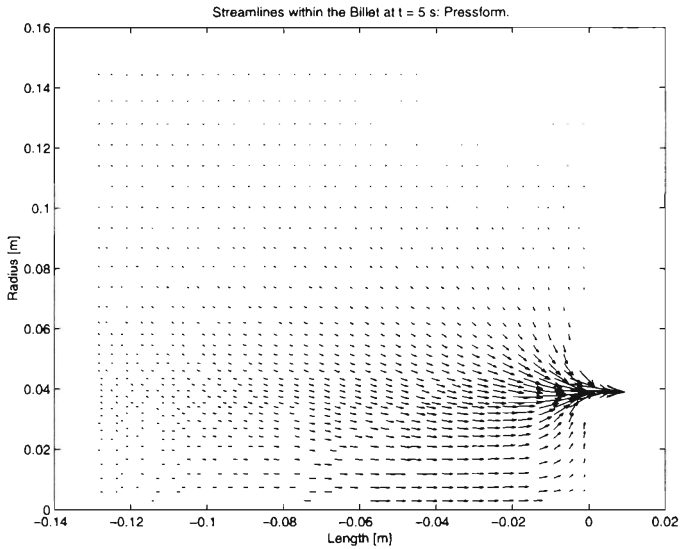


Figure 2.23: *Streamlines within the billet at  $t = 5$  s: PressForm.*

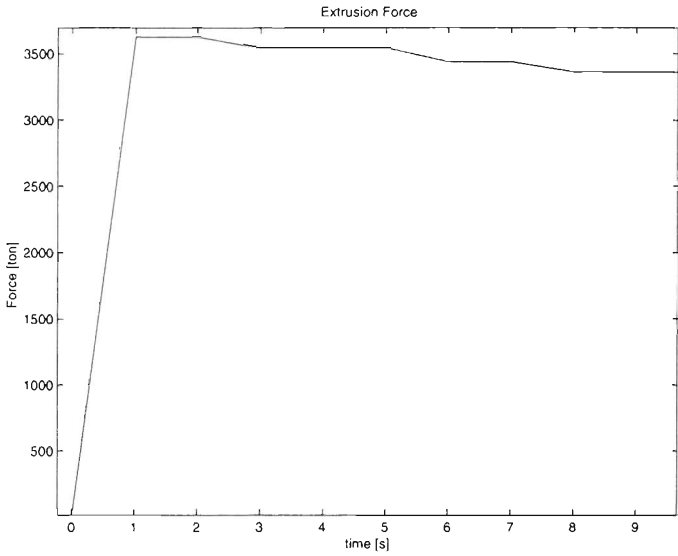


Figure 2.24: *Extrusion force.*

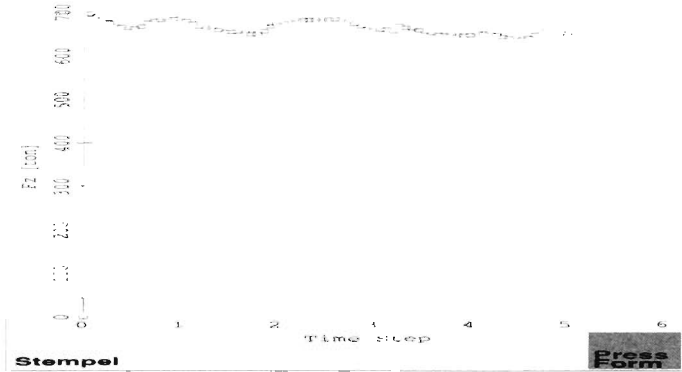


Figure 2.25: *Extrusion force: PressForm.*

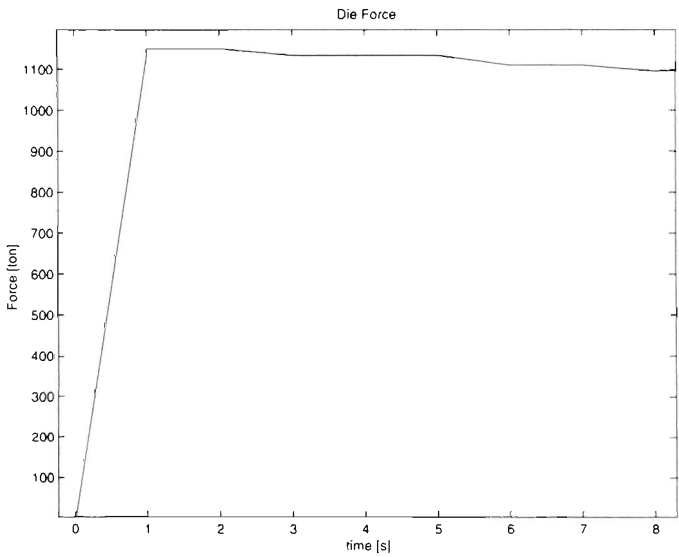


Figure 2.26: *Die force.*

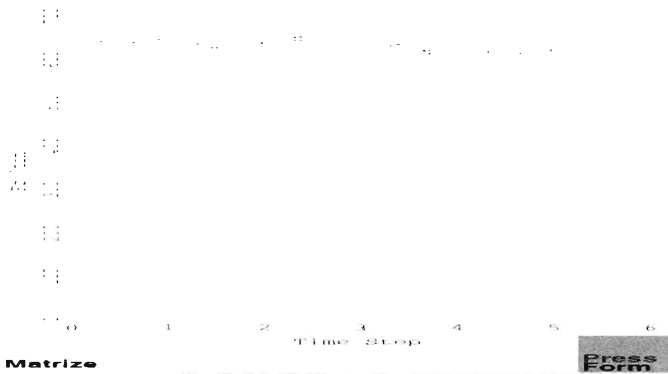


Figure 2.27: *Die force: PressForm.*

## 2.6 Model Validation

To validate the model presented in the previous sections, various experiments were conducted on an industrial aluminum extrusion press. A number of velocity trajectories were run whereby the temperature of the extrudate section was recorded. Prior to loading the billet into the container, the temperature of the billet was measured at three points along the surface of the billet. From these recorded values a linear temperature profile along the axis of the billet was inferred. The initial temperature of the container was measured at one point and assumed to be constant throughout. The measurements shown correspond to the same alloy being extruded, as well as to the same die geometry. However, the initial conditions of the billet (initial temperature distribution) were not the same. For the first measurement the initial temperature gradient of the billet was  $\Delta T = 50^\circ C$ , with the temperature at the front and rear ends of the billet being  $T_{front} = 500^\circ C$  and  $T_{rear} = 450^\circ C$ , respectively. For the second measurement  $\Delta T = 10^\circ C$ , with  $T_{front} = 500^\circ C$  and  $T_{rear} = 490^\circ C$ . Figures 2.28 and 2.29 show the response of the extrudate temperature to the corresponding velocity trajectories for each measurement.

While in the first measurement the velocity was kept almost constant throughout the whole extrusion cycle, in the second measurement the velocity was varied. The second measurement, however, must be judged with care. Here the strong variations in the velocity were not intentional. Instead they correspond to an abnormal situation within the cycle. This mishap, however, offered a unique measurement with a strong excitation of the system, something that usually is neither permitted nor desired since this causes serious load peaks that may lead to the cracking of the die. It is worth remarking that in this unusual extrusion cycle a probable partial malfunctioning of the temperature sensor is responsible for the apparent mismatch between the dynamics of the temperature measurement and the model at the beginning of the cycle. However, this last measurement provided data to verify whether the model reflects the dynamics of the extrudate temperature



when strong variations in the velocity take place. In both cases the results show quite a satisfactory agreement between measurement and model. It is worth noting that for both cycles the simulation takes less than four minutes of CPU time on a DEC AlphaServer 2100-600.

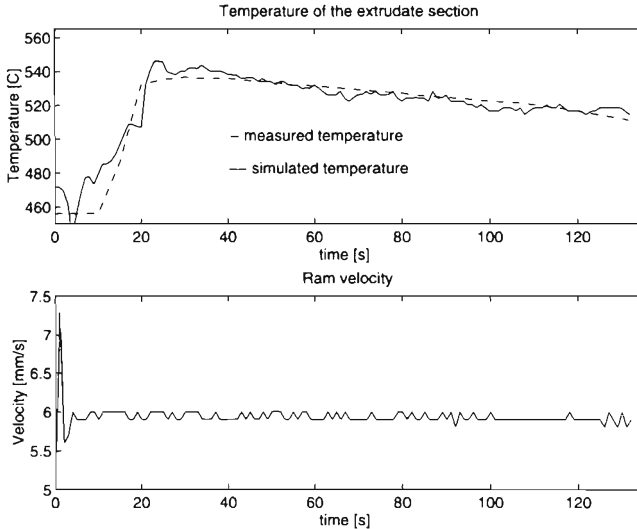


Figure 2.28: *Measured and simulated response of the extrudate temperature to a constant ram velocity.*

## 2.7 Process Control and Control Objectives

The ultimate goal of applying any control strategy to aluminum extrusion is to guarantee a homogenous product quality. Based on this, various performance criteria may be defined. In practice it is desirable to extrude isothermally to achieve product uniformity. However, the bounds of the extrusion velocity that can be achieved with the specific press in question must be taken into consideration. Mathematically this may be expressed as a constrained optimization problem.

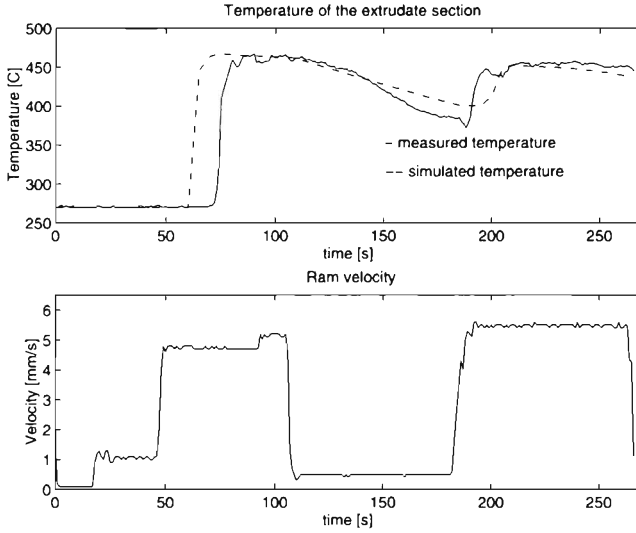


Figure 2.29: *Measured and simulated response of the extrudate temperature to a variable ram velocity.*

For example:

$$\underset{v}{\text{minimize}} \quad J(v(t)) \quad (2.90)$$

subject to:

$$v_{min} \leq v(t) \leq v_{max} \quad (2.91)$$

where:

$$J = \frac{1}{t_{final}} \int_{t=0}^{t=t_{final}} (T_{extrudate}(v(t)) - T_{setpoint})^2 dt. \quad (2.92)$$

Division by the final time  $t_{final}$  in the last equation is necessary as this time depends on the velocity profile of the extrusion cycle. If this was not done, the integral term could be minimized by maximizing the velocity, therefore minimizing the final time while disregarding the variations of the temperature from the setpoint. Although the

performance index in the last equation could have been formulated as a function of the length of the billet, the formulation as a function of time was chosen so as to avoid the conversion from exit temperature as a function of time to exit temperature as a function of length and thus save computation time.

The model developed allows the calculation of optimal velocity trajectories which minimize the performance index defined. The optimizations are carried out using a Sequential Quadratic Programming (*SQP*) method (e.g. routine *constr* from MATLAB [26]). Initial temperature distributions of the billet and tooling for these optimizations are set equal to those of the measurement in which the velocity was kept constant throughout the whole extrusion cycle (Figure 2.28). In the first optimization, the ram velocity is allowed to vary between the bounds, but it is held constant throughout the extrusion cycle. In the second optimization, the velocity is allowed to vary not only between bounds but also during the extrusion cycle (linear interpolation of the extrusion velocity through various points in time). Figure 2.30 illustrates the results of the optimizations. In the second case the temperature of the extrudate stays nearer to the setpoint through the complete cycle. Table 2.5 shows the measured and simulated extrusion times. It is worth noting that while in both cases the extrusion time is reduced, it is only in the second case that the temperature remains approximately constant and closer to the setpoint. No overshoot of the temperature is observed in this case either.

	Extrusion Time [s]
Measurement 1	132
Optimization with constant velocity	112
Optimization with variable velocity	110

Table 2.5: *Measured and simulated extrusion times.*

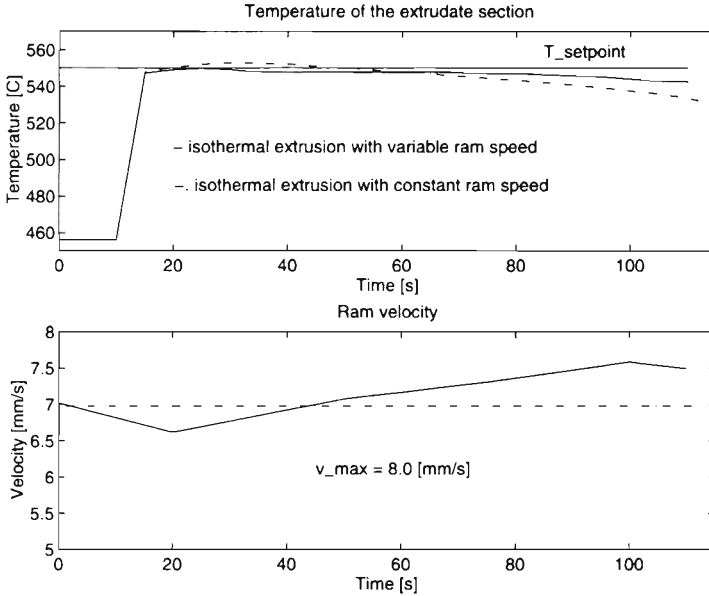


Figure 2.30: *Optimal velocity trajectories according to performance index (2.90) and subject to (2.91).*

As mentioned in Section 2.2.5, another practical approach for isothermal extrusion is *taper heating* the billet. Here an axial temperature profile is induced on the billet. The idea is to compensate the heat produced by friction/shear at the container/billet interface. Ideally, each cross-section of the billet should enter the deformation zone at the same constant temperature. This temperature gradient could then be considered in the optimization problem stated above. The idea is to predict an optimal temperature gradient and thus an optimal initial temperature distribution in the billet so as to achieve isothermal extrusion. Since in practice the furnaces used to preheat the billet are not able to produce complicated temperature profiles on the billet quickly and accurately, only linear temperature gradients are considered here. The problem of optimizing the initial temperature gradient in the billet is also stated as a constrained optimization. Due to

physical limitations this temperature gradient cannot be steeper than a certain value. This value is determined by the power of the oven that preheats the billet as well as by the residence time of the billet in the oven before it is loaded for extrusion. The optimization problem is now stated as follows:

$$\underset{v, T_{front}, T_{rear}}{\text{minimize}} \quad J(v(t)) \quad (2.93)$$

subject to:

$$v_{min} \leq v(t) \leq v_{max} \quad (2.94)$$

$$\theta_1 \leq T_{front} \leq \theta_2 \quad (2.95)$$

$$\theta_3 \leq T_{rear} \leq \theta_4 \quad (2.96)$$

where:

$$J = \frac{1}{t_{final}} \int_{t=0}^{t=t_{final}} (T_{extrudate}(v(t)) - T_{setpoint})^2 dt. \quad (2.97)$$

Here  $T_{front}$  and  $T_{rear}$  stand for the initial temperatures at the front and rear ends of the billet, respectively.  $\theta_i$  stands for the respective bounds on these parameters so that the gradient does not exceed a certain predefined value. Figures 2.31 and 2.32 illustrate the results of this optimization problem. The maximum value allowed for the temperature gradient was set to  $\Delta T = 50$  °C. Isothermal extrusion is achieved almost throughout the complete cycle.

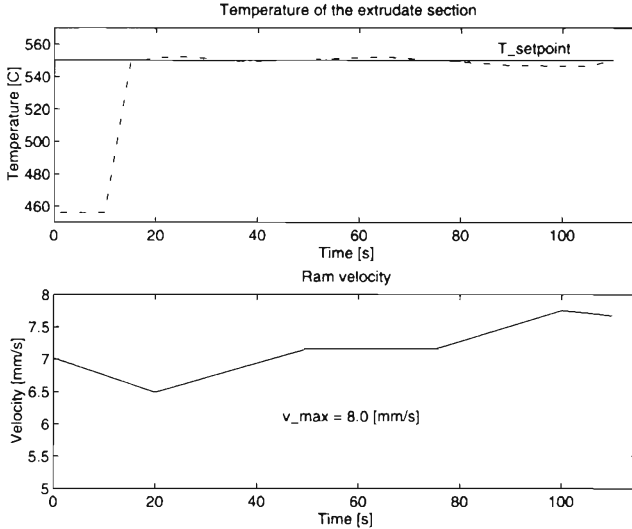


Figure 2.31: *Optimal velocity trajectories according to performance index (2.93) and subject to (2.94)-(2.96).*

## 2.8 Conclusions and Outlook

A dynamic model of the aluminum extrusion process has been derived. This model describes in detail the thermal dynamics of the most important bodies involved in the extrusion process. These are the billet, die, die holder, container, and the extrudate profile. The equations that describe the extrusion process are complicated partial differential equations. A new *semi-analytical* approach for solving these equations has been presented. In this approach the metal is treated as a highly viscous Newtonian fluid and appropriate assumptions regarding its flow are made. The velocities, pressure, strain, and strain rates distributions needed for the modeling of the process are solved analytically, leaving only the temperature distributions to be solved numerically. This innovative *semi-analytical* approach presented is of great advantage, since the computation times are drastically reduced in comparison to the classical

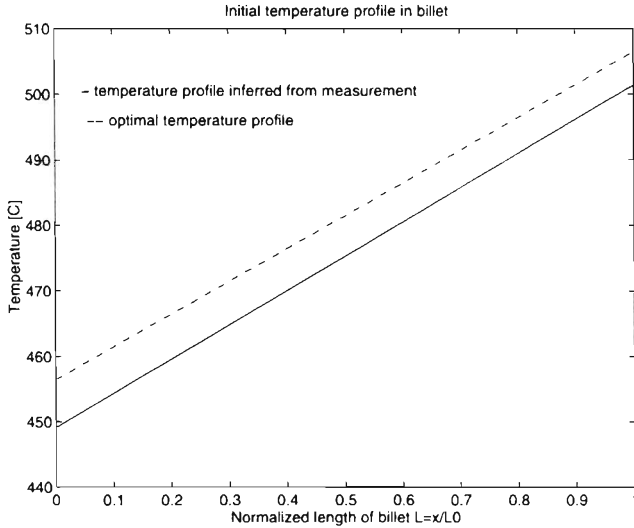


Figure 2.32: *Inferred and optimal initial temperature profiles in the billet.*

methods based on Finite Elements. Simulations of the extrusion process were conducted and the results are found to be in agreement with the physical understanding of the thermal dynamics of extrusion.

The quality of the model has been confirmed by comparison with data from an industrial aluminum extrusion press. For this purpose the parameters of the flow stress in equation (2.57) were adjusted to take into account the particular alloy in question. In addition, a qualitative comparison with the program *PressForm* [27], a well established and accepted program for the simulation of metal-forming processes, was performed. In particular it was expected that the model reflected the dynamics of the temperature of the extrudate accurately. This was important as the main purpose of the model was to design optimal control strategies that guarantee isothermal extrusion. The results of the comparison with both the industrial data and *PressForm* were satisfactory so that the

model was subsequently used to design optimal control strategies according to certain performance indexes. It has been shown that these control strategies can be used to achieve isothermal extrusion. In particular, it has been shown that the problem of controlling the temperature of the extrudate is not only a problem of properly adjusting the extrusion velocity during the extrusion cycle but also one of optimally choosing an initial temperature gradient of the billet. The combination of these two strategies allows for a considerable reduction of extrusion time while guaranteeing isothermal extrusion. Thus the quality of the product may be improved and productivity increased. Indeed, these optimal trajectories have been successfully implemented for various extrudate profiles in an industrial aluminum extrusion press located at a plant of Alusuisse in Sierre, Switzerland <sup>7</sup>.

The optimal control strategies presented in this chapter are open-loop. The introduction of feedback control may be of advantage, in particular if disturbances (e.g. noise) are taken into consideration. The constraints inherent to the system (i.e. maximum and minimum extrusion velocity that may be achieved in the particular press in question) also play a critical role in this respect. A closed-loop control strategy that takes all these facts into account is desirable. In view of all of the above, a plausible strategy could be to approach the problem of closed-loop control for the isothermal extrusion of aluminum within the framework of model predictive control (MPC). This seems reasonable as with MPC constraints may be directly taken into account while designing closed-loop control strategies. Within this context, however, a simplified dynamic model of the extrusion process is required, as the model presented here is still far too complex for the design of a model-based control strategy. Nevertheless, the model presented here may perfectly be used as a benchmark to which other simplified models may be compared.

---

<sup>7</sup>For reasons of industrial confidentiality, neither results of the implemented optimal control strategies, nor figures concerning the improvement in productivity can be disclosed.



An additional problem to be faced is that of monitoring the temperature sensors used in aluminum extrusion. Since these devices are prone to partial failure (i.e. development of bias), and since the measurement of the temperature of the extrudate is imperative for the design of any closed-loop control strategy, the detection of malfunctions in the temperature sensors is of superior importance. The derivation of a simplified dynamic model, the design of a closed-loop control strategy, as well as the monitoring and fault detection of the temperature sensors used in aluminum extrusion is the subject of subsequent chapters.

# Bibliography

- [1] Aluminum Extruders Council. Aluminum Extruders Council Industry Profile Survey. Wauconda, IL, 1991.
- [2] G. Lange. Der Wärmehaushalt beim Strangpressen. *Z. für Metallkunde*, 62, pp.571–584, 1971.
- [3] R. Akeret. A Numerical Analysis of Temperature Distribution in Extrusion. *J. Inst. of Metals*, vol. 95, pp.204–211, 1967.
- [4] A. R. E. Singer and S. H. K. Al-Samarrai. Temperature Changes Associated with Speed Variations during Extrusion. *J. Inst. of Metals*, vol. 89, pp.225–231, 1960/61.
- [5] R.V. Grandhi, A. Kumar, A. Chaudhary, and J. C. Malas. State-Space Representation and Optimal Control of Non-Linear Material Deformation Using the Finite Element Method. *Int. J. Num. Methods in Eng.*, vol.36, pp.1967–1986, 1993.
- [6] R.V. Grandhi, R. Thiagarajan, J. C. Malas, and D. Irwin. Reduced-order State Space Models for Control of Metal-forming Processes. *J. Optimal Control Appl. Methods*, vol.16, pp.19–39, 1995.
- [7] J. C. Malas, D. Irwin, and R.V. Grandhi. An Innovative Strategy for Open Loop Control of Hot Deformation Processes. *J. Mat. Eng. Perf.*, vol.2, pp.703–714, 1993.
- [8] K. Laue and H. Stenger. *Extrusion: Processes, Machinery, Tooling*. American Society for Metals, Ohio, 1981.
- [9] W. Dürrschnabel. Der Materialfluss beim Strangpressen von NE-Metallen (Literaturübersicht). *Metall*, 22, pp.426-437, 995-998, 1215-1219, 1968.

- [10] H. Weber, J. Leopold, and G. Schmidt. Visioplastizität. Wissenschaftliche Schriftenreihe der Technischen Hochschule Karl-Marx 13, Technische Hochschule Karl-Marx, Karl-Marx-Stadt, 1985.
- [11] J. Kelly and F. Kelly. Simulated Isothermal Extrusion. In *Proc. 5th International Extrusion Seminar*, Chicago, U.S.A., vol.2, pp.185–189, 1992.
- [12] S. Kobayashi, S.-I. Oh, and T. Altan. *Metal Forming and the Finite Element Method*. Oxford University Press, New York, 1989.
- [13] O. C. Zienkiewicz and R. L. Taylor. *The Finite Element Method*, volume I and II. McGraw-Hill, London, fourth edition, 1991.
- [14] M. Necati Özişik. *Heat Conduction*. John Wiley & Sons, New York, second edition, 1993.
- [15] R. B. Bird, W. E. Stewart, and E. N. Lightfoot. *Transport Phenomena*. John Wiley & Sons, New York, 1960.
- [16] T. Malvik. The Velocity Distribution Across the Bearing Channel in Aluminum Extrusion. Master's thesis, Norwegian University of Science and Technology, Trondheim, 1992.
- [17] J. W. Brown and R. V. Churchill. *Fourier Series and Boundary Value Problems*. McGraw-Hill, New York, fifth edition, 1993.
- [18] H. H. Thomann. Strömungslehre I, Vorlesungsskript. Swiss Federal Institute of Technology Zurich, 1984.
- [19] T. Altan, S. I. Oh, and H. L. Gegel. *Metal Forming: Fundamentals and Applications*. American Society for Metals, Metals Park, OH, 1983.
- [20] R. Dalheimer. Beitrag zur Frage der Spannungen, Formänderungen und Temperaturen beim axialsymmetrischen Strangpressen. Technical Report, Institut für Umformtechnik der Universität Stuttgart, 1970. Verlag W. Girardet, Essen.

- [21] R. Akeret, H. Jung, and G. Scharf. *Atlas der Warmformgebungseigenschaften von Nichteisenmetallen*, 1978.
- [22] P. Beiss and J. Broichhausen. Warmformänderungsfestigkeit von Aluminiumwerkstoffen. *Metall*, vol.33, pp.639–644, 1979.
- [23] R. H. Wagoner and J. L. Chenot. *Fundamentals of Metal Forming*. John Wiley & Sons, New York, 1997.
- [24] H. Gröber, S. Erk, and U. Grigull. *Die Grundgesetze der Wärmeübertragung*. Springer-Verlag, Heidelberg, third edition, 1981.
- [25] R. Dilger. Modellbildung und Simulation eines räumlich verteilten thermischen Prozesses. Master's thesis, Universität Kaiserslautern, Kaiserslautern, 1992.
- [26] A. Grace. *Optimization Toolbox User's Guide*. The MathWorks, Natick, MA, 1990.
- [27] Institute of Forming Technology, Swiss Federal Institute of Technology Zurich. *PressForm User's Guide, Version 1.3*, 1998.



## Chapter 3

# Nonlinear Model Predictive Control for the Isothermal Extrusion of Aluminum

By deriving a simplified model of the extrusion process, control of the temperature of the extrudate profile can be posed and solved as a nonlinear model predictive control problem. This results in a closed-loop control strategy that directly handles constraints inherent in the process, such as bounds on the extrusion velocity.

### 3.1 Introduction

From a control point of view, one of the main problems arising in the extrusion of aluminum is that of keeping the temperature of the extrudate constant throughout the extrusion cycle while extruding with maximum velocity. This is necessary to ensure product quality and homogeneity at a maximum production rate. Various model-based approaches to trying to control the temperature of the extrudate may be found in the literature. Due to the nature of the process and the complex heat phenomena that take place in extrusion, most of the models upon which these approaches are based are complex and require long computation times [1], [2]. As a consequence, most model-based control strategies for aluminum extrusion are open-loop and are based on the off-line design of optimal velocity trajectories (i.e., optimal with respect to various performance indexes) for a specific profile. Due to disturbances that may be present in an industrial environment, as

well as due to model/plant mismatch, a closed-loop control strategy would be desirable. This chapter derives a closed-loop strategy for the control of the exit temperature in aluminum extrusion. Section 3.2 of this chapter presents a simplified model that is tractable for implementing closed-loop control. In section 3.3 isothermal extrusion of aluminum is then posed and solved as a nonlinear model predictive control problem. By using this closed-loop strategy the temperature of the extrudate section can be made to remain constant throughout the whole extrusion cycle. The chapter closes with some concluding remarks in section 3.4.

## 3.2 Deriving a Simplified Model

The detailed dynamic model of the aluminum extrusion process derived in the previous chapter proved to be suitable for designing open-loop optimal control strategies for the isothermal extrusion of aluminum. Computation time was drastically reduced as compared to other approaches to modeling the extrusion process [1], [2]. Nevertheless, that model is still not suitable for designing easily any model-based feedback control strategy. Optimal velocity trajectories were calculated off-line for a class of extrudate profiles. However, designing these trajectories for the whole product range that may be present in an industrial environment is still a cumbersome task. One would have to fit the parameters of the model for each extrudate profile and then precompute the optimal velocity trajectories for each product class.

For the design of a closed-loop control strategy a simplified and more tractable model is still needed. This section is devoted to the task of deriving such a model. Based on the physical understanding of the process, a simplified model is derived and then compared to the more complex and detailed model presented in Chapter 2. The simplified model is also compared to industrial data. The model presented in this section is based on the idea of dividing the billet into various zones

and formulating heat balances around each of these zones. Although some rather strong assumptions are made with regard to the variations of temperatures in radial direction, which are neglected, as well as with regard to the deformation of the metal, which is assumed to take place only in the foremost part of the billet, the model is tractable and physically appealing. Input-output behavior (i.e., extrusion velocity and exit temperature of the extrudate section) is described well by this simplified model, so that it is attractive for subsequent use in the design of a closed-loop model-based controller for isothermal extrusion of aluminum.

### 3.2.1 Simplified Model of the Extrusion Process

The model derived in this section is based on the model presented by Akeret [3]. The billet and the tooling are divided into various discs. A cross-sectional representation of this is shown in Figure 3.1. Rotational symmetry with respect to the central axis is assumed.

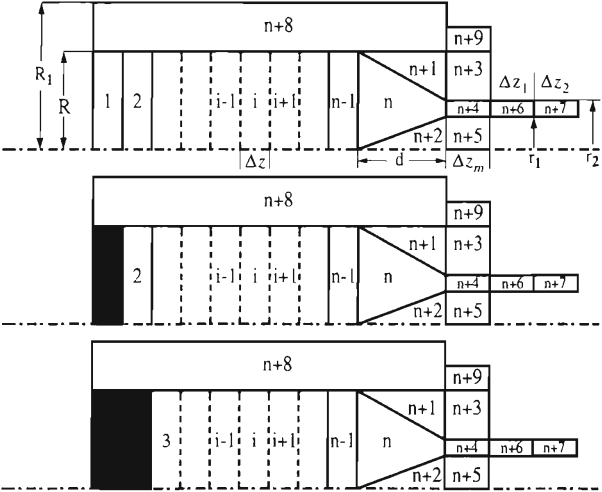


Figure 3.1: Model of the extrusion process.

Material and heat balances are formulated for each zone. The number of discs, representing the undeformed part of the billet, decreases as



the extrusion proceeds. Initially, the billet is divided into  $n - 1$  discs and the deformation zone (zones  $n$ ,  $n + 1$ , and  $n + 2$ ). The metal is treated as a noncompressible fluid, and plug flow is assumed for its flow. Further, it is assumed that deformation of the metal takes place only in the front part of the billet. Radial temperature variations within the billet are neglected. Thus, at each moment in time the temperature within each zone is assumed to be uniform. Heat within the billet flows as a result of the flow of the metal (convection), as well as through conduction. Heat is also generated as a result of friction between the billet and the container. The billet also exchanges heat with the tooling (i.e., the container, disc  $n + 8$ , die,  $n + 3$ ,  $n + 5$ , and die holder  $n + 9$ ). After a length equivalent to the width of a disc has been extruded, its temperature is assumed to remain constant in time, and the heat balance is now formulated for the remaining zones. Consider for instance disc  $i$ . The following equation represents the heat balance for this zone before it is extruded:

$$\Delta z A_0 \rho_{Al} c_{pAl} \frac{dT_i}{dt} = -A_{i/n+8} h_R (T_i - T_{n+8}) + k_{Al} A_0 \frac{(T_{i-1} - T_i)}{\Delta z} - k_{Al} A_0 \frac{(T_i - T_{i+1})}{\Delta z} + A_{i/n+8} \nu_{fr} k_f v_{ram} + \rho_{Al} c_{pAl} A_0 (T_{i-1} - T_i) v_{ram} \quad (3.1)$$

where:

- $n$  = number of discs,
- $T_i$  = temperature of zone  $i$ ,
- $k_f$  = flow stress,
- $A_0$  = cross-sectional area of billet,
- $A_{i/n+8}$  = contact area between section and container,
- $\nu_{fr}$  = coefficient of friction,
- $h_R$  = heat transfer coefficient billet/container,
- $\Delta z$  = width of disc,
- $k_{Al}$  = thermal conductivity of aluminum,
- $\rho_{Al}$  = density of aluminum,
- $c_{pAl}$  = specific heat of aluminum,
- $v_{ram}$  = ram velocity.

In equation (3.1) the first term on the right-hand side represents the heat flux between the respective disc and the container. The heat transfer coefficient  $h_R$  is given by:

$$h_R = \frac{k_{Fe}}{R_{inner} \ln(R_1/R_{inner})}. \quad (3.2)$$

Here,  $k_{Fe}$  stands for the thermal conductivity of the container (steel), while  $R_{inner}$  and  $R_1$  represent the inner and outer radius of the container, respectively. The heat transfer coefficient  $h_R$  is calculated under the steady-state assumption that the heat flux between the billet and the container can be equated to the heat flux due to radial conduction inside the container [4]. The second and third terms on the right-hand side of equation (3.1) stand for the heat flux due to conduction between the specific zone in question and its adjacent zones. The friction force between the billet and the container is given by [5]:

$$F_{friction} = A_{i/n+8} \nu_{fr} k_f. \quad (3.3)$$

Thus the work due to friction while extruding a disc of width  $dz$  is:

$$W_{friction} = A_{i/n+8} \nu_{fr} k_f dz. \quad (3.4)$$

The heat produced due to friction per unit of time is therefore given by:

$$Q_{friction} = A_{i/n+8} \nu_{fr} k_f v_{ram}. \quad (3.5)$$

This is the fourth term on the right-hand side of equation (3.1). The fifth term on the right-hand side of equation (3.1) is the heat flux due

to convection of the metal. In [6], the following empirical relationship for  $k_f$  is found:

$$k_f = A(1 - B\epsilon) \exp(-CT) \dot{\epsilon}^D. \quad (3.6)$$

The coefficients A, B, C, and D depend on the alloy under consideration. Values for various alloys can be found in [6]. The following equation for the strain rate  $\dot{\epsilon}$  is derived in [7]:

$$\dot{\epsilon} = \frac{6v_{ram}\varphi}{R_{inner}}. \quad (3.7)$$

Here,  $\varphi$  stands for the logarithm of the ratio between the cross-section of the billet and the cross-section of the extrudate profile.  $R_{inner}$  is the inner radius of the container, which can be taken to be equal to the radius  $R$  of the billet. Equation (3.7) is only valid if the geometry of the deformation zone is assumed to be constant. However, as soon as the ram reaches the deformation zone, the volume of the deformation zone no longer remains constant, but starts decreasing. This has a direct consequence for the strain rate, as the material at this point experiences a rapid acceleration as it passes through the deformation zone. To exactly describe the deformation phenomena taking place at this point, the volume of the deformation zone and thus the strain rate would have to be considered as a function of time. An alternative approach is to approximate the strain rate  $\dot{\epsilon}$  at this point of the process by the maximum strain rate at the entry of the die as given by the following expression [5]:

$$\dot{\epsilon} = \frac{2v_{exit}}{d}. \quad (3.8)$$

Here the variable  $d$  stands for the diameter of the die, and  $v_{exit}$  for the velocity of the metal at the exit of the die. Once zone  $i$  has been extruded the following is assumed:

$$\frac{dT_i}{dt} = 0. \quad (3.9)$$

The equations for the remaining zones describing the billet are posed analogously to equation (3.1) taking into consideration their respective geometries. For zones  $n + 1$  and  $n + 2$ , it is assumed that the metal does not flow (dead zone). Therefore the terms corresponding to the heat generated by both friction and convection vanish for these two sections. It is further assumed that deformation takes place only in zone  $n$ . For this zone the following term representing the heat generation rate due to deformation must be included [8]:

$$Q_{deformation} = k_f \dot{\epsilon} V_n.$$

In this equation  $V_n$  stands for the volume of section  $n$ , and  $k_f$  and  $\dot{\epsilon}$  for flow stress and strain rate, respectively. The equations for these zones are listed in Appendix F. At the beginning of the extrusion the container exchanges heat with the entire billet. The thermal behavior of the container is thus described by the following equation:

$$\begin{aligned} \rho_{Fe} c p_{Fe} V_{n+8} \frac{dT_{n+8}}{dt} = & A_{1/n+8} h_R (T_1 - T_{n+8}) + A_{2/n+8} h_R (T_2 - T_{n+8}) + \dots \\ & + A_{i/n+8} h_R (T_i - T_{n+8}) + \dots + A_{n-1/n+8} h_R (T_{n-1} - T_{n+8}) \\ & + A_{n+1/n+8} h_R (T_{n+1} - T_{n+8}) - A_{n+8} h_{Fe/Air} (T_{n+8} - T_{air}) \\ & - h_{Fe/Fe} A_{n-8;n+9} (T_{n+8} - T_{n+9}) \end{aligned} \quad (3.10)$$

where:

$$\begin{aligned} V_{n+8} &= \text{volume of section } n+8, \\ h_{Fe/Air} &= \text{heat transfer coefficient container/air,} \\ \rho_{Fe} &= \text{density of steel,} \\ c p_{Fe} &= \text{specific heat of steel,} \\ A_{i/j} &= \text{contact area between sections } i \text{ and } j, \\ A_{n+8} &= \text{outer surface of section } n + 8. \end{aligned}$$

The other variables in equation (3.10) have the same meaning as in equation (3.1). After a length equivalent to a disc has been extruded, it

is assumed that the container exchanges heat only with the remaining discs. Thus, after the first disc has been extruded, the equation which describes the thermal dynamics of the container may be posed in the following manner:

$$\begin{aligned} \rho_{Fe} c_{p_{Fe}} V_{n+8} \frac{dT_{n+8}}{dt} = & A_{2/n+8} h_R (T_2 - T_{n+8}) + \dots + A_{i/n+8} h_R (T_i - T_{n+8}) \\ & + \dots + A_{n-1/n+8} h_R (T_{n-1} - T_{n+8}) + A_{n+1/n+8} h_R (T_{n+1} - T_{n+8}) \\ & - A_{n+8} h_{Fe/Air} (T_{n+8} - T_{air}) - h_{Fe/Fe} A_{n+8/n+9} (T_{n+8} - T_{n+9}). \end{aligned} \quad (3.11)$$

### 3.2.2 Validation of the Simplified Model

The model derived in section 3.2.1 can now be compared to the more detailed model described in chapter 2. This last model has been validated with data from an industrial-scale aluminum extrusion press so that it may indeed be taken as a reference. Various simulations were conducted with both models and compared. In the first set of simulations (Figure 3.2), the initial temperature distribution of the billet was taken as a gradient with  $\Delta T = 50 \text{ }^\circ\text{C}$ . Here  $\Delta T$  stands for the difference between the initial temperatures at the front and rear end of the billet, which were chosen to be  $T_{front} = 515 \text{ }^\circ\text{C}$ , and  $T_{rear} = 465 \text{ }^\circ\text{C}$ . The simulations were stopped once the length of the billet reached  $0.1 \text{ m}$ . The number of discs into which the billet was divided was also varied to investigate its effect on the behavior of the model. The results of these simulations are presented in Figure 3.2. The subdivision of the billet in just two discs is a rather crude representation of the process so that a simulation of the extrusion process in this manner is very inaccurate. The simulations with 6, 10, and 15 discs yield better results and are presented in Figure 3.3 again, for the sake of clarity. As shown in Figure 3.3, simulating the process with 10 or 15 discs does not seem to influence the results significantly. Six discs are sufficient for describing the general input-output behavior of the process. Simulation times for an extrusion cycle using this model are under 30 seconds on a SUN ULTRA1/200E so that this model could indeed be used for a real-time implementation. In the sequel only the

simulation with six discs is considered. To investigate how well the behavior of the exit temperature is described when the velocity does not remain constant in time, further simulations were conducted in which the extrusion velocity was varied. Figure 3.4 shows the results of these simulations. The simplified model reproduces the dynamics of the temperature of the extrudate sufficiently well. It is only towards the end of the extrusion cycle that the two models diverge. In agreement with theoretical calculations [5], a temperature increase towards the end of extrusion is observed if the heat generation rate due to deformation and friction is higher than the heat exchange rate between the container and the billet. It is in this part of the process that the nonlinearities stemming from the terms describing the heat of deformation are the strongest. As expected, the simplified model is not capable of describing very accurately the dynamics of the process in this region. However, for most of the extrusion cycle the agreement between the models is satisfactory.

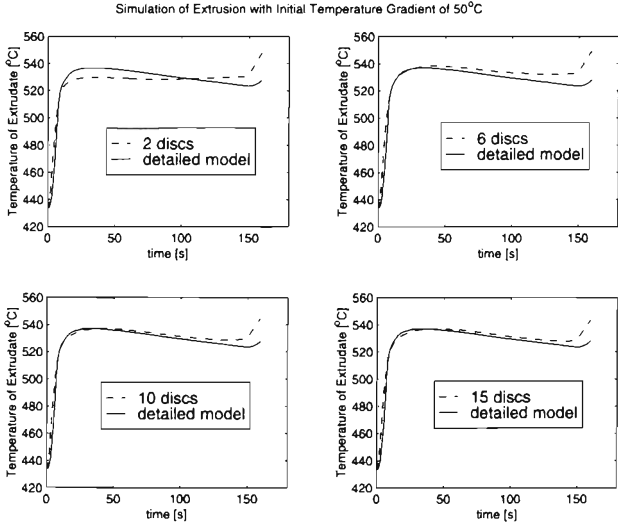


Figure 3.2: Comparison of simplified model with detailed model. Constant extrusion velocity of 6 mm/s. Initial temperature of billet:  $T_{front} = 515\text{ }^{\circ}\text{C}$ ,  $T_{rear} = 465\text{ }^{\circ}\text{C}$ .  $\varphi = \ln(A_0/A_1) = 3$ .

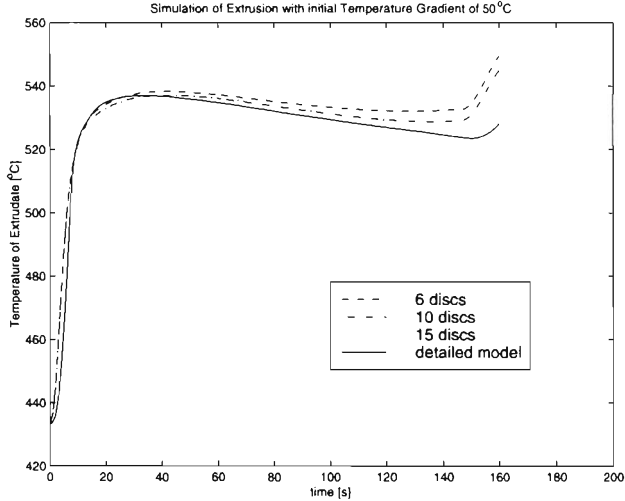


Figure 3.3: Comparison of simplified model with detailed model. Constant extrusion velocity of 6 mm/s. Initial temperature of billet:  $T_{front} = 515\text{ }^{\circ}\text{C}$ ,  $T_{rear} = 465\text{ }^{\circ}\text{C}$ .  $\varphi = \ln(A_0/A_1) = 3$ .

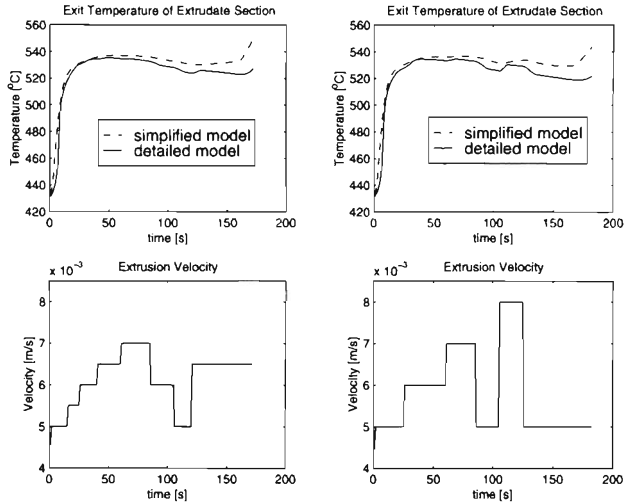


Figure 3.4: Comparison of simplified model with detailed model for various extrusion velocity profiles. Initial temperature of billet:  $T_{front} = 515\text{ }^{\circ}\text{C}$ ,  $T_{rear} = 465\text{ }^{\circ}\text{C}$ .  $\varphi = \ln(A_0/A_1) = 3$ .

For the second set of simulations an initial temperature gradient of  $\Delta T = 70 \text{ }^\circ\text{C}$  was chosen ( $T_{front} = 515 \text{ }^\circ\text{C}$ ,  $T_{rear} = 445 \text{ }^\circ\text{C}$ ). Again, the number of discs into which the billet was divided was also varied to investigate its effect on the behavior of the model. The results are presented in Figure 3.5. The simulation with six discs again reflects the input-output behavior quite well. Figure 3.6 shows the results of the simulation where the extrusion velocity was not held constant but was varied during the extrusion cycle. Once again the simulations were stopped when the remainder of the billet was  $0.1 \text{ m}$  long.

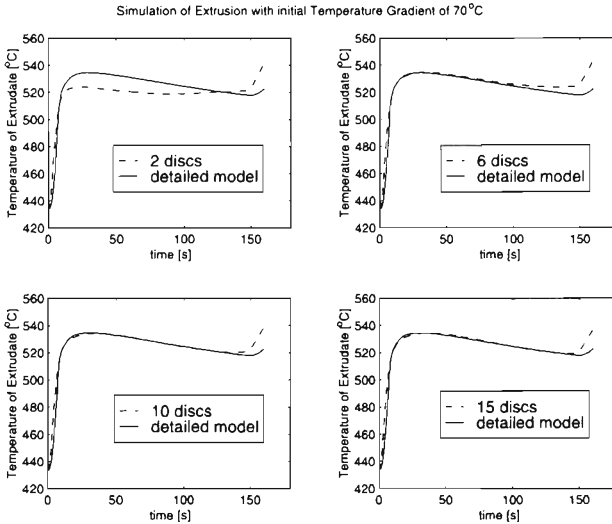


Figure 3.5: Comparison of simplified model with detailed model. Constant extrusion velocity of  $6 \text{ mm/s}$ . Initial temperature of billet:  $T_{front} = 515 \text{ }^\circ\text{C}$ ,  $T_{rear} = 445 \text{ }^\circ\text{C}$ .  $\varphi = \ln(A_0/A_1) = 3$ .



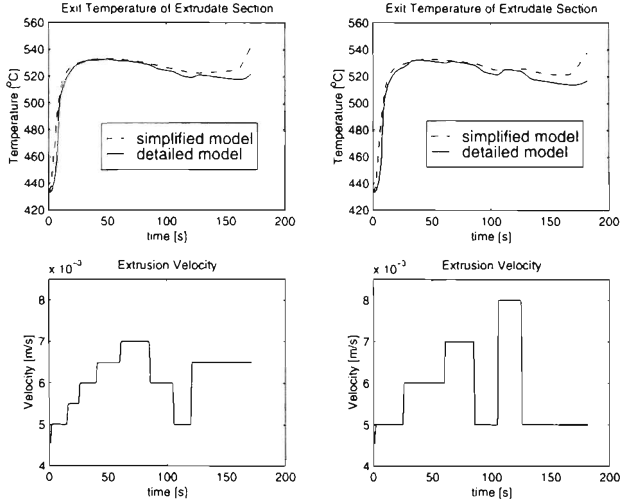


Figure 3.6: Comparison of simplified model with detailed model for various extrusion velocity profiles. Initial temperature of billet:  $T_{front} = 515 \text{ }^\circ\text{C}$ ,  $T_{rear} = 445 \text{ }^\circ\text{C}$ .  $\varphi = \ln(A_0/A_1) = 3$ .

The simulations shown previously indicate that the extrusion velocity has only limited influence on the exit temperature when the initial temperature gradient of the billet is steep. Figures 3.7 - 3.9 show the heat fluxes for the deformation zone and zone 6 for the simulation with an initial temperature gradient of  $\Delta T = 50 \text{ }^\circ\text{C}$  and with the billet divided into six discs. The velocity profile corresponds to the second velocity profile shown in Figure 3.4.

As mentioned in the previous chapter, the front part of the billet is the most important zone as it is here where the most interesting and determining phenomena take place. The rate of heat input into and out of the deformation zone may appear at a first glance to balance each other. However, the difference in these rates as shown in Figure 3.7 is clearly negative for a good part of the cycle, indicating that the temperature of this zone and therefore the exit temperature will decrease during the extrusion cycle. Only in the first part of the extrusion cycle does the rate of heat input into the deformation zone

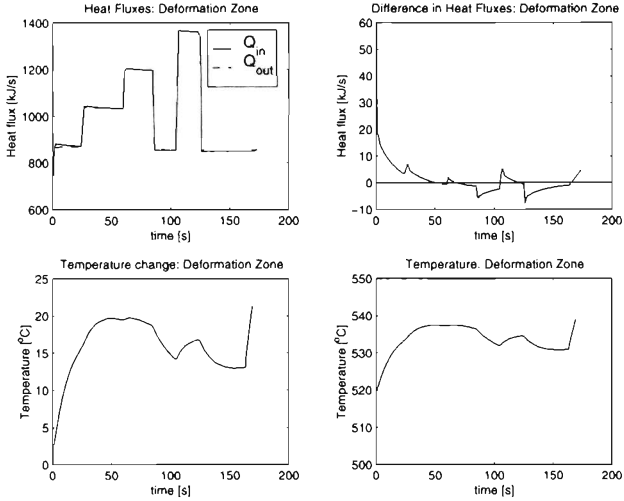


Figure 3.7: *Heat fluxes and temperature in the deformation zone. Initial temperature of billet:  $T_{front} = 515$  °C,  $T_{rear} = 465$  °C.  $\varphi = \ln(A_0/A_1) = 3$ .*

outweigh the rate of heat loss. The jumps in the extrusion velocity do have a marked effect on the heat generation rate due to deformation as clearly seen in Figure 3.8. However, the flux of the cool metal from the rear part of the billet to the front has an overall cooling effect on the different zones and the deformation zone as well. As depicted in Figure 3.8 the net heat flux due to convection for this last zone is negative. Heat is also lost due to conduction from the deformation zone into its adjacent zones so that the heat flux due to conduction is also negative (Figure 3.8). Thus, for a good part of the second half of the extrusion cycle, any increase in the temperature that the heat generation rate due to deformation may cause in the deformation zone is overridden by the heat losses. Convective cooling of the body is perhaps more clearly observed in the temperature of zone 6. This temperature drops throughout the course of the extrusion cycle (Figure 3.9) indicating that in the rear part of the billet convection is the determining factor

for the given initial temperature gradient and velocity profile. It is worth noting, once again, the increase of the heat generation rate due to deformation that can be observed towards the end of the extrusion cycle. As mentioned before, this happens when the length of billet has become small and deformation is rather strong. This heat is not dissipated fast enough, causing an increase in the temperature of the deformation zone and eventually of the exit temperature. It must be remarked that the capability of the simplified model to reflect the dynamics of the process in this part of the process is questionable. The expression for the strain rate in this region as given by equation (3.8) is only an approximation of the real behavior of the strain rate for this part of the process. However, this last segment of the process usually corresponds to the discard, so that it is of no major practical significance. In practice, the process is usually stopped before this section of the extrusion cycle is reached.

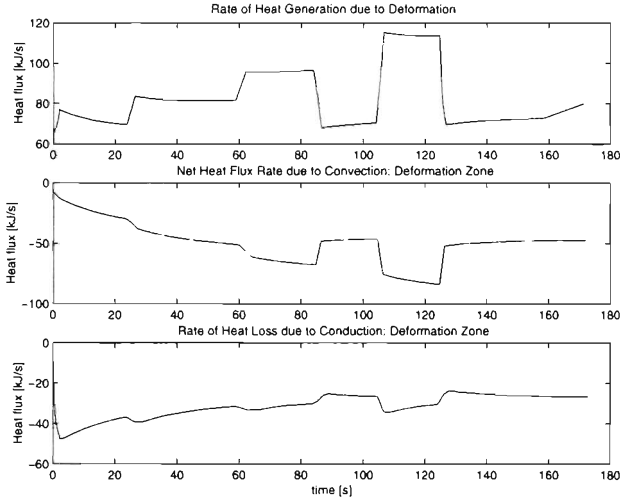


Figure 3.8: Rate of heat loss and gain: deformation zone. Initial temperature of billet:  $T_{front} = 515\text{ }^{\circ}\text{C}$ ,  $T_{rear} = 465\text{ }^{\circ}\text{C}$ .  $\varphi = \ln(A_0/A_1) = 3$ .

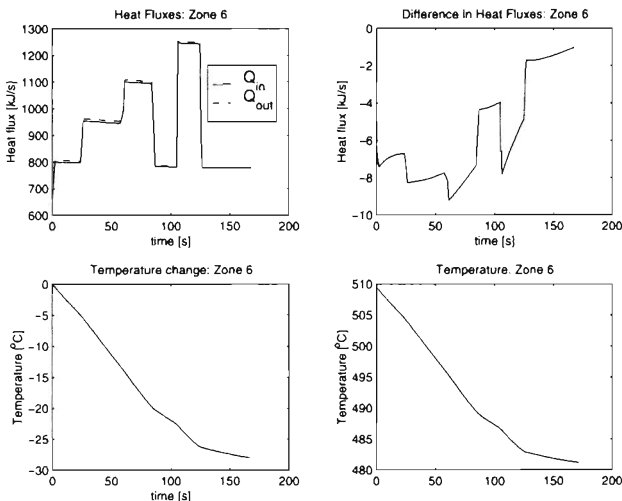


Figure 3.9: Heat fluxes and temperature in zone 6. Initial temperature of billet:  $T_{front} = 515 \text{ }^\circ\text{C}$ ,  $T_{rear} = 465 \text{ }^\circ\text{C}$ .  $\varphi = \ln(A_0/A_1) = 3$ .

### 3.2.3 Validation of the Model with Data from an Industrial Aluminum Extruder

In this section the simplified model is compared to data from an industrial aluminum extruder provided by Alusuisse Technology and Management AG. Figures 3.10–3.11 show the behavior of the temperature of the extrudate and their respective extrusion velocity profiles for different initial temperature gradients of the billet. Once again the initial temperature distributions of the billet were taken as a gradient between the temperatures measured at the front and rear ends of the billet ( $T_{front}$ ,  $T_{rear}$ ). The simplified model resembles the measurements quite reasonably. The mismatch between the model and the measurements is more pronounced on the first part of the extrusion cycle in all cases. However, the difference between measured and simulated temperatures decreases rapidly as the extrusion proceeds. The initial mismatch between the model and the measurements is mainly due to the crude assumptions made for the derivation of the model.

Another source of mismatch may come from the actual initial temperature gradient of the billet when loaded into the container. Even if the billet is loaded into the container immediately after measuring its initial temperature, the difference between this measured gradient and the actual initial temperature gradient of the billet before extrusion begins may be significant. This is why closed-loop control may be necessary in practice. Overall, however, the general dynamics of the temperature (input-output behavior) are described quite well by the simplified model.

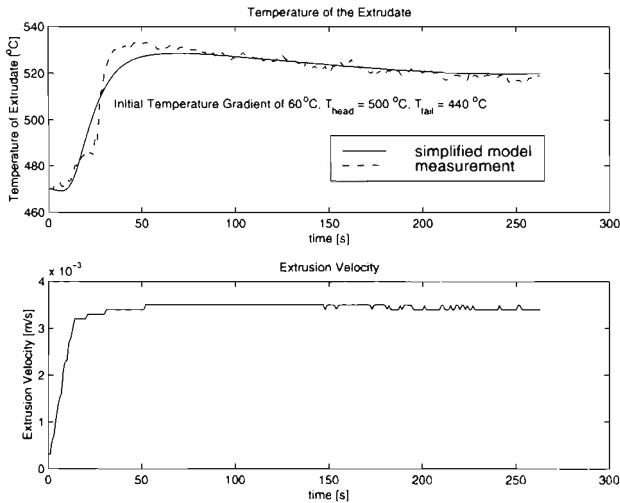


Figure 3.10: Comparison of the simplified model with measured data. Initial temperature gradient of billet:  $\Delta T = 60 \text{ }^\circ\text{C}$ .  $T_{front} = 500 \text{ }^\circ\text{C}$ ,  $T_{rear} = 440 \text{ }^\circ\text{C}$ .  $\varphi = \ln(A_0/A_1) = 3.4$ .

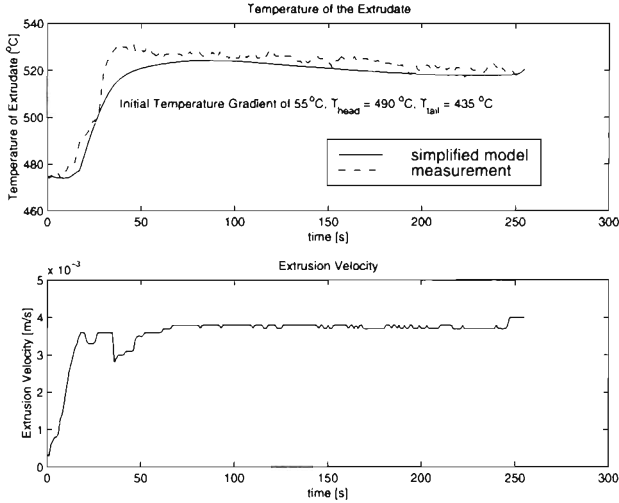


Figure 3.11: Comparison of the simplified model with measured data. Initial temperature gradient of billet:  $\Delta T = 55\text{ }^{\circ}\text{C}$ .  $T_{front} = 490\text{ }^{\circ}\text{C}$ ,  $T_{rear} = 435\text{ }^{\circ}\text{C}$ . Extrusion ratio:  $\varphi = \ln(A_0/A_1) = 3.4$ .

### 3.3 Nonlinear Model Predictive Control of Exit Temperature

The model presented in the previous section can now be used for the design of closed-loop control strategies for the isothermal extrusion of aluminum. Previous work in this direction may be found in the literature. Buchheit and Pandit [9]–[10] present an iterative learning control strategy for aluminum extrusion based on the model of the extrusion process derived by Lange [11]. Although this model makes some rather crude assumptions with respect to the thermal behavior of the billet in the extrusion process, it is tractable and well suited for real-time control. A major disadvantage of this control strategy, however, is the fact that too many iterations (extrusion cycles) may be required until isothermal extrusion is achieved. In industrial practice different types of profiles are extruded batchwise in one and the same

extrusion press. For the desired optimum to be achieved, the iterative learning control may require more learning cycles than are available for a certain profile. More recently, Schwartz et al. [12] proposed a control approach based on neural networks and a complex model described by the finite element method (*FEM*). The focus of that investigation being the control of microstructures for round-to-round extrusion using the ram force as the input signal and the ram velocity as the output of the controller, no attempt is made at controlling the exit temperature of the extrudate. One drawback of that approach is the fact that it requires cumbersome computational training of the artificial network upon which the whole control approach is based. Tibbetts et al. [13], [14] present an approach very similar to the one presented in chapter 2. However, it is unclear whether the models presented can actually be used for real-time control and whether the method used may be extended to more complicated geometries.

The approach presented in this section derives a closed-loop control strategy for isothermal extrusion of aluminum via Model Predictive Control (MPC). The following subsection provides a brief background of the theoretical principles of MPC. Further subsections show the application of MPC to the aluminum extrusion process to achieve isothermal extrusion.

### **3.3.1 MPC: Background**

Model Predictive Control is a widely used method within the chemical and petrochemical industries whereby discrete control actions are obtained solving on-line optimization problems at each time step. Its popularity within the process control community derives from the ease with which physical constraints of multivariate systems may directly be taken into account in the controller design procedure. This is done by properly defining constraints on the inputs, states, or outputs of the system and solving the optimization problem subject to these constraints. Factors reflecting marketplace variations may also be included in the performance index to be minimized, so that

the MPC framework is equally well suited for integrating economic aspects while designing control strategies.

Successful applications of MPC can be traced back to the late 1970's. Cutler and Ramaker [15], as well as Prett and Gillette [16], were among the first to successfully apply this technique to industrial processes. Since the publication of these papers, MPC has progressed rapidly, mainly in the petrochemical industries, building an impressive track record. Richalet et al. report the successful application of MPC to a PVC plant, to the main fractionator of a fluid catalytic cracker, as well as to a power plant steam generator [17]. Various applications of MPC or of some variation thereof have been reported more recently for control of wastewater treatment plants [18], for control of pulp-  
ing plants in the paper industries [19], as well as for the controlled drying of timber [20]. There exists an enormous amount of literature regarding MPC applications as well as theoretical aspects of it. The interested reader is referred to the works of García et al. [21] and Lee [22] for two very extensive and thorough survey papers on this topic.

### MPC: Formulation

A general system description is given by:

$$\begin{aligned} \dot{x}(t) &= f(x(t), u(t)), & x(t_0) &= x_0, \\ y(t) &= h(x(t), u(t)) \end{aligned} \tag{3.12}$$

where  $f: \mathbb{R}^n \times \mathbb{R}^m \rightarrow \mathbb{R}^n$  and  $h: \mathbb{R}^n \times \mathbb{R}^m \rightarrow \mathbb{R}^r$ . Here,  $x \in \mathbb{R}^n$ ,  $y \in \mathbb{R}^r$ , and  $u \in \mathbb{R}^m$  are the state, output, and control input vectors, respectively. As mentioned before, MPC is a discrete-time method, where the control action is obtained by repeatedly solving on-line finite horizon optimization problems, subject to system dynamics and constraints on the states and inputs. The optimization underlying an MPC algorithm is solved at each sampling instant  $t_k$ , and is usually



formulated as follows:

$$\begin{aligned} \min_{u_k(t)} J_k &\equiv \min_{u_k(t)} J(x_k, u_k) \\ &\equiv \min_{u_k(t)} \int_{t_k}^{t_f} L(x(t), u(t), t) dt \end{aligned} \quad (3.13)$$

subject to:

$$\dot{x}(t) - f(x(t), u(t)) = 0, \quad x(t_k) = x_k \quad (3.14)$$

$$y(t) - h(x(t)) = 0 \quad (3.15)$$

$$l(x(t), u(t)) = 0 \quad (3.16)$$

$$c(x(t), u(t)) \geq 0 \quad (3.17)$$

where:

- $J_k$  : objective function to be minimized,
- $x(t)$  : state vector of the system,
- $x_k$  : state vector of the system at time  $t_k$ ,
- $x_k(t)$  : state trajectory of the model for all  $t \in [t_k, t_f]$ , given the condition  $x_k$  at  $t_k$ ,
- $y(t)$  : output vector of the system,
- $u_k(t)$  : control trajectory to be calculated for the time interval  $t \in [t_k, t_f]$ , and the initial condition  $x_k$ ,
- $f$  : model dynamics used for state prediction,
- $h$  : model for computation of predicted outputs,
- $l, c$  : equality and inequality constraints functions, respectively,
- $t_k$  : initial time of computation,
- $t_f$  : terminal time of computation.

The terminal time of computation  $t_f$  is determined by the *prediction horizon*  $p$ , and it is given by  $t_f = t_k + pT_s$ , where  $T_s$  stands for the sampling time. The control input is calculated for a *control horizon*  $m$ , with  $m \leq p$ , and for times  $t_k + mT_s \leq t \leq t_k + pT_s$ , the input vector

$u_k(t) = 0$ . The aforementioned optimization can be reformulated in the discrete-time domain as follows:

$$\min_{\mathcal{U}(k)} J_k \equiv \min_{\mathcal{U}(k)} \sum_{i=1}^p L_i(x(k+i|k), u(k+i-1|k)) \quad (3.18)$$

where:

- $x(k+i|k)$  : predicted state vector at time  $k+i$  based on the states  $x(k|k)$  at time  $k$ , obtained by using prediction model (3.12),
- $\mathcal{U}(k)$  : control moves  $u(k+i)$ ,  $i = 0, \dots, m-1$  calculated by the optimization at time  $k$ ;  $u(k+i|k) = 0$  for  $i \geq m$ ;  $u(k|k)$  denotes the control move implemented at time  $k$ .

If for a specific problem the interest lies in the output of the system following a desired output trajectory  $r_k(t)$  (*tracking problem*), the optimization problem can be restated as follows:

$$\min_{\mathcal{U}(k)} J_k \equiv \min_{\mathcal{U}(k)} \sum_{i=1}^p L_i(e(k+i|k), u(k+i-1|k)) \quad (3.19)$$

where:

- $e(k+i|k)$  : prediction error vector given by  $e(k+i|k) = y(k+i|k) - r(k+i)$ ,
- $y(k+i|k)$  : predicted output vector based on measurement  $y(k|k)$  at time  $k$ , obtained by using the output model,
- $r(k+i)$  : reference trajectory over time interval  $[t_k, t_k + pT_s]$ .

It is sometimes more convenient to define the optimization problem in

terms of the increments in the control move  $\Delta\mathcal{U}(k) = \{\Delta u(k+i|k), i = 0, \dots, m-1\}$ , where:

$\Delta u(k|k)$  : control increments at time  $k$  given by:

$$\Delta u(k|k) = u(k|k) - u(k-1|k-1),$$

$\Delta u(k+i|k)$  : control increments at time  $k+i$  given by:

$$\Delta u(k+i|k) = u(k+i|k) - u(k+i-1|k),$$

$$i \in [1, m-1].$$

### MPC Implementation: Receding Horizon (RH)

The general control structure of an MPC scheme is depicted in Figure 3.12.

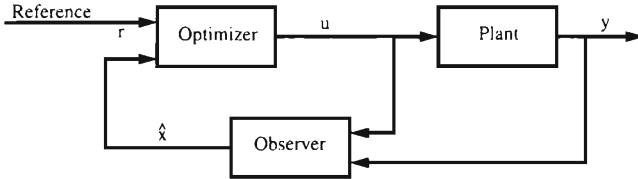


Figure 3.12: *General MPC structure.*

The state is estimated via an observer, using the inputs and measured outputs. This estimate is used to predict the trajectory of the controlled variables  $y$  over a prediction horizon  $p$  when the manipulated variables  $u$  are varied over a control horizon  $m$ . At time step  $k$ , the optimizer computes  $m$  future control moves  $(u(k|k), \dots, u(k+m-1|k))$  such that the predicted outputs deviate minimally from the selected reference trajectory. As mentioned before, constraints on the inputs and outputs are directly incorporated into the optimization. Although the open-loop optimization problem solved at time  $k$  calculates an optimal sequence of  $m$  present and future control moves, only the first control move,  $u(k|k)$ , is injected into the plant over the time  $[k, k+1]$ . At time step  $k+1$ , the prediction horizon  $p$ , and the control horizon  $m$  are shifted ahead by one step. Feedback is incorporated by using

plant measurements to update the state estimation vector  $\hat{x}$ . The optimization problem is now solved again using the estimate  $\hat{x}(k+1)$  as the initial condition for the prediction. This form of implementation is known as *receding* or *moving* horizon approach [23] and its principle is depicted in Figure 3.13.

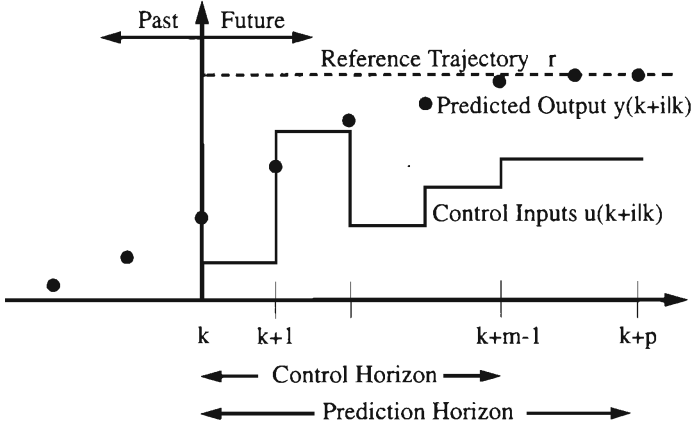


Figure 3.13: *Receding Horizon Implementation.*

The MPC framework has been briefly outlined in this section. The following sections deal with the particular application of MPC to the aluminum extrusion process.

### 3.3.2 Isothermal Extrusion via Nonlinear Model Predictive Control

Isothermal extrusion of aluminum is of interest in industrial practice to guarantee uniform product quality [5]. To achieve this, the extrusion velocity must be adjusted continuously throughout the whole extrusion cycle to balance the various heat phenomena taking place in the process. The objective is therefore the calculation of the velocity profile  $v(t)$  needed so that the temperature of the extrudate section  $T_{extrudate}(t)$  deviates minimally from the desired reference temperature

$T_{setpoint}$ . The determination of this velocity profile can be posed as an optimization problem. The target function to be minimized is the following:

$$J = \int_{t=0}^{t=t_{final}} (T_{extrudate}(t) - T_{setpoint})^2 dt . \quad (3.20)$$

This objective function should be minimized using some control input  $u(t)$ , which in this case is the extrusion velocity. An alternative way of stating the optimization problem results if the extrusion cycle is subdivided into a series of time intervals  $\Delta t$ . At each time step  $i$  a prediction of the process over a horizon  $p$  is made. The input is then chosen over a control horizon  $m$  so as to minimize the following quadratic objective:

$$J(i) = \sum_{j=1}^p [T_{extrudate}(i+j) - T_{setpoint}]^2 . \quad (3.21)$$

In order to obtain a smooth velocity profile and thus avoid strong variations of the manipulated variable, equation (3.21) is extended to:

$$J(i) = \sum_{j=1}^p [T_{extrudate}(i+j) - T_{setpoint}]^2 + \sum_{j=0}^{m-1} [\lambda \Delta u(i+j)]^2 . \quad (3.22)$$

The factor  $\lambda$  in equation (3.22) influences the behavior of the control algorithm. Large values of  $\lambda$  penalize strong variations of the manipulated variable. Small values of  $\lambda$  give more importance to the deviations of the measured output from the setpoint. Moreover, the extrusion velocity may vary only within certain bounds. These bounds correspond to the maximum and minimum extrusion velocities achievable at the extrusion press in consideration. Taking into account the nonlinear model for the extrusion process described in Section 3.2,

the nonlinear programming problem to be solved at each time step is stated as:

$$\underset{u_i \dots u_{i+m-1}}{\text{minimize}} \quad J(i) \quad (3.23)$$

subject to:

$$u_{min} \leq u_{i+j} \leq u_{max}, \quad j = 0, 1, \dots, m - 1 \quad (3.24)$$

$$\frac{d\mathbf{T}}{dt} - f[\mathbf{T}(t), u] = 0. \quad (3.25)$$

Here,  $\mathbf{T}$  is a vector of dimension  $(n + 9)$  (number of zones) and whose components are the temperatures of each of the zones. The problem stated above is a nonlinear model predictive control problem by means of a  $p$ -step ahead prediction of the behavior of the process [24].

### Estimating the States of the System

The only measurements that are usually available in the extrusion process are the temperature of the extrudate and the extrusion velocity. The former is taken to be the output of the model, while the latter is the control input. The remaining states of the model must be estimated by means of an observer. For this nonlinear system, this filtering problem may be solved by means of an extended Kalman filter (EKF) [25]. For the extrusion process, it is assumed that the system's noise is an additive purely random noise with expected value  $E(\omega_i) = \bar{\omega}_i$  and covariance matrix  $Q_i$ . Thus:

$$\mathbf{T}_{i+1} = g(\mathbf{T}_i, u_i) + \Gamma_i \omega_i. \quad (3.26)$$

The measurement is corrupted by some noise, which is also assumed to be additive purely random noise:

$$y_i = h(\mathbf{T}_i, u_i) + \nu_i \quad (3.27)$$

with expected value and covariance matrix  $E(\nu_i) = 0$  and  $R_i$ , respectively. Both noise sequences  $\omega_i$  and  $\nu_i$  are assumed to be independent.

Additionally, it is assumed that the initial state  $\mathbf{T}_0$  has an expected value  $E(\mathbf{T}_0) = \bar{\mathbf{T}}_0$ , a covariance matrix  $P_0$ , and that it is independent of the two noise sequences  $\omega_i$  and  $\nu_i$ . With these assumptions the equations for the filter are stated as follows [26]:

$$\hat{\mathbf{T}}_i = \bar{\mathbf{T}}_i + K_i(y_i - h(\bar{\mathbf{T}}_i, u_i)) \quad (3.28)$$

$$\bar{\mathbf{T}}_{i+1} = g_i(\hat{\mathbf{T}}_i, u_i) + \Gamma_i \bar{\omega}_i \quad (3.29)$$

$$K_i = P_i \left( \frac{\partial h_i}{\partial \mathbf{T}_i} \right)^T R_i^{-1} \quad (3.30)$$

$$P_i = M_i - M_i \left( \frac{\partial h_i}{\partial \mathbf{T}_i} \right)^T \left[ \frac{\partial h_i}{\partial \mathbf{T}_i} M_i \left( \frac{\partial h_i}{\partial \mathbf{T}_i} \right)^T + R_i \right]^{-1} \frac{\partial h_i}{\partial \mathbf{T}_i} M_i \quad (3.31)$$

$$M_{i+1} = \frac{\partial g_i}{\partial \mathbf{T}_i} P_i \left( \frac{\partial g_i}{\partial \mathbf{T}_i} \right)^T + \Gamma_i Q_i \Gamma_i^T. \quad (3.32)$$

Here  $\bar{\mathbf{T}}_i$  and  $\hat{\mathbf{T}}_i$  stand for the estimate of  $\mathbf{T}_i$  before and after measurement, respectively. At each time step, the partial derivatives  $\partial h_i / \partial \mathbf{T}_i$  and  $\partial g_i / \partial \mathbf{T}_i$  are evaluated at  $\mathbf{T}_i = \bar{\mathbf{T}}_i$  and  $\mathbf{T}_i = \hat{\mathbf{T}}_i$ , respectively. Figure 3.14 shows results of the estimations of some of the states of the system. For these simulations the noise sequences of the system ( $\omega_i$ ) and measurement ( $\nu_i$ ) were chosen to be zero mean, with covariance  $Q = R = 5$ . These results correspond to a model in which the billet was subdivided into six discs. The results of the estimation of the remaining states are equally satisfactory and can be found in Appendix G.

### Control of Exit Temperature

The control algorithm outlined in the previous sections can now be tested through simulations. The complete control scheme was implemented in MATLAB/SIMULINK. A block diagram is shown in Figure 3.15. For the first set of simulations the noise sequences of the measurement and the system were taken to be zero mean white noise with covariance  $Q = R = 5$ . The initial temperature gradient of

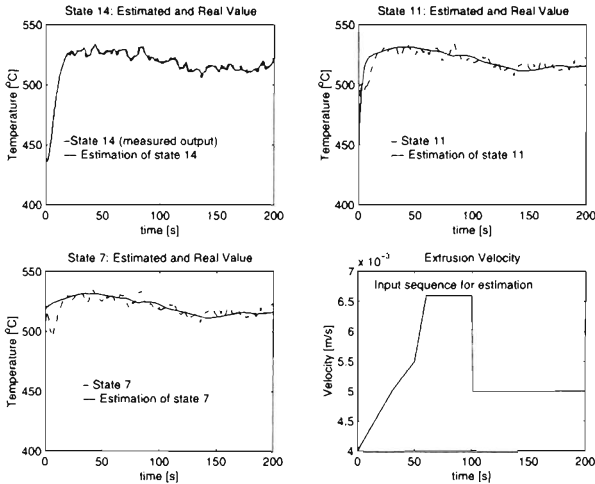


Figure 3.14: *Estimation of states via EKF.*

the billet was chosen to be  $\Delta T = 50^\circ\text{C}$  (with  $T_{front} = 515^\circ\text{C}$ , and  $T_{rear} = 465^\circ\text{C}$ ). The control and prediction horizons were set to  $m = 5\text{ s}$  and  $p = 25\text{ s}$ , respectively. A sampling time of  $T_s = 1\text{ s}$  was chosen. Figures 3.16 and 3.17 show results for  $T_{setpoint} = 520^\circ\text{C}$  and  $T_{setpoint} = 530^\circ\text{C}$ , respectively. Results for various values of the factor  $\lambda$  are shown. In all the simulations, the temperature of the extrudate stays close to the setpoint temperature  $T_{setpoint}$  throughout the complete extrusion cycle. For the simulations shown in Figure 3.18 an initial temperature gradient of the billet of  $\Delta T = 70^\circ\text{C}$  (with  $T_{front} = 515^\circ\text{C}$ , and  $T_{rear} = 445^\circ\text{C}$ ) was chosen. Once again simulations for  $T_{setpoint} = 520^\circ\text{C}$  and  $530^\circ\text{C}$  are shown.



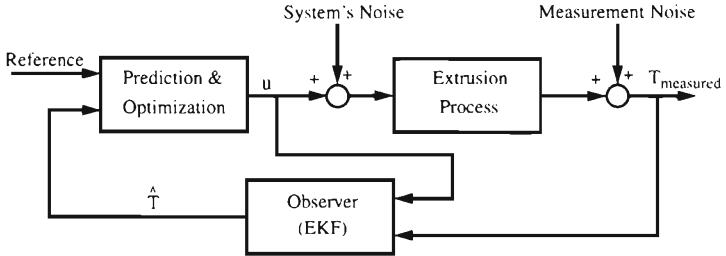


Figure 3.15: Structure of closed-loop nonlinear model predictive controller.

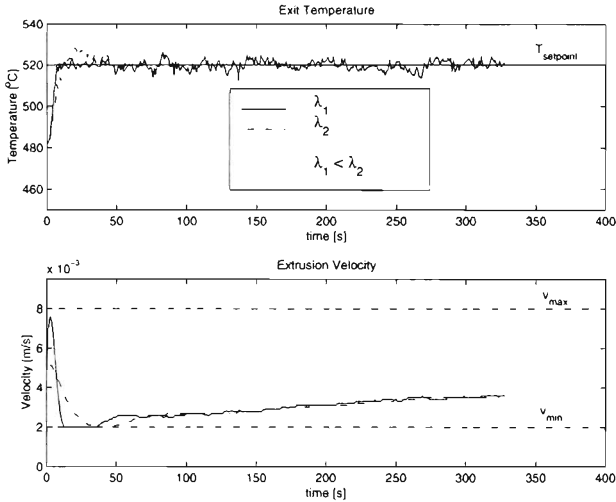


Figure 3.16: Nonlinear model predictive control: exit temperature with respective velocity trajectories for an initial temperature gradient of the billet of  $\Delta T = 50 \text{ }^\circ\text{C}$ .  $T_{\text{setpoint}} = 520 \text{ }^\circ\text{C}$ .  $\varphi = \ln(A_0/A_1) = 3$ .

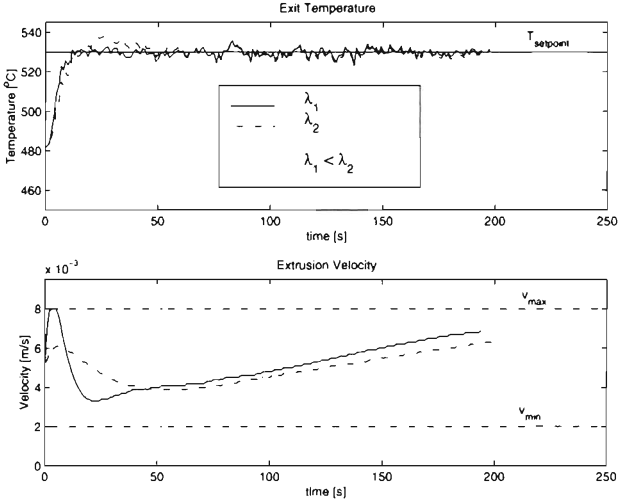


Figure 3.17: *Nonlinear model predictive control: exit temperature with respective velocity trajectories for an initial temperature gradient of the billet of  $\Delta T = 50\text{ }^{\circ}\text{C}$ .  $T_{\text{setpoint}} = 530\text{ }^{\circ}\text{C}$ .  $\varphi = \ln(A_0/A_1) = 3$ .*

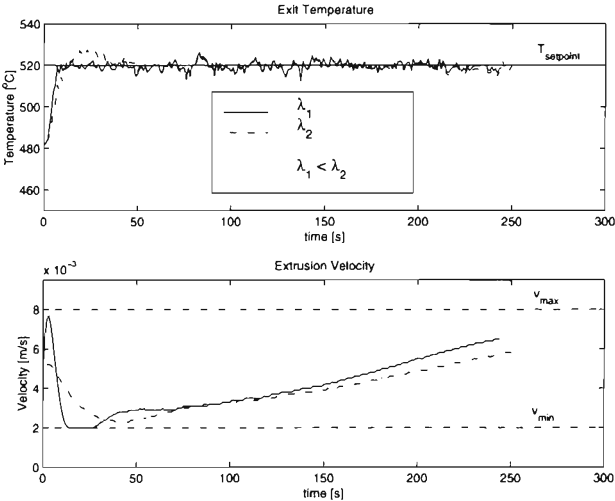


Figure 3.18: *Nonlinear model predictive control: exit temperature with respective velocity trajectories for an initial temperature gradient of the billet of  $\Delta T = 70\text{ }^{\circ}\text{C}$ .  $T_{\text{setpoint}} = 520\text{ }^{\circ}\text{C}$ .  $\varphi = \ln(A_0/A_1) = 3$ .*

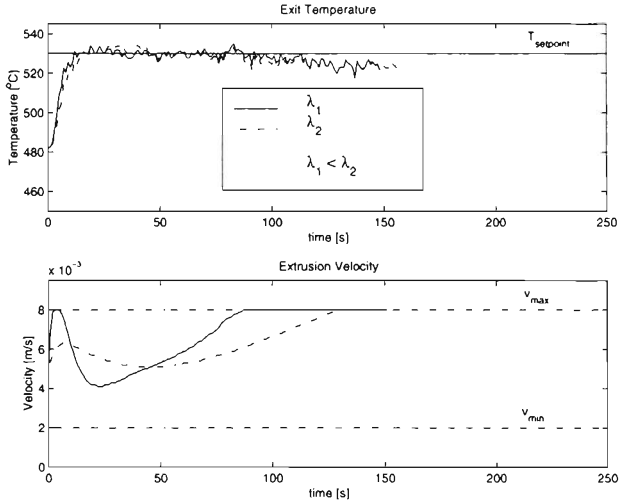


Figure 3.19: *Nonlinear model predictive control: exit temperature with respective velocity trajectories for an initial temperature gradient of the billet of  $\Delta T = 70$  °C.  $T_{setpoint} = 530$  °C.  $\varphi = \ln(A_0/A_1) = 3$ .*

In the last case, where the initial temperature gradient is  $\Delta T = 70$  °C and the temperature setpoint is  $T_{setpoint} = 530$  °C, the steep initial temperature gradient of the billet forces the velocity to hit the upper bound for a long portion of the extrusion cycle. The heat produced due to deformation is not able to balance the heat losses of the billet to the container and convection. This is shown in Figures 3.20 - 3.21, where the various heat fluxes for the deformation zone are portrayed. In Figure 3.20 the solid line represents the rate of heat gain for the deformation zone due to deformation, and convection of the metal into that zone. The dashed line represents the rate of heat loss to the container and die, and the rate of heat loss due to convection of the metal flowing out of this zone. The rate of heat loss outweighs the rate of heat gain for a significant part of the extrusion cycle. Consequently the temperature decreases. The controller tries to correct this and hits the upper bound of the velocity for most of the extrusion cycle (maximum heat production rate due to deformation).

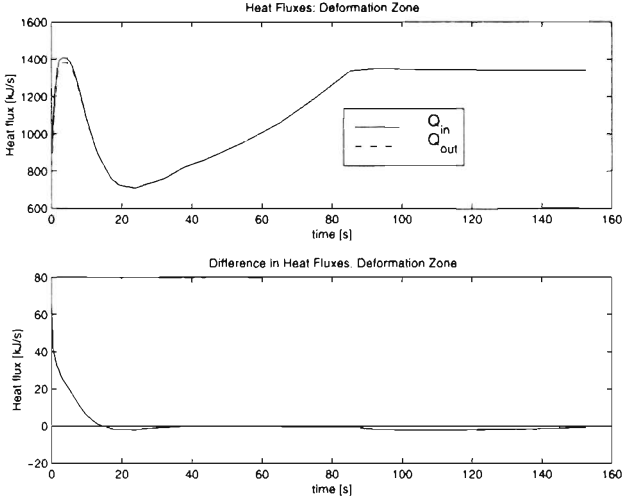


Figure 3.20: *Heat fluxes: deformation zone. Initial temperature gradient of the billet:  $\Delta T = 70\text{ }^{\circ}\text{C}$ .  $T_{\text{setpoint}} = 530\text{ }^{\circ}\text{C}$ .  $\varphi = \ln(A_0/A_1) = 3$ .*

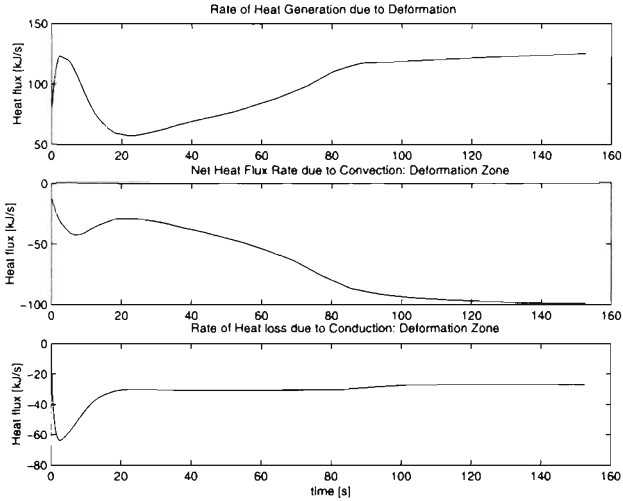


Figure 3.21: *Rate of heat loss and gain: deformation zone. Initial temperature gradient of the billet:  $\Delta T = 70\text{ }^{\circ}\text{C}$ .  $T_{\text{setpoint}} = 530\text{ }^{\circ}\text{C}$ .  $\varphi = \ln(A_0/A_1) = 3$ .*

Simulations with the velocity trajectories calculated by the MPC controller and the respective initial conditions discussed previously were conducted with the detailed model presented in the previous chapter. The results are depicted in the Figures 3.22 - 3.25. The temperature of the extrudate section as simulated by the detailed model does not exactly remain constant. However, the difference between this temperature and the setpoint temperature is always small. Once again, this confirms the capability of the simplified model to reflect the dynamics of the temperature of the extrudate. The results with the detailed model and the trajectories generated by the simplified model are meaningful. It must be stated that the use of the detailed model for MPC purposes would not be justified, considering the simulation time needed with this model and the results achieved by using the simplified model.

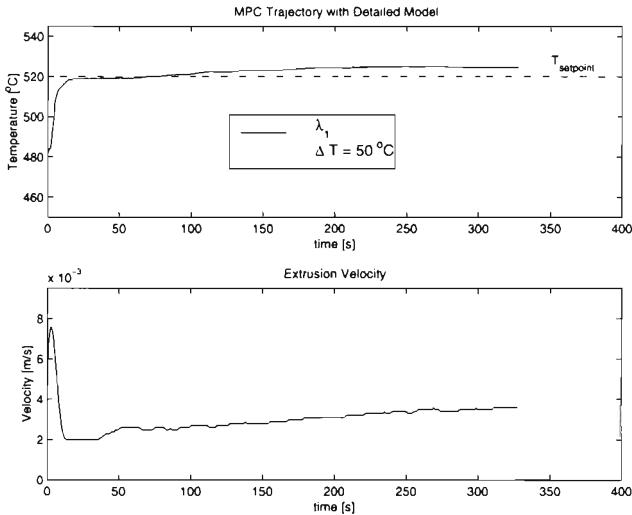


Figure 3.22: MPC trajectories with detailed model. Initial temperature gradient of the billet:  $\Delta T = 50 \text{ }^\circ\text{C}$ .  $T_{\text{setpoint}} = 520 \text{ }^\circ\text{C}$ .  $\varphi = \ln(A_0/A_1) = 3$ .

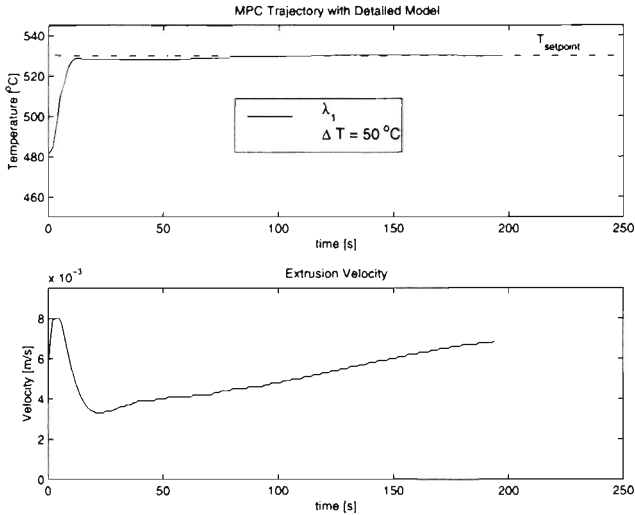


Figure 3.23: *MPC trajectories with detailed model. Initial temperature gradient of the billet:  $\Delta T = 50^\circ\text{C}$ .  $T_{setpoint} = 530^\circ\text{C}$ .  $\varphi = \ln(A_0/A_1) = 3$ .*

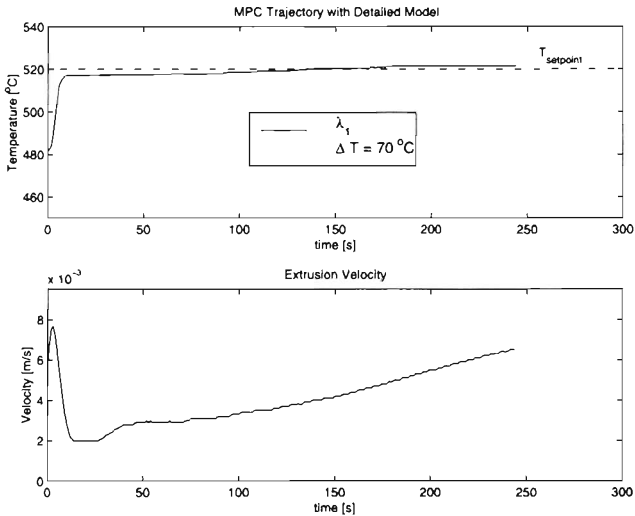


Figure 3.24: *MPC trajectories with detailed model. Initial temperature gradient of the billet:  $\Delta T = 70^\circ\text{C}$ .  $T_{setpoint} = 520^\circ\text{C}$ .  $\varphi = \ln(A_0/A_1) = 3$ .*

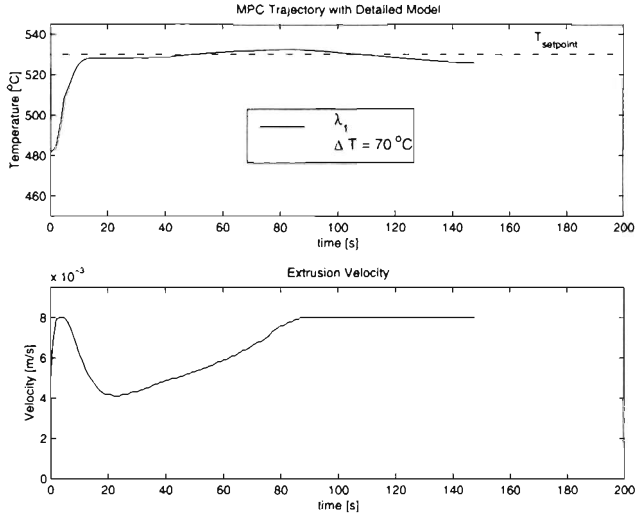


Figure 3.25: *MPC trajectories with detailed model. Initial temperature gradient of the billet:  $\Delta T = 70 \text{ }^\circ\text{C}$ .  $T_{\text{setpoint}} = 530 \text{ }^\circ\text{C}$ .  $\varphi = \ln(A_0/A_1) = 3$ .*

The MPC strategy presented previously yields good results as far as isothermal extrusion is concerned. However, as seen in the case of the simulation with an initial temperature gradient of  $\Delta T = 50 \text{ }^\circ\text{C}$  (with  $T_{\text{front}} = 515 \text{ }^\circ\text{C}$ , and  $T_{\text{rear}} = 465 \text{ }^\circ\text{C}$ ) and a setpoint temperature of  $T_{\text{setpoint}} = 520 \text{ }^\circ\text{C}$ , the extrusion time may be rather long. To achieve a constant temperature of the extrudate at a faster extrusion time, the initial temperature of the gradient has to be chosen properly. This has already been mentioned in previous chapters. A simulation was conducted again for an initial temperature gradient of  $\Delta T = 50 \text{ }^\circ\text{C}$ , this time with  $T_{\text{front}} = 490 \text{ }^\circ\text{C}$ , and  $T_{\text{rear}} = 440 \text{ }^\circ\text{C}$ , and  $T_{\text{setpoint}} = 520 \text{ }^\circ\text{C}$ . The results are portrayed in Figure 3.26. A reduction of  $25 \text{ }^\circ\text{C}$  in the temperature  $T_{\text{front}}$  from the simulation previously mentioned already causes a considerable reduction in the extrusion time while still achieving isothermal extrusion. This once again highlights the importance of properly choosing the initial temperature of the billet so as to achieve isothermal extrusion at an acceptable extrusion time.

It may be questioned at this point as to why use feedback control in the extrusion process if by properly choosing the initial temperature of the billet isothermal extrusion may be perfectly achieved by means of open-loop control. The answer to this lies in the uncertainty on the knowledge of the actual initial temperature of the billet as well as in the noise entering the system. These effects can cause performance degradation of the open-loop strategies. Feedback control is able to at least partially counterbalance these effects, therefore ensuring isothermal extrusion.

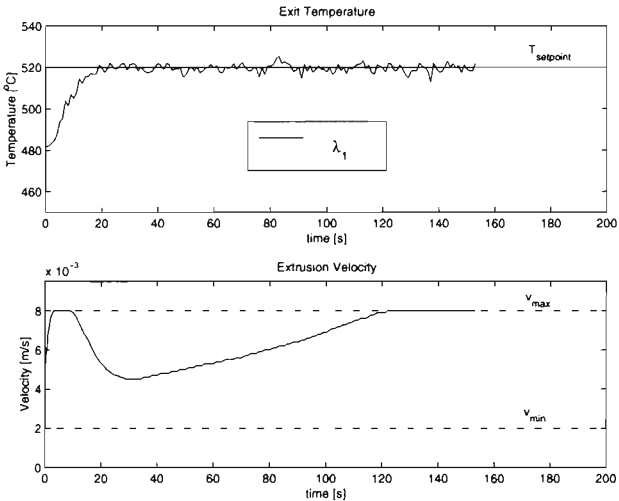


Figure 3.26: *Nonlinear model predictive control: exit temperature with respective velocity trajectories for an initial temperature gradient of the billet of  $\Delta T = 50$  °C.  $T_{front} = 490$  °C, and  $T_{rear} = 440$  °C.  $T_{setpoint} = 520$  °C.  $\varphi = \ln(A_0/A_1) = 3$ .*

### 3.4 Conclusions

In this chapter a simplified dynamic model for the extrusion of aluminum has been derived and presented. The model has been validated not only by comparison with a more detailed and exact



model, but also by comparison with measurements of an industrial aluminum extruder. The model was then used to design a feedback control strategy for the isothermal extrusion of aluminum. It has been shown that the control problem of isothermal extrusion of aluminum can be posed and solved as a nonlinear model predictive control problem. Bounds on the extrusion velocity, a natural constraint of the system, can therefore readily be taken into account while designing the control strategy. The performance of the controller has been tested through simulations for different initial conditions of the temperature gradient of the billet, as well as for different setpoint temperatures. It has been shown that if the initial temperature of the billet has been chosen in an unfavorable manner, isothermal extrusion may not be achieved even if the extrusion is carried out at the maximum speed possible on a particular extrusion press. As far as the author knows, this is the first time in the literature that a model-based closed-loop control strategy for the isothermal extrusion of aluminum has been derived and presented.

Other problems that arise in extrusion processes may be tackled in a similar manner. In many cases, requiring uniform product quality may not be as important as for example maximizing productivity (minimizing extrusion time). This problem may be posed in a similar manner by defining the appropriate target function (minimum-time control problem), taking into account the respective constraints (maximum extrusion temperature that the metal can withstand, maximum extrusion velocity, etc.) If the importance lies rather on the side of microstructure considerations, other objective functions may be defined. Constraints on the maximum extrusion temperature and maximum flow stress must then be taken into consideration.

The MPC strategy presented in this chapter has only been tested through simulations. Nevertheless, the model is simple and tractable so that an eventual implementation in an industrial environment should not pose any major problems. However, a relevant aspect

here may be the computation times required for the optimizations. Indeed, computation times still have to be reduced by a factor of 2–4 by optimizing the algorithm in order for it to be considered for implementation in an industrial environment.

# Bibliography

- [1] R. V. Grandhi, A. Kumar, A. Chaudhary, and J. C. Malas. State-Space Representation and Optimal Control of Non-Linear Material Deformation Using the Finite Element Method. *Int. J. Num. Methods in Eng.*, vol.36, pp.1967–1986, 1993.
- [2] R. V. Grandhi, R. Thiagarajan, J. C. Malas, and D. Irwin. Reduced-order State Space Models for Control of Metal-forming Processes. *J. Optimal Control Appl. Methods*, vol.16, pp.19–39, 1995.
- [3] R. Akeret. A Numerical Analysis of Temperature Distribution in Extrusion. *J. Inst. of Metals*, vol. 95, pp.204–211, 1967.
- [4] D. Q. Kern. *Process Heat Transfer*. McGraw-Hill, Singapore, 1965.
- [5] K. Laue and H. Stenger. *Extrusion: Processes, Machinery, Tooling*. American Society for Metals, Ohio, 1981.
- [6] R. Akeret, H. Jung, and G. Scharf. *Atlas der Warmformgebungseigenschaften von Nichteisenmetallen*, 1978.
- [7] H. P. Stüwe. Einige Abschätzungen zum Strangpressen. *Metall*, vol. 22, pp.1197–1200, 1968.
- [8] T. Altan, S. I. Oh, and H. L. Gegel. *Metal Forming: Fundamentals and Applications*, chapter 5. American Society for Metals, Metals Park, Ohio, 1983.
- [9] M. Pandit and K. Buchheit. Isothermes Strangpressen von Aluminium, Teil I. *Aluminium*, vol. 4, pp.483–487, 1995.

- [10] M. Pandit and K. Buchheit. Control Schemes for a Cyclically Operating Aluminum Extruder Plant. In *Proc. 3rd IEEE Conf. on Contr. Applicat.*, Glasgow, Scotland, vol.1, pp.525–531, 1994.
- [11] G. Lange. Der Wärmehaushalt beim Strangpressen. *Z. für Metallkunde*, 62, pp.571–584, 1971.
- [12] C.A. Schwartz and J. M. Berg. Neural-Network Feedback Control of an Extrusion. *IEEE Trans. on Control Systems Technology*, 6, (2), pp.180–187, 1998.
- [13] B. R. Tibbetts and J. Weng. Extrusion Process: Control, Identification, and Optimization. *IEEE Trans. on Control Systems Technology*, 6, (2), pp.134–145, 1998.
- [14] B. R. Tibbetts and J. Weng. Application of Modern Control and Modeling Techniques to Extrusion Processes. In *Proc. 4th IEEE Conf. on Contr. Applicat.*, Albany, NY, vol.1, pp.85–90, 1995.
- [15] C. R. Cutler and B. L. Ramaker. Dynamic Matrix Control – A Computer Control Algorithm. In *Proc. AIChE National Meeting*, Houston, TX, 1979.
- [16] D. M. Prett and R. D. Gillette. Optimization and Constrained Multivariable Control of a Catalytic Cracking Unit. In *Proc. AIChE National Meeting*, Houston, TX, 1979.
- [17] J. Richalet, A. Rault, J. L. Testud, and J. Papon. Model Predictive Heuristic Control: Applications to Industrial Processes. *Automatica*, 14, pp.413–428, 1978.
- [18] S. Menzi and M. Steiner. Model-based Control for Nitrogen-Eliminating Wastewater Treatment Plants. In *Proc. 4th IEEE Conf. on Contr. Applicat.*, Albany, NY, vol.2, pp.842–847, 1995.
- [19] D. di Ruscio. Model Predictive Control and Identification of a Thermo Mechanical Pulping Plant. In *Proc. Control 97*, Sydney, Australia, pp.428–433, 1997.

- [20] H. E. Musch, G. Barton, T. Langrish, and A. Brooke. Nonlinear Model Predictive Control of Timber Drying. *Comp. & Chem. Engng.*, 22, (3), pp.415–425, 1998.
- [21] C. E. García, D. M. Prett, and M. Morari. Model Predictive Control: Theory and Practice – a Survey. *Automatica*, 25, (3), pp.335–348, 1989.
- [22] J. H. Lee and B. Cooley. Recent Advances in Model Predictive Control and Other Related Areas. In J. C. Kantor, C. E. García, and B. Carnahan, editors, *Chemical Process Control – CPC-V, Proc. Fifth Int. Conf. on Chemical Process Control*, Tahoe City, CA, pp.201–216, 1997. CACHE.
- [23] A. I. Propoi. Use of LP Methods for Synthesizing Sampled-Data Automatic Systems. *Automation and Remote Control*, 24, pp.837, 1963.
- [24] A. A. Patwardhan, J. B. Rawlings, and T. F. Edgar. Nonlinear Model Predictive Control. *Chem. Eng. Comm.*, 87, pp.123–141, 1990.
- [25] A. H. Jazwinski. *Stochastic Processes and Filtering Theory*. Academic Press, New York, 1970.
- [26] A. E. Bryson and Y.-C. Ho. *Applied Optimal Control*. Hemisphere Publishing Corporation, New York, 1975.

## Chapter 4

# Monitoring and Fault Detection of Sensors in Aluminum Extrusion via Statistical Methods

The accurate measuring of the temperature of the extrudate profile in aluminum extrusion is a challenging task. The temperature sensors, mostly pyrometers usually found in industrial practice, are prone to partial failure, and hence may be unreliable. The detection of faults on these sensors via statistical methods is the main focus of this chapter.

### 4.1 Introduction

The increasing complexity of industrial processes, tighter standards on product quality, higher demands on reliability and safety of plant components, as well as an increasing awareness of the impact of industrial accidents on society and environment within the last 15 years have led the control and systems engineering community to turn its attention to the field of monitoring and fault detection of systems and industrial processes. Indeed, it could be argued that even though there are still important open questions and problems within the framework of designing automatic feedback control algorithms, most processes and systems are already being controlled rather efficiently. However, control engineers have the responsibility of ensuring that control applications are performing according to specifications. With systems becoming increasingly automated and instrumented, control engineers are finding it harder to effectively monitor the performance

of control algorithms and to diagnose problems associated therewith. As a consequence, poorly performing applications often go unnoticed for a lengthy period of time, this perhaps leading to poor quality and risk not only to personnel but ultimately to society. In addition, there exist tremendous economic incentives for industry to adequately address abnormal operations. Nimmo [1], estimates that the chemical process industries in the U.S. could save up to \$10 billion/year by better handling abnormal situations. Within the research community, the importance of the field of fault detection has been pointed out in the seminal paper of Willsky [2] as well as by Himmelblau [3], Basseville [4], and Isermann [5].

The problem of detecting faults and changes in dynamic systems usually reduces to the generation of special signals called residuals, which are derived by comparing measurements of the actual system with a model of the plant. In the "no-fault" situation these residuals ideally are zero. If a fault occurs or if the dynamics of the system shift from its normal operating mode, these residuals increase, triggering an alarm indicating that an abnormal event has occurred. The generation of these residuals is a question that must be answered based on the specific application at hand. The key question is how to generate the residuals as well as how to decide whether a fault actually did take place or not. One approach is based on parameter estimation methods. Further details to this may be found in [6]. Other approaches are based on the principles of filtering theory. Banks of filters as well as filter-based methods have been used for instance in the aerospace industries to monitor instruments and navigation systems [7], [8]. If the residual monitored is the innovation of a Kalman filter, by definition this is an independent Gaussian random sequence with zero mean. If an additive fault occurs, this sequence will violate this assumption and the fault detection problem reduces to testing the whiteness of the innovation sequence [9], [10]. Sophisticated statistical techniques are used for the on-line testing of the whiteness of the innovation. These techniques are based on

sequential statistical analysis, maximum likelihood estimation, as well as change point detection theory ([9], [11], [12]).

Detecting faults and changes in dynamic systems is only the first problem to be tackled. Equally important is the identification of the origin of the fault in order to apply proper corrective action and bring the system back to normal operation mode. For this purpose residuals can be designed in such a way that they are uniquely sensitive to certain faults and insensitive to modeling errors and disturbances, therefore triggering an alarm only when a particular fault or abnormal situation has taken place. The design of these robust failure detection systems leads to the concepts of analytical redundancy [13], [14] and the generation of residuals via parity equations [15], [16].

The detection of faults in temperature sensors used in aluminum extrusion is the focus of this chapter. In the extrusion process the importance of carefully controlling the temperature of the extrudate has already been addressed by the author [17], as well as by Tibbetts et al. [18]. This temperature is a measure of quality and must be carefully controlled. Accurate measuring of this temperature is difficult, and usually done by means of a pyrometer. However, these measuring devices are known to be unreliable and prone to partial failure, i.e. development of a bias [19]. In order to ensure the control of the temperature of the extrudate, this sensor must be monitored and a strategy should be designed so as to promptly detect any malfunctions in this sensor.

The sensor fault detection problem is tackled by using an Extended Kalman Filter to generate the appropriate residual to be monitored. Mathematically, this problem is formulated as one of the quickest detection of abrupt changes in a stochastic process. Only additive changes in dynamic systems are considered throughout the whole chapter. A cumulative sum algorithm (CUSUM), as proposed by Niki-forov [8], is used for solving the problem. In section 4.2, the framework



for fault detection via statistical methods is recast. Section 4.3 applies the technique of change point detection for the detection of sensor faults in aluminum extrusion. The chapter closes with an outlook and some concluding remarks.

## 4.2 Preliminaries

Certain types of faults in sensors, such as the onset of a bias at a particular point in time, may be modelled as additive changes in dynamic systems. As mentioned in the previous section, these changes can be detected by monitoring specifically designed residuals and statistically testing hypotheses of whether a change did take place or not. The following paragraphs outline the method used for sensor fault detection in section 4.3.

### 4.2.1 Additive Changes in Dynamic Systems

Consider the  $m$ -dimensional independent Gaussian random sequence  $(\mathbf{Y}_t)_{t \geq 1}$ . Let the distribution of  $\mathbf{Y}_t$  be  $\mathcal{L}(\mathbf{Y}_t) = \mathcal{N}(\theta, \Sigma)$ , where  $\theta$  is the mean vector and  $\Sigma$  the covariance matrix of the Gaussian distribution. We are concerned with the following problem: until time  $t_0 - 1$  included, the vector  $\theta$  is equal to  $\theta_0$  and from time  $t_0$  the vector is equal to  $\theta_1$ . The change in the parameter  $\theta$  and the change time  $t_0$  must be detected. This problem may be viewed from the hypothesis testing point of view where the null hypothesis  $\mathcal{H}_0$  corresponds to the case where no change has occurred and the hypothesis  $\mathcal{H}_1$  to the case where a change in the parameter  $\theta$  has taken place. Under the hypothesis of a change, the model of the observation can be written in the following manner:

$$\mathcal{L}(\mathbf{Y}_t) = \begin{cases} \mathcal{N}(\theta_0, \Sigma) & \text{if } t < t_0 \\ \mathcal{N}(\theta_1, \Sigma) & \text{if } t \geq t_0 \end{cases} \quad (4.1)$$

where  $t_0$  is the unknown change time. Let  $g$  be a decision function

with domain  $Y_0^N$  and range  $\{\mathcal{H}_0, \mathcal{H}_1\}$ . Here,  $Y_0^N = [y_0 \ y_1 \ \dots \ y_N]'$ . For some  $t_0$ :  $0 \leq t_0 \leq t$  consider the hypothesis  $\mathcal{H}_1$  that the observation vectors  $Y_0^N, \dots, Y_{t_0-1}^N$  are distributed according to the probability density  $p_{\theta_0}(Y_0^N)$ , and  $Y_{t_0}^N, \dots, Y_t^N$  are distributed according to  $p_{\theta_1}(Y)$ . Consider on the other hand the no-change hypothesis  $\mathcal{H}_0$ , that all observations  $Y_0^N, \dots, Y_t^N$  are distributed according to  $p_{\theta_0}(Y_0^N)$ . The decision function  $g$  is based on the likelihood ratio of the two probability densities:

$$\Lambda(Y_0^N) = \frac{p_{\theta_1}(Y_0^N)}{p_{\theta_0}(Y_0^N)}. \quad (4.2)$$

This result follows from the Neyman-Pearson lemma [20], which states that a test is optimal in the sense of maximizing the power  $\beta$  for a fixed size  $\alpha$  if and only if it is based upon the likelihood ratio. The power  $\beta$  and the size  $\alpha$  are measures of the quality of the test and are defined as follows:

$$\alpha = P(g(Y_0^N) = \mathcal{H}_1 | \mathcal{H}_0), \quad (4.3)$$

$$= 1 - P(g(Y_0^N) = \mathcal{H}_0 | \mathcal{H}_1). \quad (4.4)$$

Thus,  $\alpha$  is the probability of accepting hypothesis  $\mathcal{H}_1$  when  $\mathcal{H}_0$  is true. On the other hand,  $\beta$  is the probability of accepting  $\mathcal{H}_1$  when this is true. The size of the test  $\alpha$  can be thought of as a false alarm rate, which naturally should be kept as low as possible. Ideally, the power  $\beta$  should be close to one. The hypothesis testing problem can thus be posed as follows:

$$g(Y_0^N) = \begin{cases} \mathcal{H}_0 & \text{when } \frac{p_{\theta_1}(Y_0^N)}{p_{\theta_0}(Y_0^N)} < \lambda_\alpha \\ \mathcal{H}_1 & \text{when } \frac{p_{\theta_1}(Y_0^N)}{p_{\theta_0}(Y_0^N)} \geq \lambda_\alpha \end{cases} \quad (4.5)$$

In the last equation  $\lambda_\alpha$  is a conveniently chosen threshold. In practice it is very usual, for computational purposes, to use the logarithm of the likelihood ratio [4]. The log-likelihood ratio is therefore defined as follows:

$$S_N = \ln \left( \frac{p_{\theta_1}(Y_0^N)}{p_{\theta_0}(Y_0^N)} \right). \quad (4.6)$$

Until now the hypothesis testing problem has been solved by using a fixed sample size  $Y_0^N$ . When the sample size is not fixed *a priori* but depends upon the data that has already been observed, *sequential analysis* is the proper approach for solving hypothesis testing problems [21]. A sequential probability ratio test (SPRT) is therefore a better suited tool for the on-line detection of changes in dynamic systems. The decision function  $g$  in this case depends on the stopping time  $T$  as follows:

$$g(Y_0^T) = \begin{cases} \mathcal{H}_1 & \text{when } S_T \geq h \\ \mathcal{H}_0 & \text{when } S_T \leq -a \end{cases} \quad (4.7)$$

where:

$$T = \min \{n \geq 1 : (S_n \geq h) \cup (S_n \leq -a)\} \quad (4.8)$$

This test simply sequentially observes data  $(Y_n)_{n \geq 1}$  and makes one of the following decisions at time  $n$ :

- accept  $\mathcal{H}_0$  when  $S_n \leq -a$ ;
- accept  $\mathcal{H}_1$  when  $S_n \geq h$ ;
- continue to observe and to test when  $-a \leq S_n \leq h$ .

The change detection problem can be solved differently according to the various levels of *a priori* information available about the parameters  $\theta_0$  and  $\theta_1$ . Usually, the parameter  $\theta_0$  is known or at least may be estimated. However, information about  $\theta_1$  is usually scarce. The worst-case scenario is when neither the magnitude nor the direction of the change are known. In this case the parameter  $\theta_1$  is replaced by its maximum likelihood estimate. This results in the generalized likelihood ratio (GLR) algorithm. The GLR is defined as follows:

$$\hat{\Lambda}_n = \frac{\sup_{\theta_1} p_{\theta_1}(Y_1, \dots, Y_n)}{p_{\theta_0}(Y_1, \dots, Y_n)}. \quad (4.9)$$

The GLR solution to the change point detection problem in this case is based upon the following decision function [9]:

$$g_k = \max_{1 \leq j \leq k} \ln \frac{\sup_{\theta} \prod_{i=j}^k p_{\theta}(Y_i)}{\prod_{i=j}^k p_{\theta_0}(Y_i)}. \quad (4.10)$$

### Change Detection via GLR Algorithms

Assume that the process under consideration can be modelled in a state-space representation, i.e., the equations of the model are of the following form:

$$\begin{cases} X(k+1) = A(k)X(k) + B(k)U(k) + W(k) \\ Y(k) = C(k)X(k) + D(k)U(k) + V(k) \end{cases} \quad (4.11)$$

where the state  $X$ , the control  $U$ , and the observation  $Y$  have the dimensions  $n$ ,  $m$ ,  $r$ , respectively, and where  $W(k)$  and  $V(k)$  are two independent white noise sequences with covariance matrices  $Q$  and  $R$ ,

respectively. It is assumed that the changes enter the system in an additive form as shown below:

$$\begin{cases} X(k+1) = A(k)X(k) + B(k)U(k) + W(k) + \Gamma\Upsilon_x(k, t_0) \\ Y(k) = C(k)X(k) + D(k)U(k) + V(k) + \Xi\Upsilon_y(k, t_0) \end{cases} \quad (4.12)$$

Here,  $\Gamma$  and  $\Xi$  are matrices of dimensions  $n \times \tilde{n}$  and  $r \times \tilde{r}$ , respectively, and  $\Upsilon_x(k, t_0)$  and  $\Upsilon_y(k, t_0)$  are the dynamic profiles of the assumed changes, of dimensions  $\tilde{n} \leq n$  and  $\tilde{r} \leq r$ , respectively. The change time  $t_0$  is unknown so that the following holds:

$$\Upsilon_x(k, t_0) = \Upsilon_y(k, t_0) = 0 \quad \text{for } k < t_0. \quad (4.13)$$

Various faults may be modelled in this way. If for instance  $\Upsilon_x = 0$  and  $\Upsilon_y$  is a vector whose components are all zero except for the  $j$ th component which equals 1 for  $k \geq t_0$ , this corresponds to the onset of a bias in the  $j$ th component of  $Y$  ( $j$ th sensor). Faults in the actuators may be modelled analogously by setting  $\Upsilon_y = 0$  and  $\Upsilon_x$  to be a vector, the components of which are all zero but for the  $j$ th component. If the system on normal operation is monitored by a Kalman filter, then the filter equations are given by [22]:

$$\hat{X}(k+1|k) = A(k)\hat{X}(k|k) + B(k)U(k) \quad (4.14)$$

$$\hat{X}(k|k) = \hat{X}(k|k-1) + K(k)\epsilon(k) \quad (4.15)$$

$$\epsilon(k) = Y(k) - C(k)\hat{X}(k|k-1). \quad (4.16)$$

The Kalman gain  $K(k)$ , the state estimation error covariance  $P(k|k)$ , and the covariance of the innovation  $\Sigma(k)$  may be calculated by means

of the following equations:

$$K(k) = P(k|k-1)C(k)^T\Sigma(k)^{-1} \quad (4.17)$$

$$P(k|k) = (I_n - K(k)C(k))P(k|k-1) \quad (4.18)$$

$$P(k+1|k) = A(k)P(k|k)A(k)^T + Q \quad (4.19)$$

$$\Sigma(k) = C(k)P(k|k-1)C(k)^T + R. \quad (4.20)$$

The effect on the state, state estimate, and innovation of the filter of an additive fault entering the system is:

$$X(k) = X^0(k|k) + \alpha(k, t_0) \quad (4.21)$$

$$\hat{X}(k|k) = \hat{X}^0(k|k) + \beta(k, t_0) \quad (4.22)$$

$$\epsilon(k) = \epsilon^0(k) + \rho(k, t_0), \quad (4.23)$$

where  $X^0(k|k)$ ,  $\hat{X}^0(k|k)$ , and  $\epsilon^0(k)$  are the responses of the system if no abrupt change occurs. The terms  $\alpha(k, t_0)$ ,  $\beta(k, t_0)$ , and  $\rho(k, t_0)$  are the responses of the system due to the abrupt change taking place at  $t = t_0$ . These quantities may be computed recursively with the aid of the following equations:

$$\alpha(k, t_0) = A(k)\alpha(k-1, t_0) + \Gamma\Upsilon_x(k-1, t_0) \quad (4.24)$$

$$\beta(k, t_0) = A(k)\beta(k-1, t_0) + K(k)\rho(k, t_0) \quad (4.25)$$

$$\rho(k, t_0) = C(k)[\alpha(k, t_0) - A(k)\beta(k-1, t_0)] + \Xi\Upsilon_y(k, t_0) \quad (4.26)$$

and the initial conditions:

$$\alpha(t_0, t_0) = 0 \quad (4.27)$$

$$\beta(t_0 - 1, t_0) = 0. \quad (4.28)$$

By definition  $\epsilon(k)$  is the innovation under normal conditions and is zero mean, Gaussian, and with covariance matrix  $\Sigma(k)$ . Thus, detecting the change has been reduced to a standard detection problem in white noise [23]. The filter residuals  $\epsilon^0(k)$  are observed and to determine the presence of a change, to estimate the change time  $t_0$  and perhaps the magnitude of the change if this is unknown, the on-line GLR algorithm may be used. This consists of performing the following calculations:

$$g_k = \max_{1 \leq j \leq k} \sup_{\Upsilon} S_j^k \quad (4.29)$$

$$\sup_{\Upsilon} S_j^k = \left[ \sum_{i=j}^k \rho^T(i, j) \Sigma^{-1}(i) \epsilon(i) \right]^T V^{-1} \left[ \sum_{i=j}^k \rho^T(i, j) \Sigma^{-1}(i) \epsilon(i) \right] \quad (4.30)$$

$$V = \left[ \sum_{i=j}^k \rho^T(i, j) \Sigma^{-1}(i) \rho(i, j) \right]. \quad (4.31)$$

The stopping time is given by:

$$t_a = \min \{k \geq 1 : g_k \geq h\}. \quad (4.32)$$

## Change Detection via CUSUM Algorithms

Although the algorithm described previously has been effectively used in a wide variety of applications ([2], [7], [24], [25], [26], [27], [28]) it requires long computations. This is due to the fact that the change time  $t_0$  is estimated with the aid of the maximum likelihood estimation. This requires an exhaustive search for all possible past time instants (i.e.  $j \leq k$  in equation (4.29)). This difficulty can partially be overcome in various *ad-hoc* manners [2]. An alternative way of tackling the problem is by means of the so-called CUSUM algorithm [9], [11]. Here, the likelihood ratio is averaged with respect to all possible values of  $\theta_1$ . For this, a proper probability distribution is used as weighting function:

$$\tilde{S}_k^t = \ln \int_{-\infty}^{\infty} \frac{p_{\theta_1}(Y_0^N)}{p_{\theta_0}(Y_0^N)} dF(\theta_1). \quad (4.33)$$

If the sequence  $Y_0^N$  is a scalar Gaussian sequence with known variance  $\sigma^2$ , the distribution  $F(\theta_1)$  is concentrated on two points  $\theta_0 - \sigma b$  and  $\theta_0 + \sigma b$ . Thus, the weighted likelihood ratio (4.33) becomes [8]:

$$\begin{aligned} \tilde{S}_k^t &= \ln \int_{-\infty}^{\infty} \exp \left\{ \frac{\theta_1 - \theta_0}{\sigma^2} \sum_{j=k}^t (y_j - \theta_0) \right. \\ &\quad \left. - \frac{(\theta_1 - \theta_0)^2}{2\sigma^2} (t - k + 1) \right\} dF(\theta_1) \\ &= -(t - k + 1) \frac{b^2}{2} + \ln \cosh \left( \frac{b}{\sigma} \sum_{j=k}^t (y_j - \theta_0) \right). \end{aligned} \quad (4.34)$$

The on-line  $\chi^2$ -CUSUM algorithm is based on performing the above mentioned calculations and can be summarized as follows:

$$\begin{aligned} t_a &= \min t \geq 1 : g_t \geq h \\ g_t &= \max_{1 \leq k \leq t} \left\{ -(t - k + 1) \frac{b^2}{2} \right. \\ &\quad \left. + \ln \cosh \left( \frac{b}{\sigma} \sum_{j=k}^t (y_j - \theta_0) \right) \right\} \end{aligned} \quad (4.35)$$

where  $b = \frac{|\theta_1 - \theta_0|}{\sigma}$  is the signal-to-noise ratio. If the threshold  $h$  is chosen as the unique positive solution of the following equation:

$$h = -l \frac{b^2}{2} + \ln \cosh(bc_l), \quad (4.36)$$

equation (4.35) may be rewritten as follows:



$$t_0 = \min \left\{ t \geq 1 : \max_{1 \leq k \leq t} \left( \frac{1}{\sigma} \left| \sum_{j=k}^t (y_j - \theta_0) \right| \geq c_{t-k+1} \right) \right\}. \quad (4.37)$$

The algorithm (4.37) stops at the first time  $t$  at which the cumulative sum  $\frac{1}{\sigma} \sum_{j=k}^t (y_j - \theta_0)$  reaches the upper boundary  $c_{t-k+1}$  or the lower boundary  $-c_{t-k+1}$ .

The framework for fault detection via statistical methods has been recast. Subsequent sections deal with the applications of these techniques, in particular of the CUSUM algorithm, for the monitoring and detection of faults in the temperature sensors used in aluminum extrusion.

### 4.3 Detection of Faults in Sensors for Aluminum Extrusion

This section concerns the monitoring and fault detection in the direct aluminum extrusion process via CUSUM algorithms. Figure 4.1 shows a diagram of the process as well as the main bodies involved.

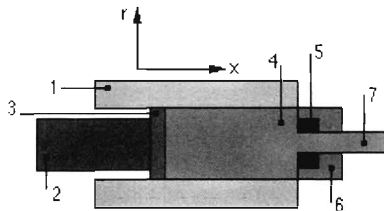


Figure 4.1: *Direct Extrusion: 1 Container, 2 Ram, 3 Dummy Block, 4 Billet, 5 Die, 6 Die Holder, 7 Extrudate.*

Accurate measuring of the temperature of the extrudate profile is a

difficult task which has been addressed in previous investigations [19]. In industrial practice, the temperature of the extrudate is recorded by means of pyrometers. These devices are prone to failure. In particular they tend to develop bias. This section presents the detection of bias in these type of sensors via CUSUM algorithms as presented in the previous section.

### 4.3.1 Tuning of the Algorithm

The design parameters of the on-line CUSUM algorithm described in section 4.2.1 are the signal-to-noise ratio  $b$  and the threshold  $h$ . The ratio  $b$  determines the minimum magnitude of change that is to be detected and lower values than the chosen one will go unnoticed. The on-line  $\chi^2$ -CUSUM algorithm described by equation (4.37) has been shown to be closely related to a two-sided CUSUM algorithm [29]. This latter algorithm can be implemented in a recursive manner and consists of the following on-line calculations:

$$t_a = \min \{t \geq 1 : (g_t^* \geq h + \ln 2) \cup (g_t^\bullet \geq h + \ln 2)\} \quad (4.38)$$

where:

$$\begin{aligned} g_t^* &= \left( g_{t-1}^* + y_t - \frac{\delta}{2} \right)^+ \\ g_t^\bullet &= \left( g_{t-1}^\bullet - y_t - \frac{\delta}{2} \right)^+ \\ g_0^* &= g_0^\bullet = 0 \\ (x)^+ &= \max(0, x), \quad \delta = \theta_1 - \theta_0. \end{aligned} \quad (4.39)$$

Measures of the performance of the algorithm are the mean detection delay  $\bar{\tau}$  and the mean time between false alarms  $\bar{T}$ . These two

quantities are defined as conditional expectations with respect to the distributions of the parameter before and after change:

$$\begin{aligned}\bar{T} &= \mathbf{E}_{\theta_0}(t_a) \\ \bar{\tau} &= \mathbf{E}_{\theta_1}(t_a).\end{aligned}\tag{4.40}$$

Intuitively, it can be said that large values for  $\bar{T}$  (few false alarms) and low values for  $\bar{\tau}$  (fast detection) are desired. In practice a trade-off for these two quantities must be accepted since they cannot be chosen independently of each other [30]. The mean time between false alarms  $\bar{T}$  and the mean detection delay  $\bar{\tau}$  are also related to the magnitude of the change  $\delta$  and the threshold  $h$  in the following manner [11]:

$$\bar{T} \geq \frac{\exp(|\delta|h) - 1 - |\delta|h}{\delta^2} - \frac{\varphi\left(-\frac{|\delta|}{2}\right)}{|\delta|\Phi\left(-\frac{|\delta|}{2}\right)} + \frac{1}{2}\tag{4.41}$$

$$\bar{\tau} \leq \frac{2h}{|\delta|} + \frac{2\varphi\left(\frac{\delta}{2}\right)}{|\delta|\Phi\left(\frac{|\delta|}{2}\right)} + 1\tag{4.42}$$

where:

$$\Phi(x) = \int_{-\infty}^x \varphi(x)dx, \quad \varphi(x) = \frac{1}{\sqrt{2\pi}} \exp(-x^2/2), \quad \delta = \theta_1 - \theta_0.$$

Thus in summary the fault detection algorithm consists of the following steps:

1. Choose a minimum magnitude,  $\delta$ , for the change to be detected.
2. Choose a convenient mean time between false alarms,  $\bar{T}$ .
3. Calculate the threshold from equation (4.41).

4. Check if the mean delay of detection  $\bar{\tau}$  as given by equation (4.42) is acceptable for the system in question. If not, go back to 2.
5. Implement the algorithm given by equation (4.39).
6. Stop the calculations when equation (4.38) is satisfied.

### 4.3.2 Simulation Results

For the simulations a minimum bias of  $\delta = 5 \text{ }^\circ\text{C}$  was chosen to be detected. The threshold  $h$  is chosen in accordance with the two-sided CUSUM algorithm (4.39). A mean time between false alarms of  $\bar{T} = 600 \text{ s}$  was chosen. Figure 4.2 shows the behavior of the decision function in the case of a fault which is introduced at time  $t = 55 \text{ s}$ . Figure 4.3 shows the temperature of the extrudate for the whole extrusion cycle. The algorithm successfully detects the onset of the bias with a delay of detection of  $\bar{\tau} \approx 10 \text{ s}$ .

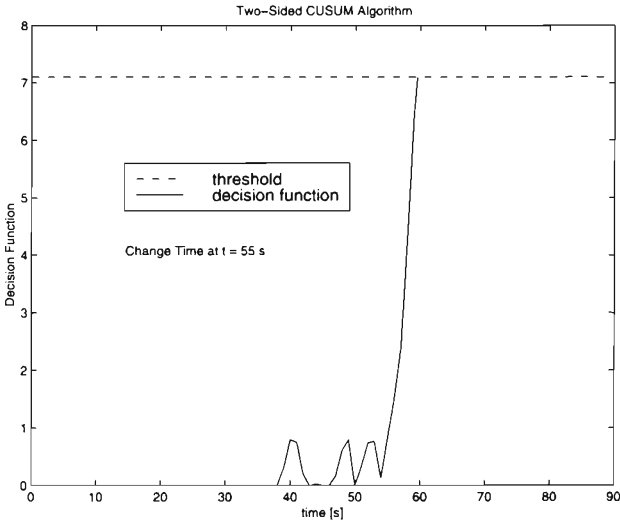


Figure 4.2: Behavior of the decision function: introduction of a fault (onset of bias) in the sensor at  $t = 55 \text{ s}$ .

Although the two-sided CUSUM algorithm(4.39) is derived under the assumption that the magnitude of the change is known *apriori*, this algorithm may still be used to detect other types of faults (i.e. drifts). A drift with a slope of  $m = 0.1 \text{ } ^\circ\text{C}/\text{s}$  is introduced, again at time  $t = 55 \text{ s}$ . Figure 4.4 shows the behavior of the decision function when a fault of this type is present. The fault is detected, however, with a longer delay of detection  $\bar{\tau}$  than before. For aluminum extrusion, however, this delay of detection is not so critical so that it may be tolerated.

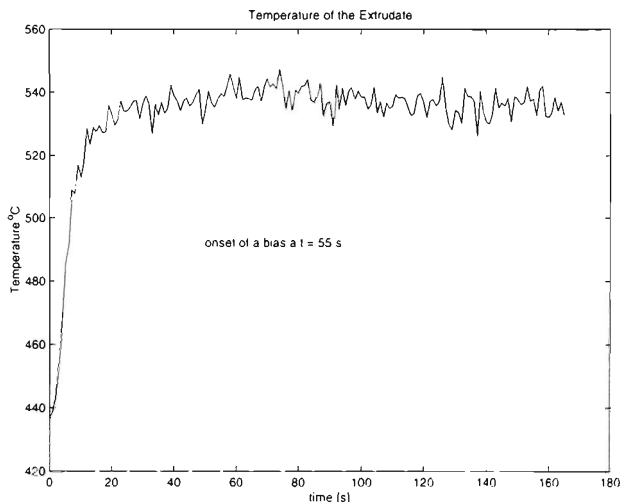


Figure 4.3: *Temperature of the extrudate for the onset of a bias in the sensor at  $t = 55 \text{ s}$ .*

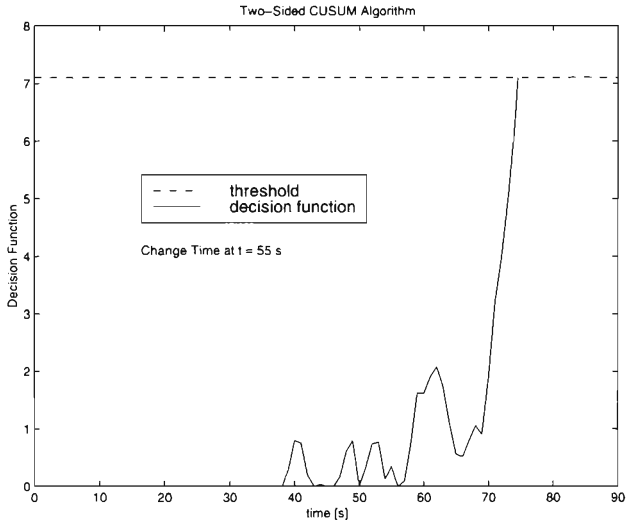


Figure 4.4: Behavior of the decision function: detection of a drift in the sensor.

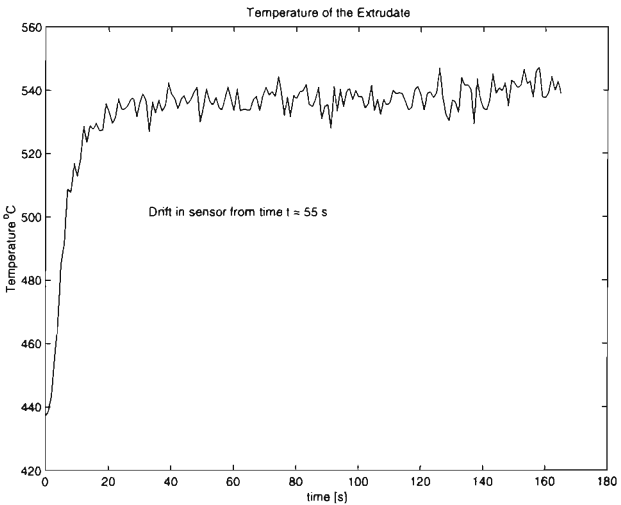


Figure 4.5: Temperature of the extrudate for a drift in the sensor starting at  $t = 55$  s.

## 4.4 Conclusions

Sensors used in aluminum extrusion for measuring the temperature of the extrudate are prone to partial failure. The monitoring of these sensors and the detection of certain types of faults via statistical methods has been shown through simulations. The problem of detecting a fault in the sensor has been treated as the on-line detection of a change in the mean of a stochastic process. For this purpose a CUSUM algorithm has been used. It has been shown that the onset of bias as well as the detection of drifts in the sensors can be successfully detected using this method. This algorithm may be easily implemented on-line in a recursive manner. For its use in practice, however, either the chosen parameter  $\delta$  or the threshold  $h$  calculated theoretically by means of equation (4.41) once an adequate mean time between false alarms has been chosen, must be properly adjusted to compensate for model inadequacies. This is the part of the procedure that must be adjusted empirically once the model/plant mismatch has been estimated. Naturally, the mean detection delay  $\bar{\tau}$  in this case will not be the optimal one as given by the theory. However, as for this process this is not too critical, a detection delay greater than the optimal one can be tolerated.

A further point may be worth mentioning at this point. This fault detection scheme could perfectly serve as the basis for a more sophisticated and complete monitoring and fault detection scheme of the overall process, whereby malfunctions in the actuators, pressure valves and remaining devices which are prone to failure could be detected promptly. This would invariably pave the way to enhanced device-diagnostics capabilities, allowing plant personnel to perform predictive maintenance without waiting for a scheduled shutdown and ultimately decreasing downtime of the plant. Enhanced diagnostics capabilities would also provide earlier warnings of current and prospective hazardous conditions, thereby reducing potential risks to field personnel.

# Bibliography

- [1] I. Nimmo. Adequately Address Abnormal Operations. *Chemical Engineering Progress*, 91, No. 9, pp.36-45, 1995.
- [2] A. S. Willsky. A Survey of Design Methods for Failure Detection in Dynamic Systems. *Automatica*, 12, pp.601-611, 1976.
- [3] D. M. Himmelblau. *Fault Detection and Diagnosis in Chemical and Petrochemical Processes*. Elsevier, Amsterdam, 1978.
- [4] M. Basseville. Detecting Changes in Signals and Systems – A Survey. *Automatica*, 24, No. 3, pp.309-326, 1988.
- [5] R. Isermann. Process Fault Detection Based on Modeling and Estimation Methods – a Survey. *Automatica*, 20, No. 4, pp.387-404, 1984.
- [6] R. Isermann. Process Fault Diagnosis Based on Dynamic Models and Parameter Estimation Methods. In R. Patton, P. Frank, and R. Clark, editors, *Fault Diagnosis in Dynamic Systems*, chapter 7. Prentice Hall, Inc., New York, 1989.
- [7] J. C. Deckert, M. N. Desai, J. J. Deyst, and A. S. Willsky. F8-DFBW Sensor Failure Identification Using Analytic Redundancy. *IEEE Trans. Automatic Control*, AC-22, No. 5, pp.795-803, 1977.
- [8] I. Nikiforov, V. Varavva, and V. Kireichikov. Application of Statistical Fault Detection Algorithms to Navigation Systems Monitoring. *Automatica*, 29, No. 5, pp.1275-1290, 1993.
- [9] M. Basseville and I. Nikiforov. *Detection of Abrupt Changes: Theory and Application*. Prentice-Hall Information and Systems Series. Prentice-Hall, Inc., Englewood Cliffs, NJ, 1993.



- [10] A. S. Willsky. Detection of Abrupt Changes in Dynamic Systems. In M. Basseville and A. Benveniste, editors, *Detection of Abrupt Changes in Signals and Dynamical Systems*, Lecture Notes in Control and Information Sciences, chapter 2. Springer-Verlag, Berlin, 1986.
- [11] I. Nikiforov. Sequential Detection of Changes in Stochastic Systems. In M. Basseville and A. Benveniste, editors, *Detection of Abrupt Changes in Signals and Dynamical Systems*, Lecture Notes in Control and Information Sciences, chapter 7. Springer-Verlag, Berlin, 1986.
- [12] T. L. Lai. Sequential Change-point Detection in Quality Control and Dynamical Systems. *J. R. Statist. Soc.*, 57, No. 4, pp.613-658, 1995.
- [13] E. Y. Chow and A. S. Willsky. Analytical Redundancy and the Design of Robust Failure Detection Systems. *IEEE Trans. Automatic Control*, AC-29, No. 7, pp.603-614, 1984.
- [14] X. C. Lou, A. S. Willsky, and G. C. Verghese. Optimally Robust Redundancy Relations for Failure Detection in Uncertain Systems. *Automatica*, 22, No. 3, pp.333-344, 1986.
- [15] J. Gertler. Structured Residuals for Fault Isolation Disturbance Decoupling and Modelling Error Robustness. In *Proc. IFAC Workshop on On-Line Fault Detection and Supervision in the Chemical Process Industries*, Wilmington, DE, pp.15-23, 1992.
- [16] J. Gertler. *Fault Detection and Diagnosis in Engineering Systems*. Marcel Dekker, Inc., New York, 1998.
- [17] C. Cuéllar, A. Schmid, and M. Steiner. Dynamic Modeling and Optimal Control Strategies for Aluminum Extrusion. In *Proc. Control 97*, Sydney, pp.91-96, 1997.
- [18] B. R. Tibbetts and J. Weng. Extrusion Process: Control, Identification, and Optimization. *IEEE Trans. on Control Systems Technology*, 6, (2), pp.134-145, 1998.

- [19] K. Buchheit. *Iterativ Lernende Regelungen für Zyklische Systeme*. PhD thesis, Universität Kaiserslautern, Kaiserslautern, Germany, 1994.
- [20] J. Neyman and E. S. Pearson. Sufficient Statistics and Uniformly Most Powerful Tests of Statistical Hypotheses. *Statistical Research Memoirs*, vol. 1, pp.113-137, 1936.
- [21] D. Siegmund. *Sequential Analysis: Tests and Confidence Intervals*. Series in Statistics. Springer-Verlag, New York, 1985.
- [22] H. W. Sorenson, editor. *Kalman Filtering: Theory and Application*. Selected reprint series. IEEE Press, New York, 1985.
- [23] H. V. Poor. *An Introduction to Signal Detection and Estimation*. Springer Verlag, New York, 1988.
- [24] M. Basseville and M. Benveniste. Design and Comparative Study of Some Sequential Jump Detection Algorithms for Digital Signals. *IEEE Trans. Acoustics, Speech, Signal Processing*, vol.ASSP-31, No. 3, pp.521-535, 1983.
- [25] A. S. Willsky, E. Y. Chow, S. B. Gershwin, C. S. Greene, P. K. Houpt, and A. L. Kurkjian. Dynamic Model-Based Techniques for the Detection of Incidents on Freeways. *IEEE Trans. Automatic Control*, vol. AC-25, 1980.
- [26] A. L. Kurkjian, S. B. Gershwin, P. K. Houpt, A. S. Willsky, C. S. Greene, , and E. Y. Chow. Estimation of Roadway Traffic Density on Freeways Using Presence Detector Data. *Transportation Sciences*, 1980.
- [27] J. R. Dowdle, A. S. Willsky, and S. W. Gully. Nonlinear Generalized Likelihood Ratio Algorithms for Maneuver Detection and Estimation. In *Proc. American Control Conference*, Arlington, VA, 1983.
- [28] R. R. Tenney, R. S. Hebbert, and N. R. Sandell. A Tracking Filter for Maneuvering Sources. *IEEE Trans. Automatic Control*, vol. AC-22, No. 4, pp.246-251, 1977.

- [29] E. S. Page. Continous Inspection Schemes. *Biometrika*, vol. 41, pp.100-115, 1954.
- [30] G. Lorden. Procedures for Reacting to a Change in Distribution. *Annals of Mathematical Statistics*, vol. 26, pp.7-22, 1971.

# Contributions of the Thesis

Upon ending this dissertation, a brief summary of the contributions of the thesis is presented in this chapter.

- For the purpose of deriving model-based optimal control strategies for the isothermal extrusion of aluminum a dynamic model of the process has been presented. Although the physics of the process is well known, the main challenge in deriving a first-principles dynamic model of the process that is suited for control purposes consists of achieving reasonable computation times. By treating the metal as a highly viscous fluid and by making appropriate assumptions regarding its flow, it was possible to analytically solve the velocity, pressure, strain, and strain rates distributions needed for the modeling of the process, leaving only the temperature distributions to be solved numerically. By means of this innovative *semi-analytical* approach for solving the partial differential equations describing the physical phenomena taking place in extrusion, computation times have been drastically reduced as compared to other methods of modeling this process (e.g. Finite Element Method). An immediate consequence of this was the straightforward design of open-loop control strategies to achieve isothermal extrusion. These optimal velocity trajectories were obtained by minimizing performance indexes related to practical measures of product quality.
- The open-loop control strategies, which have been tested and implemented in various industrial extruders, optimally adjust the extrusion velocity throughout the extrusion cycle, thereby achieving a constant temperature of the extrudate profile during a significant part of the extrusion cycle. Moreover, since on average the extrusion velocities calculated by these strategies are higher than those usually achieved by experienced operators, productivity has been increased. In some cases the duration of the extrusion cycles has been reduced by as much as 20-25%.

- Assisted by the model, it was possible to show that the problem of isothermal extrusion is not solely a problem of optimally adjusting the velocity throughout the whole extrusion cycle, but also one of optimally choosing the initial temperature gradient of the billet. In some cases, if the initial gradient is not chosen properly, isothermal extrusion is not achieved during the entire cycle even if the extrusion is carried out at the maximum velocity allowed at a particular press. Although this is physically intuitive and may seem trivial, in practice sometimes isothermal extrusion is demanded when in fact it is not physically realizable given the initial conditions and the pre-heating ovens at hand. The question then is not how to optimally adjust the extrusion velocity, but how to optimally control the ovens heating the billets to achieve an optimal initial temperature gradient.
- Based on model predictive control (MPC) principles, closed-loop control strategies have been derived and tested through simulations. This was possible due to the development of a simplified dynamic model of the process. This model is described by means of ordinary nonlinear differential equations and has been thoroughly validated, not only by comparison to the complex model previously mentioned, but also by comparing it to industrial data. MPC allows to take into account constraints inherent to the system directly during the controller design procedure. Advantageous here is the fact that noise entering the system and uncertainties (e.g. lack of knowledge of the initial temperature gradient of the billet) may be at least partially counterbalanced.
- A methodology has been presented for detecting faults in the sensors measuring the temperature of the extrudate. This was necessary as these sensors are prone to partial failure and the measurements of the temperature are critical for any closed-loop control strategy. Through simulations it has been shown that bias and drifts in these sensors can be detected on-line by means of sophisticated statistical methods.

# Appendix A

## Assumed Geometry of Profile

For the detailed model of the extrusion process the geometry of the profile is always assumed to be a ring with a cross-sectional area and perimeter equivalent to the actual profile in question. Let  $A_{profile}$  be the actual cross-sectional area of the profile and  $U_{profile}$  its perimeter. To obtain the inner and outer radius  $r_1$  and  $r_2$  of a ring with equal cross-sectional area and perimeter we have:

$$A_{profile} = \pi(r_2^2 - r_1^2) \quad (\text{A.1})$$

$$U_{profile} = 2\pi(r_2 + r_1). \quad (\text{A.2})$$

From these equations it is trivial to obtain the following relationship for the inner and outer radius of a ring with equal cross-section and perimeter:

$$r_1 = \frac{U_{profile}}{4\pi} - \frac{A_{profile}}{U_{profile}}, \quad (\text{A.3})$$

$$r_2 = \frac{U_{profile}}{4\pi} + \frac{A_{profile}}{U_{profile}}. \quad (\text{A.4})$$

For example, if the cross-sectional area of a profile is a square with the side  $a$  (and thus the area  $a^2$  and the perimeter  $4a$ ) from the equations

derived above a ring with the same cross-sectional area will have a inner and outer radius equal to:

$$r_1 = \frac{a}{4} - \frac{a}{\pi} \quad (\text{A.5})$$

$$r_2 = \frac{a}{4} + \frac{a}{\pi} \quad (\text{A.6})$$

By making this transformation of geometry, the solution for the velocity distributions at the exit of the die is simplified and can be readily solved as discussed in section 2.3.1.

## Appendix B

### Method of Separation of Variables for the Solution of a Fourth Order Linear Partial Differential Equation

The equation to be solved is the following:

$$\frac{\partial^4 \Psi}{\partial r^4} + 2 \frac{\partial^4 \Psi}{\partial r^2 \partial x^2} + \frac{\partial^4 \Psi}{\partial x^4} - \frac{2}{r} \frac{\partial^3 \Psi}{\partial r \partial x^2} - \frac{2}{r} \frac{\partial^3 \Psi}{\partial r^3} + \frac{3}{r^2} \frac{\partial^2 \Psi}{\partial r^2} - \frac{3}{r^3} \frac{\partial \Psi}{\partial r} = 0 \quad (\text{B.1})$$

with the following boundary conditions:

$$v_r|_{r=0} = 0 ; \forall x \quad (\text{B.2})$$

$$v_r|_{x=0} = 0 ; \forall r \quad (\text{B.3})$$

$$v_r|_{r=R} = 0 ; \forall x \quad (\text{B.4})$$

$$v_r|_{x=L} = 0 ; \forall r \quad (\text{B.5})$$

$$v_x|_{x=0} = v_{ram} ; \forall r \quad (\text{B.6})$$

$$v_x|_{r=R} = v_x(x, R) \quad (\text{B.7})$$

$$v_x|_{x=L} = v(L, r) \quad (\text{B.8})$$

$$\Psi(r = 0, x) = \text{constant} \forall x. \quad (\text{B.9})$$

In the last equation  $\Psi$  stands for the stream function which is defined



as follows:

$$v_r = -\frac{1}{r} \frac{\partial \Psi}{\partial x}, \quad v_x = \frac{1}{r} \frac{\partial \Psi}{\partial r}. \quad (\text{B.10})$$

To solve this boundary value problem it is assumed that the function  $\Psi(r, x)$  may be separated into two functions, each of them depending only on one of the space variables  $r, x$ , in the form:

$$\Psi(r, x) = \Upsilon(r) \Xi(x). \quad (\text{B.11})$$

Combining equations (B.11) and (B.1) yields:

$$\Upsilon'''' \Xi + 2 \Upsilon'' \Xi'' + \Upsilon \Xi'''' - \frac{2}{r} \Upsilon' \Xi'' - \frac{2}{r} \Upsilon''' \Xi + \frac{3}{r^2} \Upsilon'' \Xi - \frac{3}{r^3} \Upsilon' \Xi = 0. \quad (\text{B.12})$$

Taking into account the definition of the stream function as expressed by equation (B.10), the boundary conditions yield:

$$v_r|_{r=0} = \frac{1}{r} \Upsilon(r) \Xi'(x) = 0; \quad \forall x \implies \frac{1}{r} \Upsilon(r) \Big|_{r=0} = 0 \quad (\text{B.13})$$

$$v_r|_{r=R} = \frac{1}{r} \Upsilon(r) \Xi'(x) = 0; \quad \forall x \implies \frac{1}{r} \Upsilon(r) \Big|_{r=R} = 0 \quad (\text{B.14})$$

$$v_r|_{x=0} = \frac{1}{r} \Upsilon(r) \Xi'(x) = 0; \quad \forall r \implies \Xi'(x) \Big|_{x=0} = 0 \quad (\text{B.15})$$

$$v_r|_{x=L} = \frac{1}{r} \Upsilon(r) \Xi'(x) = 0; \quad \forall r \implies \Xi'(x) \Big|_{x=L} = 0 \quad (\text{B.16})$$

$$v_x|_{x=0} = \frac{1}{r} \Upsilon'(r) \Xi(x) \Big|_{x=0} = v_{ram} \quad (\text{B.17})$$

$$v_x|_{x=L} = \frac{1}{r} \Upsilon'(r) \Xi(x) \Big|_{x=L} = v(L, r) \quad (\text{B.18})$$

$$v_x|_{r=R} = \frac{1}{r} \Upsilon'(r) \Xi(x) \Big|_{r=R} = v_x(x, R) \quad (\text{B.19})$$

$$\Upsilon(0) = \text{constant}. \quad (\text{B.20})$$

Rearranging equation (B.12) in descending order of derivatives of  $\Xi$  (first separation) yields:

$$\Xi'''' \Upsilon + \Xi'' \left( 2 \Upsilon'' - \frac{2}{r} \Upsilon' \right) + \Xi \left( \Upsilon'''' - \frac{2}{r} \Upsilon''' + \frac{3}{r^2} \Upsilon'' - \frac{3}{r^3} \Upsilon' \right) = 0. \quad (\text{B.21})$$

A separation is feasible if  $\Xi$  satisfies the following fourth-order differential equation:

$$\Xi'''' + \alpha \Xi'' + \beta \Xi = 0 \quad (\text{B.22})$$

where  $\alpha$  and  $\beta$  are constants. This implies that the following differential equations are valid:

$$2 \Upsilon'' - \frac{2}{r} \Upsilon' - \alpha \Upsilon = 0 \quad (\text{B.23})$$

$$\Upsilon'''' - \frac{2}{r} \Upsilon''' + \frac{3}{r^2} \Upsilon'' - \frac{3}{r^3} \Upsilon' - \beta \Upsilon = 0. \quad (\text{B.24})$$

Solving equation B.23 for  $\Upsilon''$  yields:

$$\Upsilon'' = \frac{1}{r} \Upsilon' + \frac{\alpha}{2} \Upsilon \quad (\text{B.25})$$

which is further differentiated to provide the following equations:

$$\Upsilon''' = \left( -\frac{1}{r^2} + \frac{\alpha}{2} \right) \Upsilon' + \frac{1}{r} \left( \frac{1}{r} \Upsilon' + \frac{\alpha}{2} \Upsilon \right) = \frac{\alpha}{2} \Upsilon' + \frac{\alpha}{2r} \Upsilon \quad (\text{B.26})$$

$$\Upsilon'''' = \frac{\alpha}{2r} \Upsilon' - \frac{\alpha}{2r^2} \Upsilon + \frac{\alpha}{2} \left( \frac{1}{r} \Upsilon' + \frac{\alpha}{2} \Upsilon \right) = \frac{\alpha}{r} \Upsilon' + \left( \frac{\alpha^2}{4} - \frac{\alpha}{2r^2} \right) \Upsilon. \quad (\text{B.27})$$

Substitution of the corresponding terms into equation (B.24) results in

$$\begin{aligned} \frac{\alpha}{r} \Upsilon' + \left( \frac{\alpha^2}{4} - \frac{\alpha}{2r^2} \right) \Upsilon - \frac{2}{r} \left( \frac{\alpha}{2} \Upsilon' + \frac{\alpha}{2r} \Upsilon \right) + \frac{3}{r^2} \left( \frac{1}{r} \Upsilon' + \frac{\alpha}{2} \Upsilon \right) \\ - \frac{3}{r^3} \Upsilon' - \beta \Upsilon = \left( \frac{\alpha^2}{4} - \beta \right) \Upsilon = 0. \quad (\text{B.28}) \end{aligned}$$

This last equation reveals that (B.1) may be separated only if its eigenvalues satisfy the following relationship:

$$\frac{\alpha^2}{4} = \beta. \quad (\text{B.29})$$

Equations (B.23) and (B.24) thus provide no additional information for the solution of the problem. This is reflected in the fact that not all the boundary conditions may be satisfied. If the problem of indirect extrusion is taken into consideration ( $v_x(x, r)|_{x=0} = 0$ ,  $v_x(x, r)|_{x=L} = -v_{ram}$ ), the boundary conditions are easier to satisfy. The problem can therefore be solved. The result for the axial velocity must be compensated to account for the difference to the axial velocity component in the case of direct extrusion. Equation (B.1) shows that adding a constant correction factor of  $\Delta v$  to any of the velocity

components does not have any influence on the solution as long as a correction factor of:

$$\frac{r^2}{2} \Delta v \quad (\text{B.30})$$

is added to the stream function  $\Psi$ . For this new formulation of the problem the boundary conditions are:

$$v_r|_{r=0} = \frac{1}{r} \Upsilon(r) \Xi'(x) = 0 ; \forall x \implies \frac{1}{r} \Upsilon(r) \Big|_{r=0} = 0 \quad (\text{B.31})$$

$$v_r|_{r=R} = \frac{1}{r} \Upsilon(r) \Xi'(x) = 0 ; \forall x \implies \frac{1}{r} \Upsilon(r) \Big|_{r=R} = 0 \quad (\text{B.32})$$

$$v_r|_{x=0} = \frac{1}{r} \Upsilon(r) \Xi'(x) = 0 ; \forall r \implies \Xi'(x) \Big|_{x=0} = 0 \quad (\text{B.33})$$

$$v_r|_{x=L} = \frac{1}{r} \Upsilon(r) \Xi'(x) = 0 ; \forall r \implies \Xi'(x) \Big|_{x=L} = 0 \quad (\text{B.34})$$

$$v_x|_{x=0} = \frac{1}{r} \Upsilon'(r) \Xi(x) \Big|_{x=0} = 0 \implies \Xi(x) \Big|_{x=0} = 0 \quad (\text{B.35})$$

$$v_x|_{x=L} = \frac{1}{r} \Upsilon'(r) \Xi(x) \Big|_{x=L} = v(L, r) - v_{ram} \quad (\text{B.36})$$

$$v_x|_{r=R} = \frac{1}{r} \Upsilon'(r) \Xi(x) \Big|_{r=R} = v_x(x, R) - v_{ram}. \quad (\text{B.37})$$

From the first boundary condition, it can immediately be deduced that the stream function  $\Psi$  vanishes at the axis of symmetry ( $r = 0$ ), and is therefore constant. The introduction of the following transformation:

$$f(r) = \frac{1}{r} \Upsilon'(r) \quad (\text{B.38})$$

into equation (B.25) yields the following expression:

$$f''(r) + \frac{1}{r} f'(r) - \frac{\alpha}{2} f(r) = 0. \quad (\text{B.39})$$

The inverse transform of (B.38) thus reads as follows:

$$\Upsilon(r) = \frac{2r}{\alpha} f'(r) \quad (\text{B.40})$$

which, together with the following substitution,

$$-\frac{\alpha}{2} = \omega^2 \quad (\text{B.41})$$

leads to the following *Bessel* equation of zero order<sup>1</sup>:

$$f''(r) + \frac{1}{r} f'(r) + \omega^2 f(r) = 0. \quad (\text{B.42})$$

The boundary conditions

$$\frac{1}{r} \Upsilon(r) \Big|_{r=0} = 0 \quad (\text{B.43})$$

$$\frac{1}{r} \Upsilon(r) \Big|_{r=R} = 0, \quad (\text{B.44})$$

under consideration of equation (B.40), lead to:

$$f'(r) \Big|_{r=0} = 0 \quad (\text{B.45})$$

$$f'(r) \Big|_{r=R} = 0. \quad (\text{B.46})$$

---

<sup>1</sup>See M. N. Özışık. *Heat Conduction*, Wiley & Sons, 2nd edition, 1993; J.W. Brown, R. and V. Churchill. *Fourier Series and Boundary Value Problems*, McGraw-Hill, 5th edition, 1993.

The eigenvalues  $\omega_i$  for a normed radius of one may now be calculated. The functions  $f_i(r)$  corresponding to each eigenvalue  $\omega_i$  are the *Bessel* functions of zero order. Any velocity distribution  $v_x(r)$  can now be expressed as a linear combination of the *Bessel* functions  $f_i(r)$ . The coefficients of the *Bessel* functions,  $\kappa_i$ , may be calculated by means of the following formula:

$$\kappa_i = \frac{\int_{r=0}^{r=1} r v_x(r) f_i(r) dr}{\int_{r=0}^{r=1} r f_i^2(r) dr}. \quad (\text{B.47})$$

Numerical values of the *Bessel* functions may be found tabulated in standard references<sup>2</sup>. If equation (B.1) is solved as indicated above (first separation), the boundary condition:

$$v_x|_{r=R} = \frac{1}{r} \Upsilon'(r) \Xi(x) \Big|_{r=R} = v_{surface}(x) - v_{ram} \quad (\text{B.48})$$

cannot be satisfied for a general velocity distribution  $v_x(x, r)$ . This velocity distribution  $v_x(x, r)$  will result from the solution and may not be predetermined. If the velocity at the surface  $v_x(x, R)$  is predetermined and the aforementioned boundary condition must be satisfied, another approach must be taken to find a solution. In this case equation (B.12) must be rearranged in descending order of derivatives of  $\Upsilon$  (second separation). The solution is then developed in a similar manner to the one shown for the first separation. For the model in question the first separation was chosen<sup>3</sup>.

<sup>2</sup>See, for instance, H. S. Carslaw and J.C. Jaeger. *Conduction of Heat in Solids*. Oxford University Press, 2nd. edition, 1959.

<sup>3</sup>Details to the solution with the second separation are found in: A.Schmid. Basisinformationen der Modellbildung des Strangprozesses, Technical Report 96/01. Alusuisse-Lonza Services AG, 1996.



## Appendix C

### Solving the Equation for the Distribution of Pressure

The pressure distribution, as already described, may also be expressed in terms of the stream function  $\Psi$ . It then takes the following form:

$$\frac{\partial p(r, x)}{\partial r} = \mu \left[ \frac{\partial}{\partial r} \left( -\frac{1}{r} \frac{\partial^2 \Psi}{\partial r \partial x} \right) - \frac{1}{r} \frac{\partial^3 \Psi}{\partial x^3} \right]. \quad (\text{C.1})$$

Introduction of the two separation functions  $\Upsilon$  and  $\Xi$  into the last equation leads to the following expression:

$$\frac{\partial p(r, x)}{\partial r} = \mu \left[ -\frac{\partial}{\partial r} \left( \frac{1}{r} \Upsilon'(r) \Xi'(x) \right) - \frac{1}{r} \Upsilon(r) \Xi'''(x) \right]. \quad (\text{C.2})$$

Applying the identities (B.38) and (B.40) to the last equation results in:

$$\frac{\partial p(r, x)}{\partial r} = \mu \left[ -\frac{\partial}{\partial r} (f \Xi'(x)) + \frac{f'}{\omega^2} \Xi'''(x) \right]. \quad (\text{C.3})$$

By integrating the last equation the following result is obtained:

$$p(r, x) = \mu f \left[ -\Xi'(x) + \frac{\Xi'''(x)}{\omega^2} \right] + \varphi(x), \quad (\text{C.4})$$



where  $\varphi(x)$  is an unknown function of the space coordinate  $x$ . To determine  $\varphi(x)$  we first derive the last equation with respect to the spatial coordinate  $x$ :

$$\frac{\partial p(r, x)}{\partial x} = \mu f \left[ -\Xi''(x) + \frac{\Xi''''(x)}{\omega^2} \right] + \varphi'(x). \quad (\text{C.5})$$

The introduction of the stream function into equation (2.22) and subsequent applications of identities (B.38) and (B.40) yield the following expression for the distribution of pressure:

$$\frac{\partial p(r, x)}{\partial x} = \mu \left[ \Xi(x) \left( \frac{1}{r} \Upsilon'''(r) + \frac{1}{r^3} \Upsilon'(r) - \frac{1}{r^2} \Upsilon''(r) \right) + \frac{1}{r} \Upsilon'(r) \Xi''(x) \right]. \quad (\text{C.6})$$

Considering equations (B.25) and (B.26) as well as the identities (B.40) and (B.41), the last two equations may be set equal to provide:

$$\mu f \left[ \omega^2 \Xi(x) - 2\Xi''(x) + \frac{\Xi''''(x)}{\omega^2} \right] + \varphi'(x) = 0 \quad (\text{C.7})$$

Equation (B.22) forces the term in parentheses to vanish. It may thus be concluded that:

$$\varphi'(x) = 0 \longrightarrow \varphi(x) = \text{constant}. \quad (\text{C.8})$$

The pressure distribution is therefore given by:

$$p(r, x) = \mu \sum_i f_i(r) \left[ -\Xi'_i(x) + \frac{\Xi'''(x)}{\omega_i^2} \right] + c \quad (\text{C.9})$$

where  $c$  is an integration constant. The integration constant may be determined by assuming zero pressure at the exit of the die. The assumptions for the velocity and pressure distributions within the die (*Hagen-Poiseuille* flow) mentioned in chapter 2 imply that:

$$\frac{\partial p(r, x)}{\partial x} = \mu \frac{1}{r} \frac{\partial}{\partial r} \left( r \frac{\partial v_x}{\partial r} \right) = \text{constant}. \quad (\text{C.10})$$

The above equation leads to the following expression for the pressure drop in the die:

$$\Delta p(x) = 2\mu \Delta x \frac{CA}{R^2} \quad (\text{C.11})$$

where  $\Delta x$  is width of the die.  $C$  and  $A$  are the constants defined in equation (2.50). The integration constant in equation (2.65) is readily derived from the following relationship:

$$\mu \sum_i f_i(0) \left[ -\Xi'_i(L) + \frac{\Xi'''(L)}{\omega_i^2} \right] - 2\mu \Delta x \frac{CA}{R^2} + c = 0. \quad (\text{C.12})$$



# Appendix D

## Smoothing Algorithm

When the heat conduction equation with heat generation terms as given by:

$$\frac{\partial T}{\partial t} = \alpha \nabla^2 T - \nabla v + \frac{1}{\rho c_p} q(\mathbf{p}, t) \quad (\text{D.1})$$

is solved numerically, oscillations may show up if the size of the discretization mesh used is not properly chosen. This problem can be avoided by reducing the mesh size of the discretization grid. However, since the computation time rises markedly when the size of the mesh is reduced, it is convenient to tackle the problem of numerical oscillations by means of a different approach. In this thesis a smoothing algorithm was used for the solution of the above equation by means of numerical methods.

First, it is convenient to recast the classical approximation approach. Let three neighboring points  $i - 1$ ,  $i$ , and  $i + 1$  of the mesh be given. The size of the mesh is denoted by  $h$ , and the values of the function at these points are denoted by  $f_{i-1}$ ,  $f_i$ , and  $f_{i+1}$ , respectively. A second degree polynomial is fitted through these points, such that the origin lies at point  $i$ , and that it exactly passes through  $f_{i-1}$ ,  $f_i$ , and  $f_{i+1}$ . That is:

$$P(x) = ax^2 + bx + c \quad (\text{D.2})$$

with the following conditions:

$$P(0) = f_i \quad (\text{D.3})$$

$$P(-h) = f_{i-1} \quad (\text{D.4})$$

$$P(+h) = f_{i+1}. \quad (\text{D.5})$$

The coefficients  $a$ ,  $b$ , and  $c$  are readily derived from the last equations:

$$c = f_i \quad (\text{D.6})$$

$$b = \frac{f_{i+1} - f_{i-1}}{2h} \quad (\text{D.7})$$

$$a = \frac{f_{i+1} + f_{i-1} - 2f_i}{2h^2}. \quad (\text{D.8})$$

For the first and second derivatives at the origin (point  $i$ ) the following expressions are obtained:

$$P'(0) = \frac{f_{i+1} - f_{i-1}}{2h} \quad (\text{D.9})$$

$$P''(0) = \frac{f_{i+1} + f_{i-1} - 2f_i}{h^2}. \quad (\text{D.10})$$

It is clear from the last equations that only immediate neighbors have an influence on the subsequent development of each point. Since the fitted polynomial passes exactly through the function values  $f_{i-1}$ ,  $f_i$ , and  $f_{i+1}$  at the given points, numerical oscillations are fully transferred to immediate neighboring points. Natural damping of these oscillations can sometimes take place if the process is self-dissipative. However, if the convection term  $-\nabla v$  in equation (D.1) is dominant, this natural dissipation and therefore numerical damping of the oscillations does not take place. The numerical values must be smoothed.

The smoothing algorithm proposed in this thesis is based on the following idea: let five points  $i - 2$ ,  $i - 1$ ,  $i$ ,  $i + 1$ , and  $i + 2$  with their respective function values  $f_{i-2}$ ,  $f_{i-1}$ ,  $f_i$ ,  $f_{i+1}$ , and  $f_{i+2}$  be given. The

size of the mesh is denoted by  $h$ . A second-degree polynomial in  $x$ ,  $P(x)$  with origin at  $i$ , is fitted through these points in such a manner that it exactly passes through  $f_i$  and that the difference between the remaining function values  $f_{i-2}, f_{i-1}, f_{i+1}, f_{i+2}$  and the approximated function values at points  $i - 2, i - 1, i + 1, i + 2$  is minimized in a least-squares sense. That is:

$$\begin{aligned}
 P(x) &= ax^2 + bx + c \\
 P(0) &= f_i = c \\
 P(-h) &= ah^2 - bh + f_i \\
 P(-2h) &= 4ah^2 - 2bh + f_i \\
 P(h) &= ah^2 + bh + f_i \\
 P(2h) &= 4ah^2 + 2bh + f_i \\
 \Delta_{-1} &= (ah^2 - bh + f_i - f_{i-1}) \\
 \Delta_{-2} &= (4ah^2 - 2bh + f_i - f_{i-2}) \\
 \Delta_{+1} &= (ah^2 + bh + f_i - f_{i+1}) \\
 \Delta_{+2} &= (4ah^2 + 2bh + f_i - f_{i+2})
 \end{aligned}$$

with:

$$\begin{aligned}
 \frac{\partial(\Delta_{-1}^2 + \Delta_{-2}^2 + \Delta_{+1}^2 + \Delta_{+2}^2)}{\partial a} &= 0 \\
 \frac{\partial(\Delta_{-1}^2 + \Delta_{-2}^2 + \Delta_{+1}^2 + \Delta_{+2}^2)}{\partial b} &= 0.
 \end{aligned}$$

From the above equations the following expressions results:

$$P(0) = f_i \quad (\text{D.11})$$

$$P'(0) = \frac{2f_{i+2} + f_{i+1} - f_{i-1} - 2f_{i-2}}{10h} \quad (\text{D.12})$$

$$P''(0) = \frac{4f_{i+2} + f_{i+1} + f_{i-1} + 4f_{i-2} - 10f_i}{17h^2}. \quad (\text{D.13})$$

In this case the function value for a particular point is not only influenced by its immediate neighboring points, but also by neighboring points of the latter. In the model presented in this thesis,

two different types of boundary conditions are found. Boundary conditions between different bodies (physical boundary) and boundary conditions between the various zones into which the billet was divided (numerical boundary). It is common for boundary conditions<sup>1</sup> to introduce fictitious nodes and fictitious temperatures at the borders of the body or zone in question.

In the case of a physical boundary, the boundary condition is expressed as follows:

$$\frac{\partial T}{\partial n} = \frac{h_c}{k} (T_p - T).$$

Here,  $T$  stands for the temperature at the surface of the body,  $T_p$  for its respective partner temperature,  $h_c$  for the contact conductance, and  $k$  for the thermal conductivity.  $n$  is a normal vector to the surface. With the usual approximation algorithm this fictitious temperature is given by:

$$T_F = \frac{2hh_c}{k} (T_p - f_i) + f_{i\pm 1}.$$

The smoothing algorithm proposed here yields the following expression:

$$T_{F1} + 2T_{F2} = \frac{10hh_c}{k} (T_p - f_i) + f_{i\pm 1} + 2f_{i\pm 2}.$$

Since the boundary condition is of rank 1, there is still one degree of freedom that may be exploited. This could be used for example for the following simplification:

$$T_{F1} = T_{F2}$$

In the case of a numerical boundary the idea is to choose the fictitious temperature such that the transfer from one zone to the other is as smooth as possible. In the case of the classical approximation, only the continuity of the temperature gradient can be demanded. With the smoothing algorithm previously presented, the curvature of the gradient may also be forced to be continuous. Let  $H$  be the mesh size outside of, and  $h$  the mesh size in the interior of the zone in question.

<sup>1</sup>See M. N. Özışık. Heat Conduction, Wiley & Sons, 2nd. edition, 1993

Let  $\varepsilon$  be:

$$\varepsilon = \frac{H}{h}.$$

The following expressions result for the smoothing algorithm:

$$T_{F+1} = -34\tilde{a} + 20\tilde{b} - 10f_i + 8f_{i-2} + 3f_{i-1}$$

$$T_{F+2} = 17\tilde{a} - 5\tilde{b} + 5f_i - 3f_{i-2} - f_{i-1}$$

$$T_{F-1} = -34\tilde{a} - 20\tilde{b} - 10f_i + 8f_{i-2} + 3f_{i-1}$$

$$T_{F-2} = 17\tilde{a} + 5\tilde{b} + 5f_i - 3f_{i-2} - f_{i-1}.$$

The following variables must be calculated on-line:

$$\tilde{a} = a_{11}\Gamma_2 + a_{12}\Gamma_1$$

$$\tilde{b} = a_{12}\Gamma_2 + a_{22}\Gamma_1$$

$$c = f_i$$

where:

$$\Gamma_2 = -4T_{P\pm 2}\varepsilon^2 - T_{P\pm 1}\varepsilon^2 + 5(\varepsilon^2 + 1)f_i - 4f_{i\pm 2} - f_{i\pm 1}$$

$$\Gamma_1 = \pm (2T_{P\pm 2}\varepsilon + T_{P\pm 1}\varepsilon + 3(1 - \varepsilon)f_i - 2f_{i\pm 2} - f_{i\pm 1}).$$

The coefficients  $a_{11}$ ,  $a_{12}$ , and  $a_{22}$  may be calculated a priori by means of the following relationships:

$$a_{11} = \frac{-\gamma}{(\alpha\gamma - \beta^2)}$$

$$a_{12} = \frac{\beta}{(\alpha\gamma - \beta^2)}$$

$$a_{22} + \frac{\alpha}{(\alpha\gamma - \beta^2)}$$

where:

$$\alpha = 17(1 + \varepsilon^4)$$

$$\beta = 9(1 - \varepsilon^3)$$

$$\gamma = 5(1 + \varepsilon^2)$$





# Appendix E

## Simulation of the Extrusion Process

### E.1 Simulation of the Container

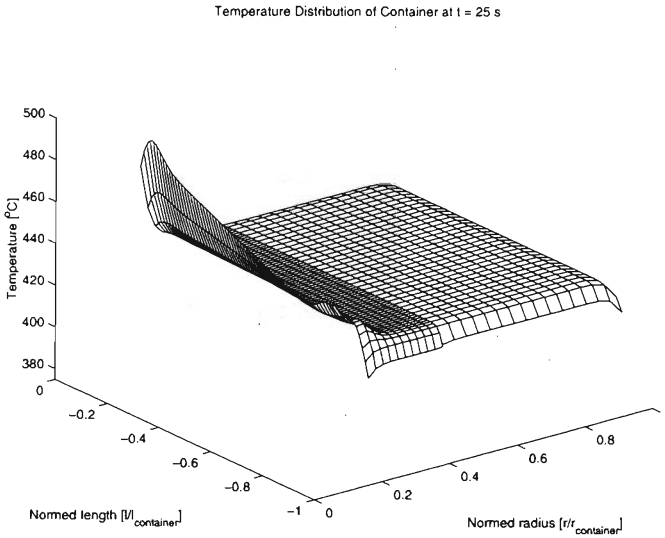
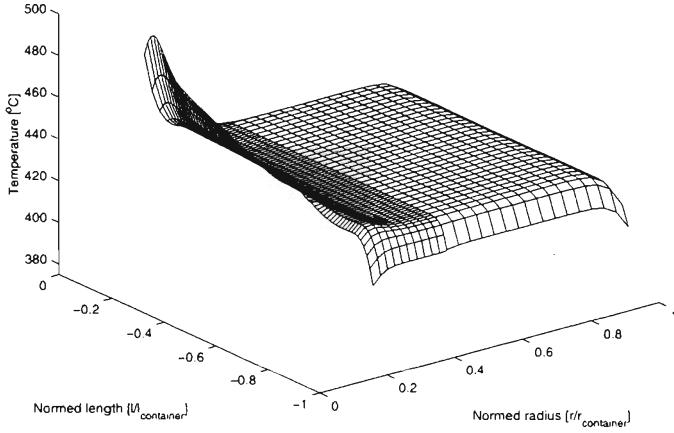


Figure E.1: *Temperature distribution of the container.*

Temperature Distribution of Container at  $t = 50$  s



Temperature Distribution of Container at  $t = 75$  s

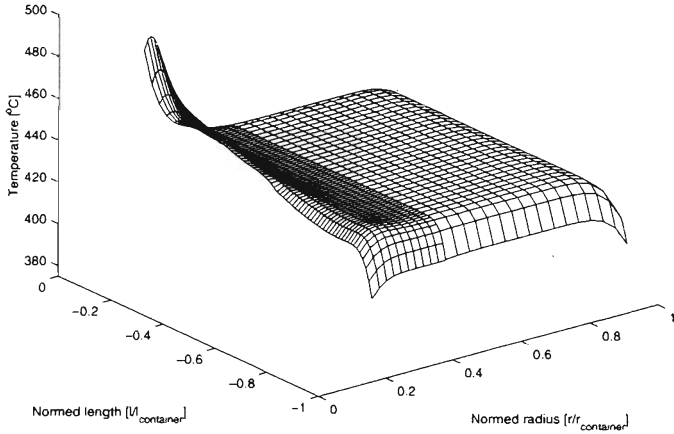
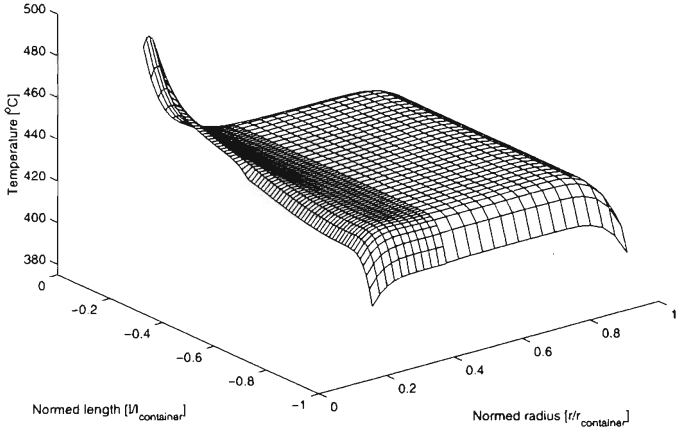


Figure E.2: *Temperature distribution in the container.*

Temperature Distribution of Container at  $t = 100$  s



Temperature Distribution of Container at  $t = 125$  s

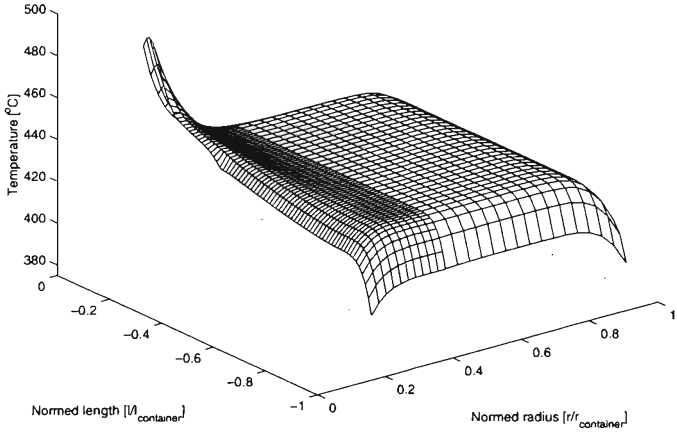


Figure E.3: *Temperature distribution in the container.*

Temperature Distribution of Container at  $t = 150$  s

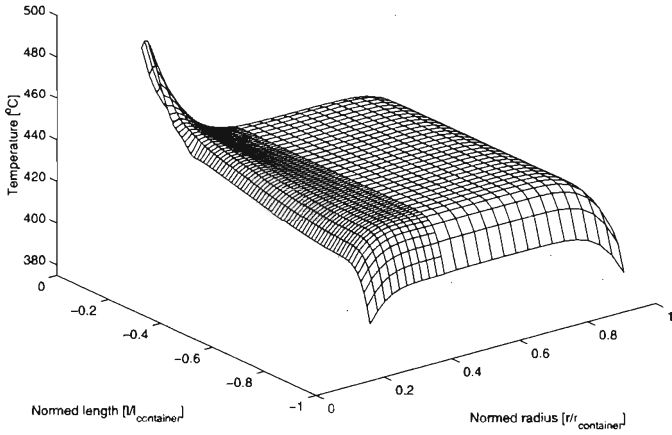


Figure E.4: *Temperature distribution in the container.*

## E.2 Simulation of the Die

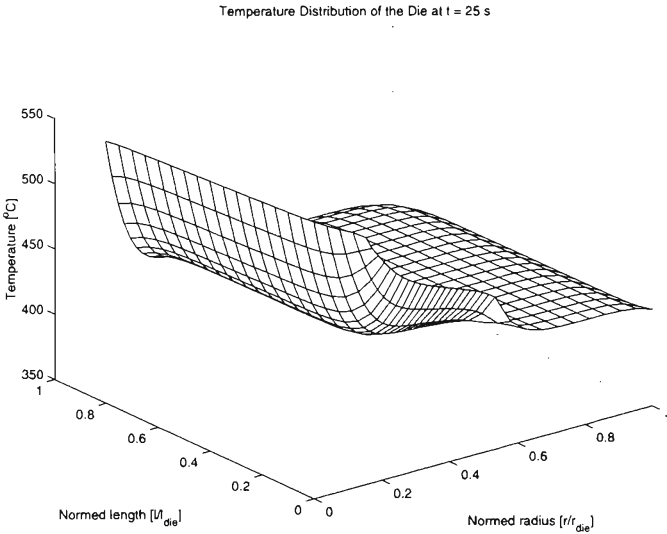
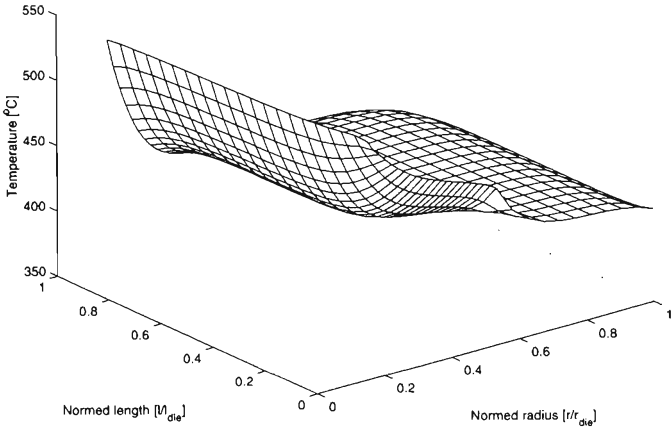


Figure E.5: *Temperature distribution of the die.*

Temperature Distribution of the Die at  $t = 50$  s



Temperature Distribution of the Die at  $t = 75$  s

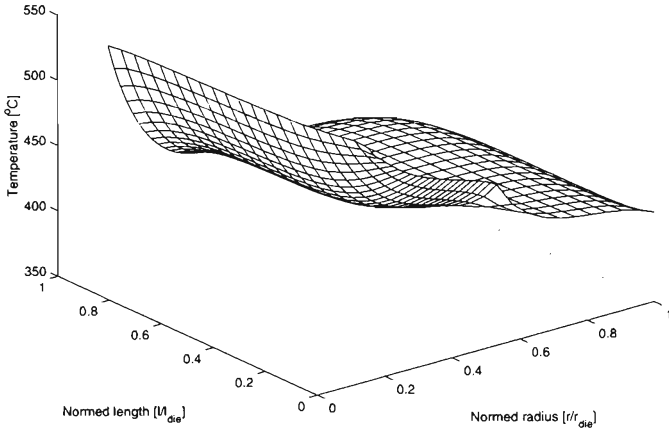
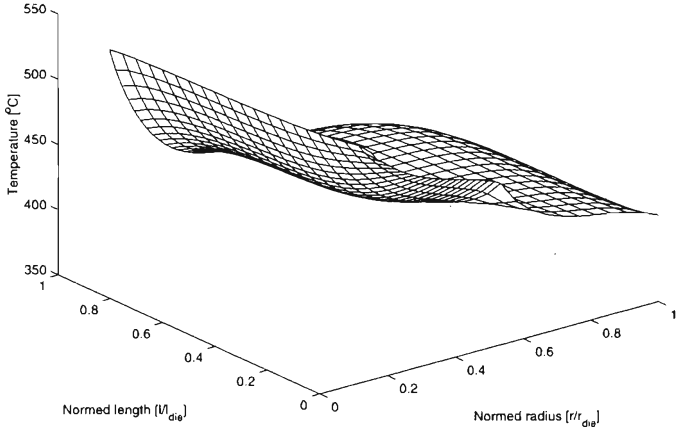


Figure E.6: *Temperature distribution of the die.*

Temperature Distribution of the Die at  $t = 100$  s



Temperature Distribution of the Die at  $t = 125$  s

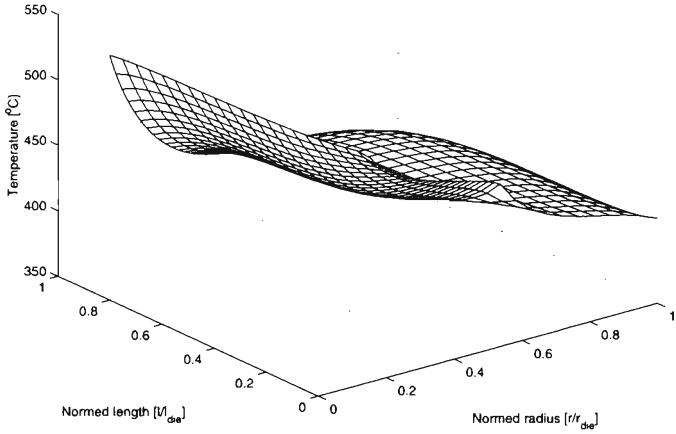


Figure E.7: *Temperature distribution of the die.*



Temperature Distribution of the Die at  $t = 150$  s

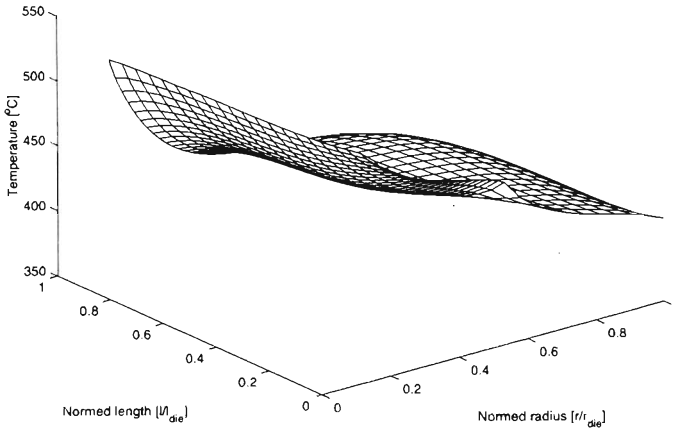


Figure E.8: *Temperature distribution of the die.*

### E.3 Simulation of the Mandrel

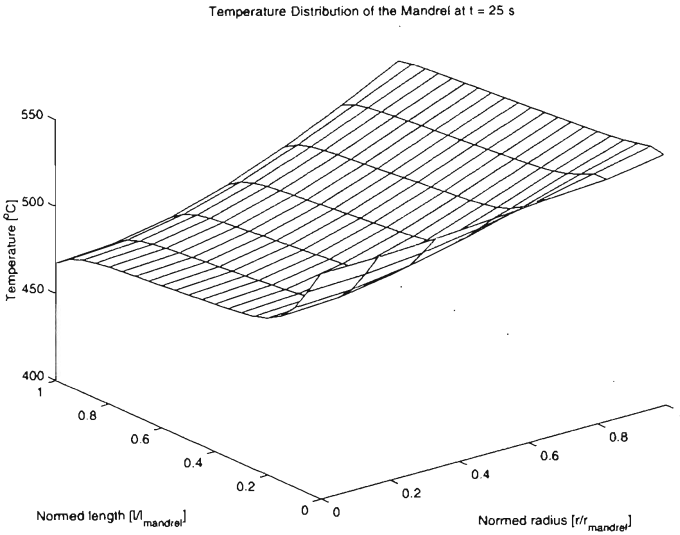
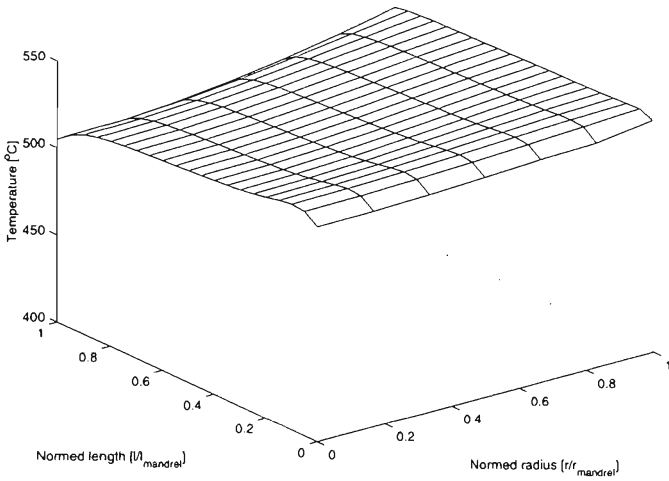


Figure E.9: *Temperature distribution of the mandrel.*

Temperature Distribution of the Mandrel at  $t = 50$  s



Temperature Distribution of the Mandrel at  $t = 75$  s

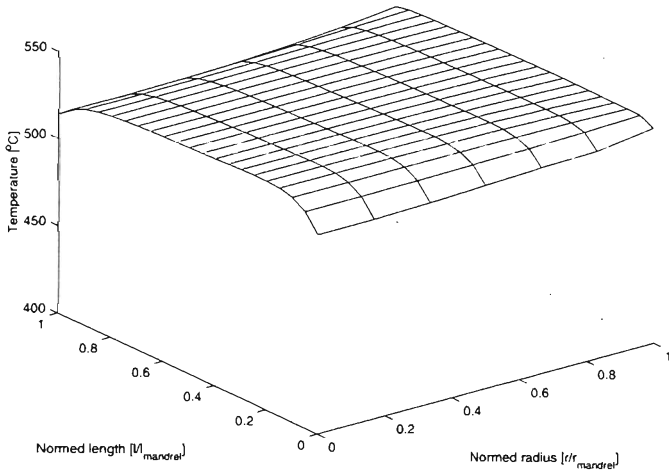
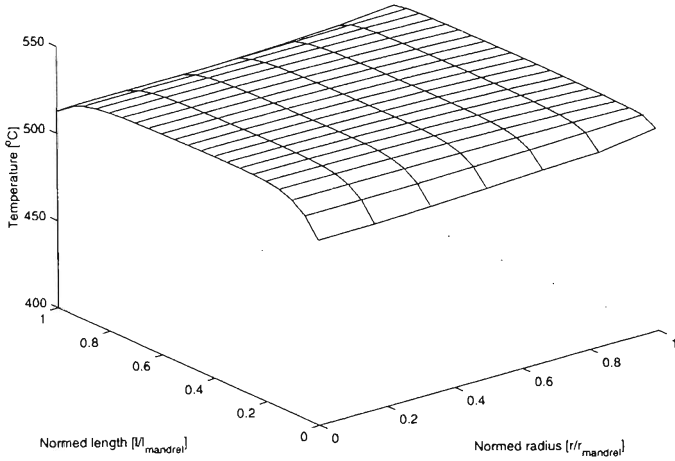


Figure E.10: *Temperature distribution of the mandrel.*

Temperature Distribution of the Mandrel at  $t = 100$  s



Temperature Distribution of the Mandrel at  $t = 125$  s

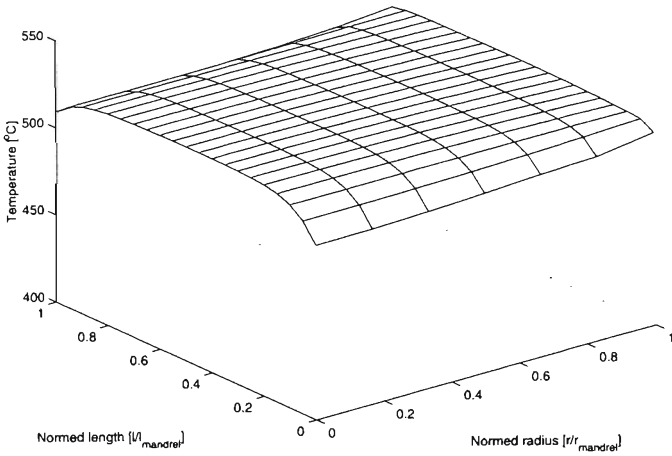


Figure E.11: *Temperature distribution of the mandrel.*

Temperature Distribution of the Mandrel at  $t = 150$  s

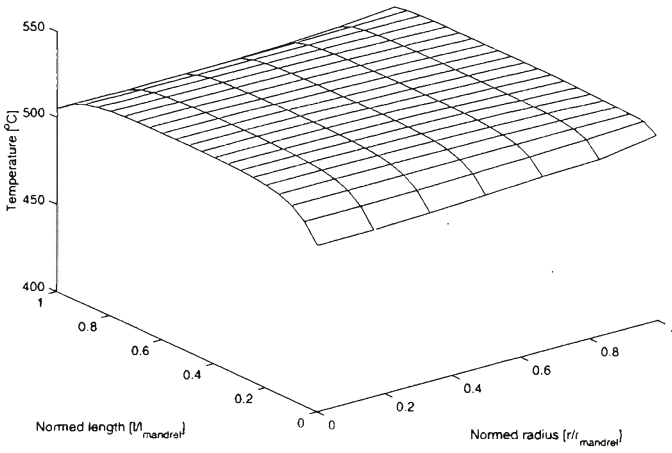


Figure E.12: *Temperature distribution of the mandrel.*

# Appendix F

## Equations of the Simplified Model for the Various Bodies Involved

### F.1 Equations of the Model Before the First Disc is Extruded

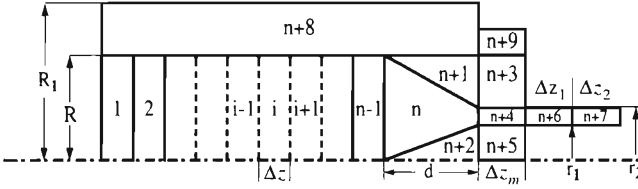


Figure F.1: *Disc model of extrusion before the first disc is extruded.*

For disc 1:

$$\begin{aligned} \Delta z A_0 \rho_{Al} c p_{Al} \frac{dT_1}{dt} = & -A_{1/n+8} h_R (T_1 - T_{n+8}) - k_{Al} A_0 \frac{(T_1 - T_2)}{\Delta z} \\ & + A_{1/n+8} \nu_{fr} k_f v_{ram} - \rho_{Al} c p_{Al} A_0 T_1 v_{ram} \quad (F.1) \end{aligned}$$

For discs  $2 \leq i \leq n-1$ :

$$\begin{aligned} \Delta z A_0 \rho_{Al} c p_{Al} \frac{dT_i}{dt} = & -A_{i/n+8} h_R (T_i - T_{n+8}) + k_{Al} A_0 \frac{(T_{i-1} - T_i)}{\Delta z} \\ & - k_{Al} A_0 \frac{(T_i - T_{i+1})}{\Delta z} + A_{i/n+8} \nu_{fr} k_f v_{ram} + \rho_{Al} c p_{Al} A_0 (T_{i-1} - T_i) v_{ram} \quad (F.2) \end{aligned}$$

**For discs  $n$  to  $n + 2$  (deformation zone):**

$$\begin{aligned}
 V_n \rho_{Al} c_{pAl} \frac{dT_n}{dt} &= 2k_{Al} A_0 \frac{(T_{n-1} - T_n)}{(\Delta z + d)} - 2k_{Al} A_{n/n+1} \frac{(T_n - T_{n+1})}{(R - r_2)} \\
 &\quad - 2k_{Al} A_{n/n+2} \frac{(T_n - T_{n+2})}{r_1} - 2k_{Al} A_1 \frac{(T_n - T_{n+4})}{(\Delta z_m + d)} \\
 &\quad + \rho_{Al} c_{pAl} A_0 (T_{n-1} - T_n) v_{ram} + k_f \dot{\epsilon} V_n \quad (F.3)
 \end{aligned}$$

$$\begin{aligned}
 V_{n+1} \rho_{Al} c_{pAl} \frac{dT_{n+1}}{dt} &= -2k_{Al} A_{n/n+1} \frac{(T_{n+1} - T_n)}{(R - r_2)} \\
 - A_{n+1/n+8} h_R (T_{n+1} - T_{n+8}) &- A_{n+1/n+3} h_{Fe/Al} (T_{n+1} - T_{n+3}) \quad (F.4)
 \end{aligned}$$

$$\begin{aligned}
 V_{n+2} \rho_{Al} c_{pAl} \frac{dT_{n+2}}{dt} &= -2k_{Al} A_{n/n+2} \frac{(T_{n+2} - T_n)}{r_1} \\
 - A_{n+2/n+5} h_{Fe/Al} (T_{n+2} - T_{n+5}) &\quad (F.5)
 \end{aligned}$$

**For disc  $n + 3$ :**

$$\begin{aligned}
 V_{n+3} \rho_{Fe} c_{pFe} \frac{dT_{n+3}}{dt} &= h_{Fe/Al} A_{n+1/n+3} (T_{n+1} - T_{n+3}) \\
 &\quad - h_{Fe/Fe} A_{n+3/n+9} (T_{n+3} - T_{n+9}) \\
 &\quad - A_{n+3} h_{Fe/Air} (T_{n+3} - T_{air}) \\
 &\quad + h_{Fe/Al} A_{n+3/n+4} (T_{n+4} - T_{n+3}) \quad (F.6)
 \end{aligned}$$

**For disc  $n + 4$ :**

$$\begin{aligned}
 V_{n+4} \rho_{Al} c_{pAl} \frac{dT_{n+4}}{dt} &= 2k_{Al} A_1 \frac{(T_n - T_{n+4})}{(\Delta z_m + d)} + 2k_{Al} A_1 \frac{(T_{n+6} - T_{n+4})}{(\Delta z_m + \Delta z_1)} \\
 &\quad - h_{Fe/Al} A_{n+3/n+4} (T_{n+4} - T_{n+3}) \\
 &\quad - h_{Fe/Al} A_{n+4/n+5} (T_{n+4} - T_{n+5}) \\
 &\quad + \rho_{Al} c_{pAl} A_0 (T_n - T_{n+4}) v_{ram} \quad (F.7)
 \end{aligned}$$

**For disc  $n + 5$ :**

$$\begin{aligned}
 V_{n+5}\rho_{Fe}c\rho_{Fe}\frac{dT_{n+5}}{dt} &= -h_{Fe/Al}A_{n+2/n+5}(T_{n+5} - T_{n+2}) \\
 &\quad + h_{Fe/Fe}A_{n+4/n+5}(T_{n+4} - T_{n+5}) \\
 &\quad - A_{n+5}h_{Fe/Air}(T_{n+5} - T_{air}) \quad (F.8)
 \end{aligned}$$

**For disc  $n + 6$ :**

$$\begin{aligned}
 V_{n+6}\rho_{Al}c\rho_{Al}\frac{dT_{n+6}}{dt} &= 2k_{Al}A_1\frac{(T_{n+7} - T_{n+6})}{(\Delta z_1 + \Delta z_2)} - 2k_{Al}A_1\frac{(T_{n+6} - T_{n+4})}{(\Delta z_m + \Delta z_1)} \\
 &\quad - h_{Fe/Air}A_{n+6}(T_{n+6} - T_{air}) \\
 &\quad + \rho_{Al}c\rho_{Al}A_0(T_{n+4} - T_{n+6})v_{ram} \quad (F.9)
 \end{aligned}$$

**For disc  $n + 7$ :**

$$\begin{aligned}
 V_{n+7}\rho_{Al}c\rho_{Al}\frac{dT_{n+7}}{dt} &= -2k_{Al}A_1\frac{(T_{n+7} - T_{n+6})}{(\Delta z_1 + \Delta z_2)} \\
 &\quad - h_{Fe/Air}A_{n+7}(T_{n+7} - T_{air}) \\
 &\quad + \rho_{Al}c\rho_{Al}A_0(T_{n+6} - T_{n+7})v_{ram} \quad (F.10)
 \end{aligned}$$

**For disc  $n + 8$  (container):**

$$\begin{aligned}
 V_{n+8}\rho_{Fe}c\rho_{Fe}\frac{dT_{n+8}}{dt} &= A_{1/n+8}h_R(T_1 - T_{n+8}) + A_{2/n+8}h_R(T_2 - T_{n+8}) + \dots \\
 &\quad + A_{i/n+8}h_R(T_i - T_{n+8}) + \dots + A_{n-1/n+8}h_R(T_{n-1} - T_{n+8}) \\
 &\quad + A_{n+1/n+8}h_R(T_{n+1} - T_{n+8}) - A_{n+8}h_{Fe/Air}(T_{n+8} - T_{air}) \\
 &\quad - h_{Fe/Fe}A_{n+8/n+9}(T_{n+8} - T_{n+9}) \quad (F.11)
 \end{aligned}$$



For disc  $n + 9$ :

$$\begin{aligned}
 V_{n+9} \rho_{Fe} c_{p_{Fe}} \frac{dT_{n+9}}{dt} &= h_{Fe/Fe} A_{n+8/n+9} (T_{n+8} - T_{n+9}) \\
 &\quad + h_{Fe/Fe} A_{n+3/n+9} (T_{n+3} - T_{n+9}) \\
 &\quad - A_{n+9} h_{Fe/Air} (T_{n+9} - T_{air}) \quad (F.12)
 \end{aligned}$$

## F.2 Equations of the Model Before the Second Disc is Extruded

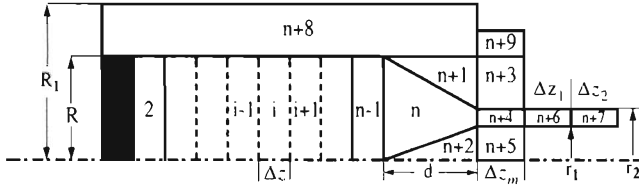


Figure F.2: Disc model of extrusion before second disc is extruded.

For disc 1:

$$\frac{dT_1}{dt} = 0 \quad (F.13)$$

For disc 2:

$$\begin{aligned}
 \Delta z A_0 \rho_{Al} c_{p_{Al}} \frac{dT_2}{dt} &= -A_{2/n+8} h_R (T_2 - T_{n+8}) - k_{Al} A_0 \frac{(T_2 - T_3)}{\Delta z} \\
 &\quad + A_{2/n+8} \nu_{fr} k_f v_{ram} - \rho_{Al} c_{p_{Al}} A_0 T_2 v_{ram} \quad (F.14)
 \end{aligned}$$

For discs  $3 \leq i \leq n - 1$ :

$$\begin{aligned}
 \Delta z A_0 \rho_{Al} c_{p_{Al}} \frac{dT_i}{dt} &= -A_{i/n+8} h_R (T_i - T_{n+8}) + k_{Al} A_0 \frac{(T_{i-1} - T_i)}{\Delta z} \\
 - k_{Al} A_0 \frac{(T_i - T_{i+1})}{\Delta z} &+ A_{i/n+8} \nu_{fr} k_f v_{ram} + \rho_{Al} c_{p_{Al}} A_0 (T_{i-1} - T_i) v_{ram} \quad (F.15)
 \end{aligned}$$

**For disc  $n + 8$  (container):**

$$\begin{aligned}
 V_{n+8} \rho_{Fc} c_{pFc} \frac{dT_{n+8}}{dt} = & A_{2/n+8} h_R (T_2 - T_{n+8}) + \dots + A_{i/n+8} h_R (T_i - T_{n+8}) \\
 & + \dots + A_{n-1/n+8} h_R (T_{n-1} - T_{n+8}) + A_{n+1/n+8} h_R (T_{n+1} - T_{n+8}) \\
 & - A_{n+8} h_{Fe/Air} (T_{n+8} - T_{air}) - h_{Fe/Fe} A_{n+8/n+9} (T_{n+8} - T_{n+9}) \quad (\text{F.16})
 \end{aligned}$$

For the remaining zones, the respective equations stated in section F.1 are still valid.



# Appendix G

## State Estimation via Extended Kalman Filtering

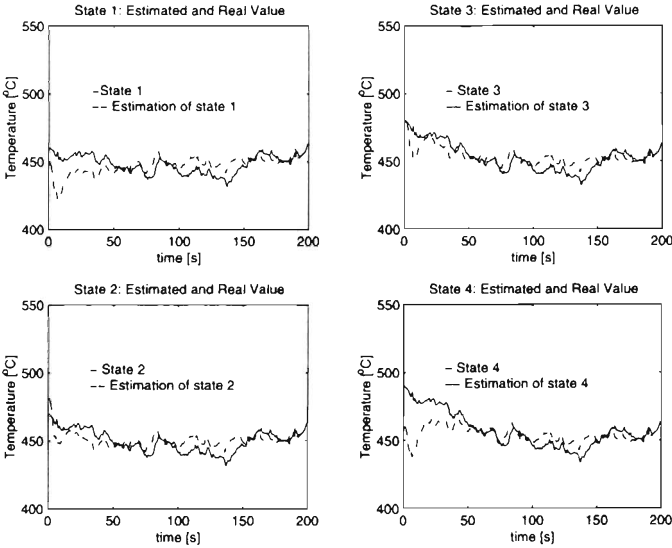


Figure G.1: Estimation of states via EKF.

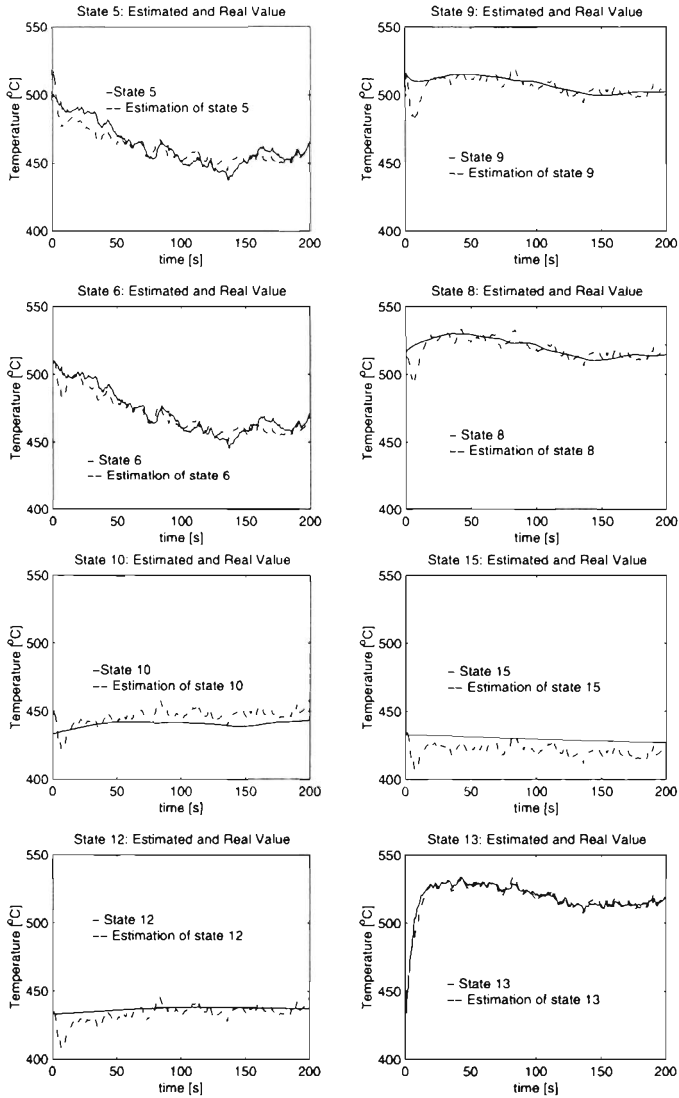


Figure G.2: Estimation of states via EKF.





# Curriculum Vitae

I was born on the 28th of October, 1967 to E. Alfredo Cuéllar and Lygia M. de Cuéllar in San Salvador, El Salvador. I am the youngest of four children: Alfredo, José Ernesto, and Lygia being my brothers and sister.

I received my entire elementary, secondary, and high school education at the German School in San Salvador, with the exception of my junior year in high school in 1984/85, which I spent as an exchange student at the Enrico Fermi High School in Enfield, Connecticut, U.S.A. I graduated from high school in November 1986 and started my Chemical Engineering studies in January 1987 at the Universidad Centroamericana José Simeón Cañas in San Salvador. In February 1988 I went to Germany to continue my studies at the Technical University in Darmstadt, from which I received my Pre-Diploma (Vordiplom) in Chemistry in September 1991. I then moved to Switzerland, where I completed my studies at the Swiss Federal Institute of Technology (ETH) in Zurich, obtaining my Diploma in Chemical Engineering in October 1993.

In January 1994, I started working as a research assistant at the Laboratory for Technical Chemistry of the ETH, and in October of the same year I transferred to the Measurement and Control Laboratory at the Department of Mechanical Engineering of the ETH as a research and teaching assistant. Here I pursued my PhD studies in automatic process control.